Microchemical Systems for Rapid Optimization of Organic Syntheses

by

Edward Robert Murphy
B.S. Chemical Engineering, Georgia Institute of Technology (2001)
S.M. Chemical Engineering Practice, Massachusetts Institute of Technology (2003)

Submitted to the Department of Chemical Engineering
in partial fulfillment of the requirements for the degree of
Doctor of Philosophy in Chemical Engineering
at the
MASSACHUSETTS INSTITUTE OF TECHNOLOGY
June 2006

Author .....
Department of Chemical Engineering
June 1, 2006

Certified by .....
Klavs F. Jensen
Lammot du Pont Professor of Chemical Engineering
Professor of Materials Science and Engineering
Thesis Supervisor

Certified by .....
Martin A. Schmidt
Professor of Electrical Engineering and Computer Science
Thesis Supervisor

Accepted by .....
William M. Deen
Carbon P. Dubbs Professor of Chemical Engineering
Chairman, Committee for Graduate Students

Microchemical Systems for Rapid Optimization of Organic Syntheses

by
Edward Robert Murphy

Submitted to the Department of Chemical Engineering on June 1, 2006,
in partial fulfillment of the requirements for the degree of
Doctor of Philosophy in Chemical Engineering

Abstract

In the chemistry laboratory, the desire to use smaller quantities of material to minimize both reagent cost and waste generation has driven chemists to develop new experimental techniques. The current approach to small scale experimentation has mostly been a simple reduction in the size of batch reaction apparatus. Working with these smaller volumes has increased the efficiency of experiments by accelerating the typically time consuming processes of heating, filtration, and drying. Furthermore, when working with hazardous materials, smaller scales minimize the exposure of a chemist to toxic materials and enable easier containment of potentially flammable or explosive systems.

The use of microfluidic devices has shown several improvements when compared to traditional batch synthesis. The precise control of reaction conditions enabled within the microreactor format has proved advantageous for a wide range of single and multiphase reactions. Also, unlike conventional bench-top batch reactions, continuous microreactors are capable of producing both analytical and preparative quantities of material by simply changing the amount of reactor effluent collected. The aim of this work was to harness the microsystem advantages of improved safety and process intensification while demonstrating both improved quality and speed of data collection, especially for chemistries that were challenging to explore using standard laboratory techniques. This work required improvements to reactor design, packaging technologies, and experimental techniques in order to use microreactors as a platform for rapidly determining optimum reaction conditions as well as reaction kinetics.

Three model reactions were selected to highlight the advantages of microchemical laboratory tools. The synthesis of oligosaccharides served as an example of rapid profiling of the effects of temperature and reaction time. Microreactors improved reaction optimization by reducing waste and dramatically increasing the rate of data collection. High-pressure carbonylation of aryl halides was also explored to characterize the effects of pressure, temperature, and various substrates on product yields. With microreactors, previously inaccessible reaction conditions were explored thus obtaining improved insights into the reaction mechanism. Finally, the production of sodium nitrotetrazolate was used to demonstrate the improved flexibility and safety of a modular microchemical system. The kinetics and pH effects for each step of the synthesis of this energetic compound were measured. This system was also optimized so that the microreactors used to characterize the reaction could be run in parallel as a production method.

Thesis Supervisor: Klavs F. Jensen
Title: Lammot du Pont Professor of Chemical Engineering
Professor of Materials Science and Engineering
Thesis Supervisor: Martin A. Schmidt
Title: Professor of Electrical Engineering and Computer Science

Acknowledgements

This thesis would not have been possible without the guidance of my thesis advisors Professors Klavs F. Jensen and Martin A. Schmidt. In addition to their technical advice, they provided a supportive environment in which to explore my own ideas. I also wish to thank the members of my thesis committee, Professors William M. Deen and Patrick S. Doyle. Their expertise and input proved invaluable to this project.

I am deeply indebted to my collaborators from the Department of Chemistry at MIT, particularly Dr. Daniel M. Ratner of Professor Peter H. Seeberger's group for his help with oligosaccharide synthesis and Joseph R. Martinelli from Professor Steven L. Buchwald's group for his help with organometallic chemistries. Thanks to Dr. Tomoya Inoue for looking over my shoulder during my first few months in the fab as well as his help in getting me started on high-pressure packaging. Thanks also to Dr. Jason G. Kralj, my collaborator on diazonium chemistry. Many thanks also to Dr. Yongbae Jeon, Hemantkumar Sahoo, and Nicolas Imlinger for their help with chip-to chip and optical packaging. I would especially like to thank Nikolay Zaborenko who, for the last 6 months, helped me be in two places at once.

None of my devices would ever have made it out of the fab without the help of the excellent MTL staff. The advice and aid of Dennis Ward, Dave Terry, and Kurt Broderick were crucial to producing functional microreactors.

I gratefully acknowledge the μChemical Systems Technology Center, Pacific Scientific, and the Deshpande Center for Technological Innovation for their financial support.

Joan Chisholm, thanks for everything... especially the chocolate.

Special thanks to the Movienight crew: Saif, Jamil, Andre, Hemant, Ben, Jodie, Jason, Marianne, Nico, Nick, Ahmed, and Zardoz.

Finally, I would like to thank Mom, Dad, Cindy, and Leah for their love and support

Contents

List of Figures

List of Tables

List of Reaction Schemes

Chapter 1

Introduction

1.1 Microchemical Systems

Microfabrication techniques revolutionized the electronics industry with the advent of the MOSFET transistor and integrated circuit. These techniques have also enabled new methods for the construction of miniaturized actuators, detectors, and analysis tools with a high degree of precision.[1] Interest in these devices led to further refinement of surface and bulk micromachining techniques, creating the field of microelectromechanical systems (MEMS).[2] One of the earliest uses of silicon micromachining for fluidic systems was the use of anisotropic wet etching to form ink jet print nozzles by Bassous *et al*. in 1977.[3] The combination of bulk micromachining and anodic bonding of silicon to glass by Terry *et al*. in 1979 was also used to fabricate sealed fluidic channels for a gas chromatograph with an integrated thermal conductivity detector.[4] While this work highlighted the great promise of microchemical devices, the microscale advantages of rapid separation, nanoliter sample handling, and compact packaging were not widely recognized until the development of the first micro total analysis system (μTAS) by Manz *et al*. in 1990.[5]

The theoretical analysis of gas chromatography and its analogy to liquid systems led to the prediction that open tubular liquid chromatography columns would be 100-fold more efficient in separating components than packed columns for a given pressure drop.[6,7] Unlike gas phase capillary columns, however, which range from 50μm to 500μm in diameter,[8] in order to achieve this improvement in separation efficiency, the required diameters for liquid capillary columns were calculated to be 0.25μm to 8μm.[9] Columns with diameters of 15μm to 50μm had been fabricated by the drawing of glass capillaries

and showed improved performance over packed columns, but the dispersion due to the injection and detection techniques made the use of these columns impractical.[10,11] Silicon microfabrication and similar patterning of glass substrates, on the other hand, provided a robust method for defining channels of the necessary diameters with integrated detectors capable of analyzing the minute quantities of column effluent.[12] The ability to use electroosmotic flows with these devices enabled sub-nanoliter injections of aqueous samples and separations of up to 75000 theoretical plates within 15 seconds.[13,14]

The precision with which samples could be manipulated and controlled encouraged the development of other microfluidic systems, including microsystems for chemical processing. One of the earliest microfabricated chemical systems was developed at DuPont in the early 1990's whereby several silicon wafers were patterned, etched, and bonded to produce a system of interconnected microfabricated unit operations. This system harnessed the high thermal conductivity of silicon (148 W/mK)[15] and its superior chemical compatibility to construct mixing units, microscale chemical reactors, heat exchangers, and sensors for precise control and monitoring of reaction conditions.[16-18]

In addition to precise monitoring, microreactors also have proved to be much safer than their traditional counterparts. The high surface area to volume ratio of the small diameter channels has demonstrated not only improved reaction control through both enhanced heat and mass transfer but also suppressing flame formation by quenching free radical generation.[19] These advantages were highlighted in a study of catalytic oxidation of ammonia in a silicon microreactor by Srinivasan *et al*. in 1997. In this work, a silicon microreactor, with the integration of on-chip temperature and flow sensors as well as resistive heaters, was capable of igniting and monitoring the partial oxidation of ammonia with highly flammable gas mixtures at several concentrations of hydrogen, oxygen, and ammonia without explosive failure.[20]

The rapid heat transfer in silicon microreactors has enabled other chemistries that had been considered too exothermic to attempt with traditional techniques. One such reaction of particular industrial interest is direct fluorination of organics for use as pharmaceutical precursors.[21] Due to their highly exothermic nature, these reactions had been considered uncontrollable, leading to the use of more stable, nitrogen containing fluorination agents.[22] Additionally the reactivities of both fluorine and hydrofluoric acid require

special considerations of materials compatibility. A nickel-lined silicon microreactor was constructed by de Mas *et al*. through a combination of bulk micromachining and subsequent nickel deposition. As demonstrated by the successful selective direct fluorination of toluene, this microreactor was capable of withstanding chemical attack without sacrificing the excellent heat transfer characteristics of silicon necessary to control the high heats of reaction that can exceed -473 kJ/mol.[23]

The success of microreactors in managing hazardous chemistries has raised the possibility of on-demand synthesis of hazardous intermediates.[24] An example of an on-demand synthesis system was a packed bed silicon microreactor in which complete conversion of chlorine to phosgene was demonstrated by Ajmera *et al*.[25] Production of phosgene on an as-needed basis in a microreactor, as opposed to delivery from a storage tank, reduces the phosgene inventory required for a subsequent process to the volume of the microreactor. By minimizing the volume of toxic material, in the event of a containment failure, only a microliter-scale volume of phosgene would be released, as opposed to a significantly larger release from a tank failure.

Fabrication of microreactors in chemically inert silicon, along with the wide range of coatings available though thermal oxidation and metal deposition, has made silicon microreactors compatible with a wide range of chemistries. In addition, the heat and mass transfer enhancements due to the submillimeter dimensions of the reaction channels singularly suits the microreactor as a platform for reaction characterization. Much reaction characterization work in microreactors has focused on catalyst screening and catalyst testing, as reactions are localized only to the catalyst bed and can be readily characterized by differential kinetics.[26,27] Furthermore, the use of microreactors minimized the consumption of catalyst and enabled high-throughput screening, greatly accelerating the discovery and characterization of catalytic systems.[28,29]

In improving the speed and reliability of obtaining chemical information, the microreactor has served as a bridge between the research lab and the plant floor. This bridge is reinforced by the possibility of using microreactors in parallel to increase throughput to production levels.[30] This scale-out method of increasing capacity enables the same platform to be used for both characterization and production, thus eliminating the costly and time-consuming scale-up process of traditional plant design. The prospect

of extending the applicability of the microreactor, even to the chemistry lab bench, further raises the possibility of the microreactor as a universal chemical discovery, characterization, and production tool. Such a tool would not only unify these branches of chemical development but also, through the advantages of microscale processing, improve process safety and accelerate the progress of chemical research.

1.2 Motivation: Microsystems as Laboratory Tools

In the chemistry laboratory, the desire to use smaller quantities of material to minimize both reagent cost and waste generation has driven chemists to develop new experimental techniques. While the current approach to small scale experimentation has mostly been a simple reduction in the size of batch reaction apparatus, working with smaller volumes has increased the efficiency of experiments by accelerating the typically time consuming processes of heating, filtration, and drying. Furthermore, when working with hazardous materials, smaller scales minimize the exposure of a chemist to toxic materials and enable easier containment of potentially flammable or explosive systems.[31]

In the case of sequential reactions where intermediates are not commercially available, the process of reaction optimization is crucial. The process of optimizing reactions can be very time consuming and requires a significant investment of reagents that themselves are often the result of several synthesis steps. This is particularly true for the field of total synthesis of natural compounds such as oligosaccharides. The synthesis of the individual saccharide building blocks must be optimized such that these compounds are available in sufficient quantity to investigate the subsequent linkage of these building blocks. These long synthesis chains, often involving several protection and deprotection reactions for each synthetic transformation, has led to the development of robotic automated synthesizers.[32] One such system was constructed from a peptide synthesizer in which a batch reaction vessel was sequentially loaded with reagents by either a series of injectors or by pumping form liquid reagent reservoirs maintained under a pressurized argon atmosphere. Unless such systems can become sufficiently flexible to handle both small quantities for characterization reactions and larger quantities for preparation of reagents for subsequent manipulations, they will not be a viable alternative to manual manipulations by a bench chemist.[33]

The use of microfluidic devices has shown several advantages when compared to traditional batch synthesis. The capability of microsystems to manipulate small quantities of material has proved particularly helpful in biochemical applications. With precise handling of samples in the range of nanoliters, high throughput screening and characterization of natural compounds, often present in only femtomolar quantities, has become feasible.[34] The precise control of reaction conditions enabled within the microreactor format has also proven advantageous for organic synthesis optimization over a wide range of single and multiphase organic reactions.[35,36] Furthermore, unlike conventional bench-top batch reactions, continuous microreactors are capable of producing both analytical and preparative quantities of material by simply changing the amount of reactor effluent collected.

1.3 Thesis Objectives and Overview

To be a viable alternative to standard laboratory techniques, a small set of basic microreactor configurations must be able to accommodate a wide range of chemistries. In operating these reactors, typical packaging schemes, such as those that relied on epoxy and compression sealing, were found to be insufficient for the high pressures, low temperatures, and aggressive solvents used that are of interest in many areas of active chemical research. To this end a new packaging technique based on direct solder bonding was developed for both chip to world and chip to chip packaging. The design and fabrication of these reactors, as well as the development of the packaging schemes necessary to connect these are described in Chapter 2.

The first class of chemistries to be explored was the synthesis of oligosaccharides. As described in Chapter 3, this chemistry was particularly challenging since the starting materials of interest were not commercially available and required significant investment of both reagents and time to generate significant material before any optimization of the desired reaction could begin. Thus, the microreactor was used to both minimize the waste generated in profiling the effect of reaction conditions as well as greatly accelerate the process of data collection.

Chapter 4 describes the optimization of aryl halide carbonylation syntheses. This study is an example of how microreactors can greatly increase the safety of working with

toxic gases while opening up new reaction conditions that could not be explored using traditional means. This study was also an example of how microreactors could serve as multipurpose chemical tools. The same reactor used for the homogeneous oligosaccharide studies was also used for the multiphase carbonylation experiments in this study.

Finally, the nitrotetrazolate synthesis described in Chapter 5 demonstrated the utility of microreactors for kinetic studies of multi-step syntheses. The synthesis of this energetic compound was too hazardous to characterize through batch experiments but, when transferred to microreactors, both the kinetic parameters of each reaction step and the equilibrium of the reactive intermediate could safely be determined. This study also highlighted the advantages of a modular microreactor design. By fabricating separate rapid mixers and using standardized tubing for the reaction zone, a customized reactor could be readily assembled with an adjustable residence time. By attaching two of these reactor chains in series, multiple steps in the synthesis could be independently monitored. This standard set of tools also allowed for the rapid parallelization or "scale-out" such that the same reactor system that was used for the kinetic studies could also generate production scale quantities of material.

Chapter 2

Microreactor Packaging

Constructing a microsystem compatible with a wide range of chemistries required a system design that would be flexible for a wide range of compounds and conditions. While silicon is highly resistant to most chemistries, the cryogenic temperatures, high pressures, and aggressive solvents required the development of a new fluidic packaging scheme. Solder based connections were designed and implemented on silicon microreactors and showed excellent resistance to a wide range of reaction conditions[37].

Joint failure tests revealed solder based connections to be highly robust to elevated pressures (200 bar) a wide range of temperatures (-78°C to 160°C) and a large number of solvent systems. Through the deposition of metal bonding pads directly onto silicon devices, solder-based chip-to-tube connections could be reliably formed using handheld soldering tools. Additional packaging techniques allowing microfluidic modules to be directly connected were also developed. Direct chip-to-chip solder bonding enabled the construction of a larger integrated platform for synthesis and optimization. This prototype board consists of 3 parallel reaction chains with integrated flow control and on-line detection.

2.1 Microsystem Packaging

The packaging requirements for microfluidic devices are much more challenging than those for the packaging of integrated circuits. The integrated circuit package is required to isolate the device from environmental influences and facilitate only the removal of heat and provide electrical connections. These limited requirements has enabled the development of a general packaging technology that can be applied to most devices regardless of function.[2] The design of the microfluidic package, on the other hand, is extremely dependent upon, not only compatibility with the fluids being processed but also the number of fluid ports required for the device and the degree of integration of those devices with optical, electronic, or mechanical functionalities.[38] The performance of the device package can determine the success or failure of a microfluidic device and the packaging cost can be 50%-90% of the total cost of a MEMS device.[39] However, academic publication on the subject of packaging has been sparse as packaging has been considered an intrinsically industrial or commercial field.[1] As a result, packaging techniques have varied greatly from application to application and it has been very difficult to develop a universal packaging scheme for microfluidic devices.[40]

2.1.1 Microfluidic Packaging Techniques

One of the more prevalent packaging techniques has been the sealing of tubing to a microfluidic device via adhesives.[41] The advantage to the use of adhesives, particularly epoxy, for device sealing has been the simplicity of the application. Without specialized tooling, both glass capillary and polymer tubing have been attached to microfluidic devices facilitating connections to standard chromatography fittings. This technique, as shown in Figure 2-1a can be used for devices a high density of connections and does not obscure the device, a critical feature for devices in which optical measurements are required.[42] This technique has been particularly effective for devices fabricated in poly(dimethylsiloxane) or PDMS as holes into which tubing can be inserted were easily bored and epoxy subsequently applied to the exterior of both the tubing and device.[43,44] The main difficulty with the use of epoxy or other adhesives has been the limited compatibility of the epoxies with organic solvents. Furthermore, it is difficult to prevent

epoxy from clogging the device channels when, as in the case of most silicon devices, the tubes are attached to the planar surface of the device and the procedure requires manual alignment.

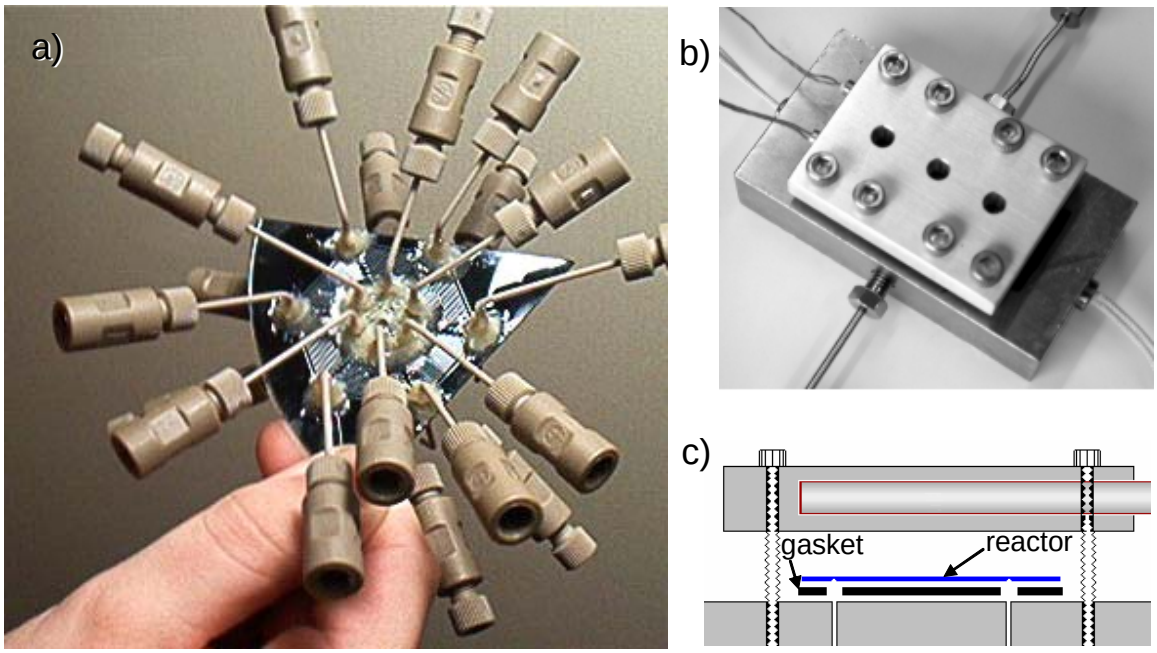

Figure 2-1: Silicon Microreactor Packaging Examples
a) Epoxy based packaging technique[42] b) Compression sealing technique[27]
c) Schematic of compression sealing

Fluidic seals have also been achieved, as shown in Figure 2-1b, by the compression of a device within a fluidic module or chuck. With this technique, a flexible O-ring or gasket creates a seal between the fluid ports on the device and the corresponding flow channels in the chuck.[45] For particularly small devices, such chucks enabled the use of fluid ports separated by only 800µm which would have been unfeasible to achieve with adhesive sealing.[46,47] The primary difficulty with this technique has been ensuring even compression across the large surface area of the device to form a proper seal. This has been especially difficult for chemically resistant gasket materials such as Teflon® with a high modulus requiring a high degree of compression to form a seal. To reduce breakage of devices, the softer Kalrez® or Viton® have been typically used as gasket materials; however, this increase in pliability is obtained at the expense of chemical compatibility with many organic solvents.[27] Compression sealing techniques have also required custom

fabricated pieces that must be built to tight tolerances otherwise, these fluidic chucks can be plagued by leaks.[48]

Other methods for microfluidic packaging have involved the use of microfabrication techniques to form integrated chip-to-tube couplers. In one design, pyramidal couplers were fabricated in silicon by either a potassium hydroxide (KOH) etch or deep reactive ion etch (DRIE) such that the coupler would fit directly into a similarly etched fluid port. These couplers were connected to PEEK™ (polyetheretherketone) tubing by cooling the tubing in liquid nitrogen and immediately inserting the tube into the coupler. Thus, when the tube warms, the thermal expansion compressed the tube against the coupler creating a seal that was reinforced with epoxy when the coupler was glued to the device.[49] Additional coupler designs have been fabricated directly into silicon devices. One technique involves DRIE rings that are etched around flow ports such that tubing can be placed directly into the flow port for sealing. The sealing of tubing to these couplers has been accomplished by adhesive sealing and molded plastic fittings[50] or through the use of polyolefin heat shrink tubing which was used as a sleeve that, upon heating, contracts around both the DRIE coupler and standard tubing.[51]

In addition to chip-to-tube connections there is also a great desire for chip-to-chip packaging. A reliable connection between devices would facilitate the construction of integrated microsystems as the separation of different microfluidic functionalities into modules would greatly simplify the fabrication of each unit.[52] While most successful integration techniques involved connection through external tubing to standard fluidic and analytical equipment,[24] the possibility of integration on the micro-scale with low dead-volumes would reduce required sample sizes and accelerate the pace of data collection. A common inspiration for chip-to-chip bonding has been the idea of reversibly interlocking LEGO® bricks with different functionality. An example of such a packaging scheme was machined in silicon where the use of (110) and (100) silicon wafers allowed the formation of interlocking fingers and protruding tubes which were coupled with silicone gaskets to allow direct chip-to-chip and chip-to-tube interfaces at low pressures (2.4 bar).[53] Another chip-to-chip bonding technique involves the use of adhesives to attach devices directly. It has been shown that the use of a UV crosslinking epoxy can

join glass chips and that these devices can subsequently be released by immersion in dichloromethane.[54]

2.1.2 Solder-Based Packaging

Tin-lead (SnPb) solder has been a favorite interconnect material of electronic hobbyists due to the ease of its application and the reliability of the joint produced. As a secondary packaging material for integrated circuits, SnPb and other solder formulations have served as the backbone for both electrical and mechanical connections between packaged electronic components and printed circuit boards (PCBs); thus, the robustness of the solder joint to withstand both mechanical wear and thermal cycling has been thoroughly investigated.[55]

The necessity of ever higher densities of electrical interconnects on modern integrated circuits has led to the development of flip-chip bonding in which solder bumps on the silicon chip are directly bonded to the circuit board. The joint has typically been prepared by deposition of metal bond pads composed of copper, nickel, gold, or palladium and SnPb solder by one of several means including, evaporation, electroplating, and electroless plating.[56,57] Heating reflows the solder forming the flip-chip joint which has been found to be quite robust. With epoxy reinforcement, SnPb flip-chip interconnects have been found to withstand thousands of thermal cycles between -40°C and 125°C.[57,58]

The flip-chip joint, compared to the more traditional wire bonding has the additional advantage of self-alignment. With SnPb solder and Cu bonding pads, the surface tension of the molten solder has been shown to pull the device into alignment with the corresponding bond pads on the substrate.[57] For these materials, there is also no need for a forming gas atmosphere as oxide formation on the bond pads can be removed through pretreatment with chemicals such as acetic acid and ammonium hydroxide and prevented through the use of rosin fluxes which prevent oxidation and reduce the solder surface tension.[57,59] Furthermore, since the melting point of SnPb solder (63%Sn, 37%Pb) is 183°C and the intermetallic compounds are formed between 200°C and 220°C no specialized equipment is required for bonding, and this connection has been reliably formed on laboratory hotplates.[60,61]

Optoelectronic devices have been the primary MEMS field in which solder-based packaging has been put to the greatest use. Due to the tight alignment required for chip to fiber and chip to amplifier connections the self-alignment of the molten solder to the bonding pads enabled much more precise optical component placement and greatly reduced loss.[62,63] In fact, since this surface tension alignment depended almost entirely on the photolithography used to position the bond pads, alignment precision of 1μm has been achieved.[64]

Solder-based connections, as a completely metallic seal, are known to be compatible with a wide range of solvents and conditions. As such, solder joints have found wide use in tube fittings and plumbing;[65] however, solder-based microfluidic packaging has not been common. Flip-chip techniques have been use in microfluidic devices, although this use has been limited to the integration of integrated circuit modules onto the separately constructed fluidic device or the connection of external device electrodes to a printed circuit board.[66,67] Thermocompression bonding, like solder bonding, uses deposited metal layers to form a hermetic seal and fluidic seals have been achieved using electroplated gold layers to form a gold-silicon eutectic seal.[68] This technique has been useful for wafer level bonding at temperatures between 260°C to 450°C,[69] but the pressures and surface conditions required preclude its use as a practical chip-to-tube bonding process. Glass brazing to Kovar® tubing, which also involves the thermal reflow of a sealant, has been used to package microfluidic devices.[70] The high pressure (127 bar) and temperature (530°C) tolerated by this packaging scheme enabled the construction of a microfabricated rocket engine.[71] This technique, with a lower temperature braze, has also been found to work with glass capillaries producing a chemically compatible glass seal; however, this bond required temperatures in excess of 630°C and tight control of the bonding process to complete the seal. Additionally, the resulting joint was brittle, requiring careful device handling and external packaging.[27]

While solder bonding would enable a lower temperature range than possible with a glass braze, the possibility of its use in both chip-to-tube and chip-to-chip bonds suggests that this technique would be a significant improvement over current microfluidic packaging techniques in both design flexibility and solvent resistance. The compatibility of solder bonding with current fabrication techniques, and the ability to join parts with

standard laboratory equipment, also would make solder-bonding a more economical process than those requiring precisely machined chucks or high temperature processing. Finally, as this process would use the same materials used for flip-chip bonding the same fabrication processes could be used to create a unified fluidic and electronic packaging scheme.

2.2 Packaging Design and Methodology

In order to use as many standard components as possible, the solder joint was designed to form a seal between 1/16" OD tubing and either the glass or silicon surface of a microfluidic device. Since a solder wetting surface is required to bond to the tubing, the joint was designed to bond to brass ferrules that could be swaged onto the desired tubing. Figure 2-2 shows a schematic of the bond where the swaged ferrule would be placed over the device bond pad and a solder preform would be heated, reflowing around the ferrule and creating a seal. For chip-to-chip bonding, solder would be applied between the bond pads of two devices creating a direct chip-to-chip seal.

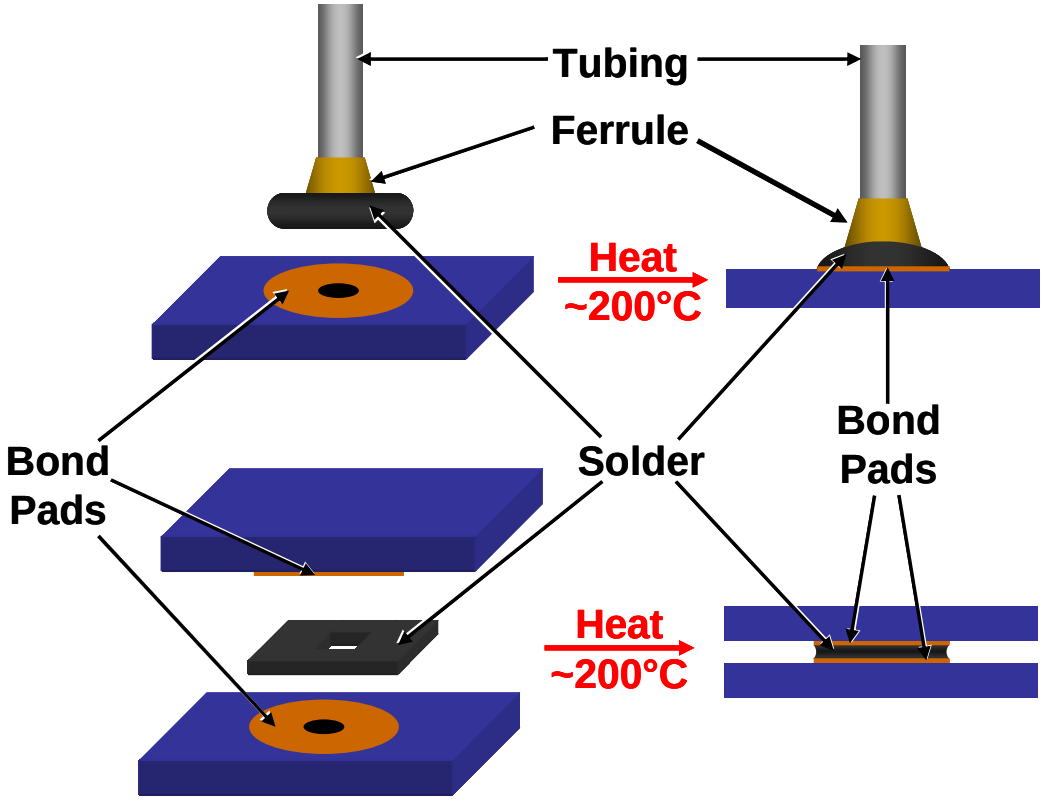

Figure 2-2: Solder-Based Packaging Schematic
Chip-to-Tube and Chip-to-Chip Bonding

2.2.1 Test Device Fabrication Process

In order to test the viability of the solder interconnect, test devices consisting of a single channel 600µm wide and 300µm deep with one inlet and one outlet were fabricated in silicon. Figure 2-3 outlines the fabrication process whereby the channels and flow ports were etched into a 500µm thick silicon wafer by deep reactive ion etching (DRIE). This wafer was then anodically bonded to a Pyrex® wafer to seal the flow channels. Once sealed, photoresist was spun and patterned onto the wafer so that, after electron beam deposition of the metal layers, 5mm diameter bond pads could be defined by acetone lift-off. Since the photoresist was spun onto the wafer after the holes were etched, a thick coating was required to ensure full coverage. The bond pads consist of a 1000Å titanium layer that promotes adhesion between the silicon and the 5000Å copper bonding layer. The use of a lift-off pattern enabled the simultaneous deposition of metal connectors such that every bond pad could be electrically connected for subsequent electroplating. It was originally intended that the bond pads would be electroplated with additional copper to a thickness of 50µm but it was found that the thicker bond pads showed no improvement in bond quality or bond reversibility over bonding directly to the original 5000Å thick seed layer.

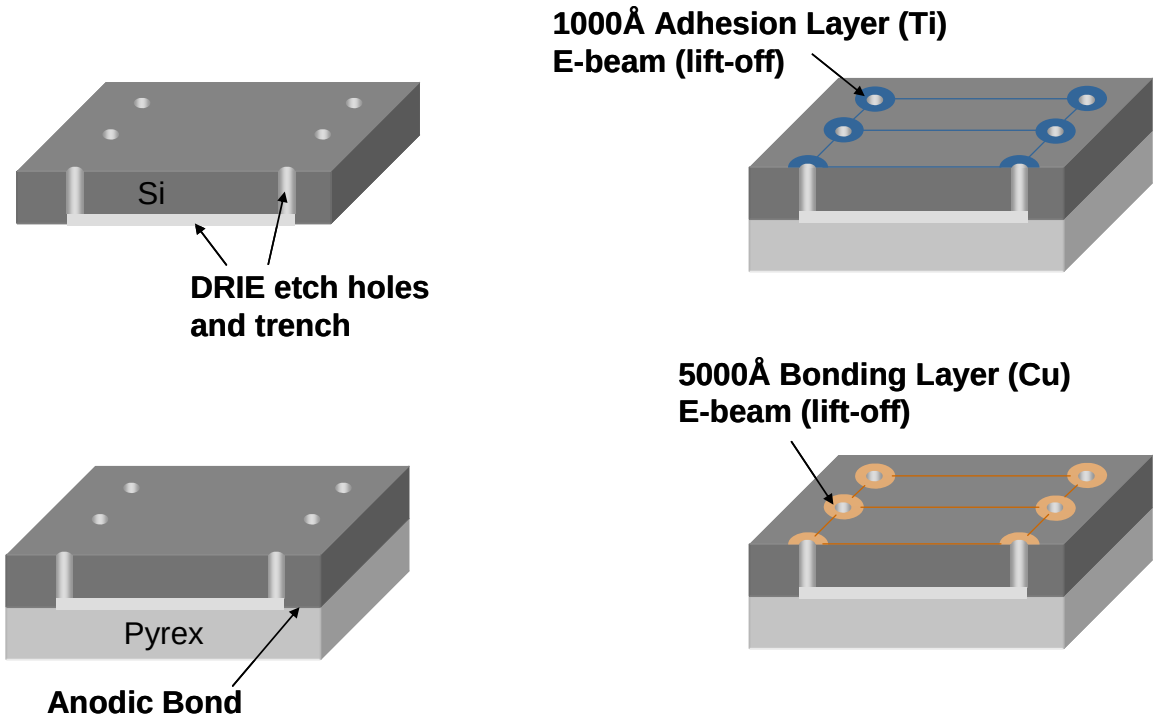

Figure 2-3: Test Device Fabrication Process

2.2.2 Test Device Chip-to-Tube Bonding

Tubing Preparation

The tubing for the test devices was 5cm lengths of 316 stainless steel tubing (Upchurch U-101 1/16" OD 0.02" ID or Upchurch U-115 1/16" OD 0.03" ID). This tubing was chosen for its high pressure and temperature tolerance as well as for its chemical compatibility. As shown in Figure 2-4a, each tube was preswaged with a 1/16" Swagelok® two-part ferrule. The ferrule is a combination of two Swagelok® parts. The conical portion is a 1/16" stainless steel front ferrule (Swagelok SS-103-1) and the flat portion at the end of the tube is a 1/16" brass back ferrule (Swagelok B-104-1). The ferrule parts were assembled over the tubing such that the flat, brass piece was positioned at the end of the tube. The use of a mixed metal ferrule assembly ensured that only the brass portion of the ferrule, nearest the device bond pad, would wet the solder. In this way, the solder was localized at the device surface, minimizing the amount of solder required for the bond. The ferrule was swaged onto the tube with a 1/16" bored-through union (Swagelok SS-100-6BT). The bored-through union was necessary as the fitting was designed to mate to a ferrule such that the conical portion pointed toward the end of the tube. After swaging, the union was removed and excess tubing was filed back to the surface of the brass ferrule. Once the tubing was prepared, 0.032" rosin-core SnPb solder wire (RadioShack® 64-009) was wrapped once around the ferrule to form a circular solder preform as shown in Figure 2-4b.

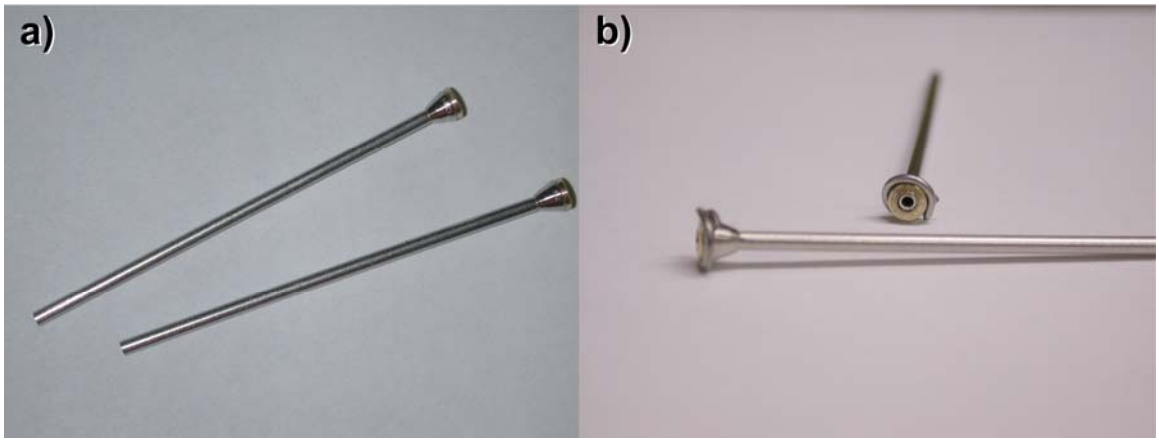

Figure 2-4: Stainless Steel Tubing Preparation
a) Pre-Swaged Ferrules b) Solder Preforms

Bonding Process

Prior to bonding, copper oxide was removed by wiping the pads with either a swab or tissue wetted with a 5%-10% acetic acid solution. The surface of the device was subsequently cleaned with acetone and ethanol. Two methods were used to bond the tubing to the test devices. For single connections, tubing could be connected manually by holding the tubing with swaged ferrule and solder perform against the device bond pad and heating the joint with a soldering iron. This method was simple and successful, but if the device was overheated, the copper bond pad adjacent to the joint being soldered could be oxidized. Therefore, for simultaneous bonding of both tubes, the device was placed on a hotplate (VWR Model 351) on top of a flat thermocouple (Omega® CO2-K) connected to a digital thermometer (Omega® HH21). As shown in Figure 2-5, the tubes were then positioned over the bond pads by clamps attached to ring stands. The hotplate was then activated and the temperature was raised to 200°C. Within 1 to 2 minutes after reaching 200°C the solder had completely reflowed around the ferrule. The hotplate was then turned off and the device was allowed to cool to 80°C before removal.

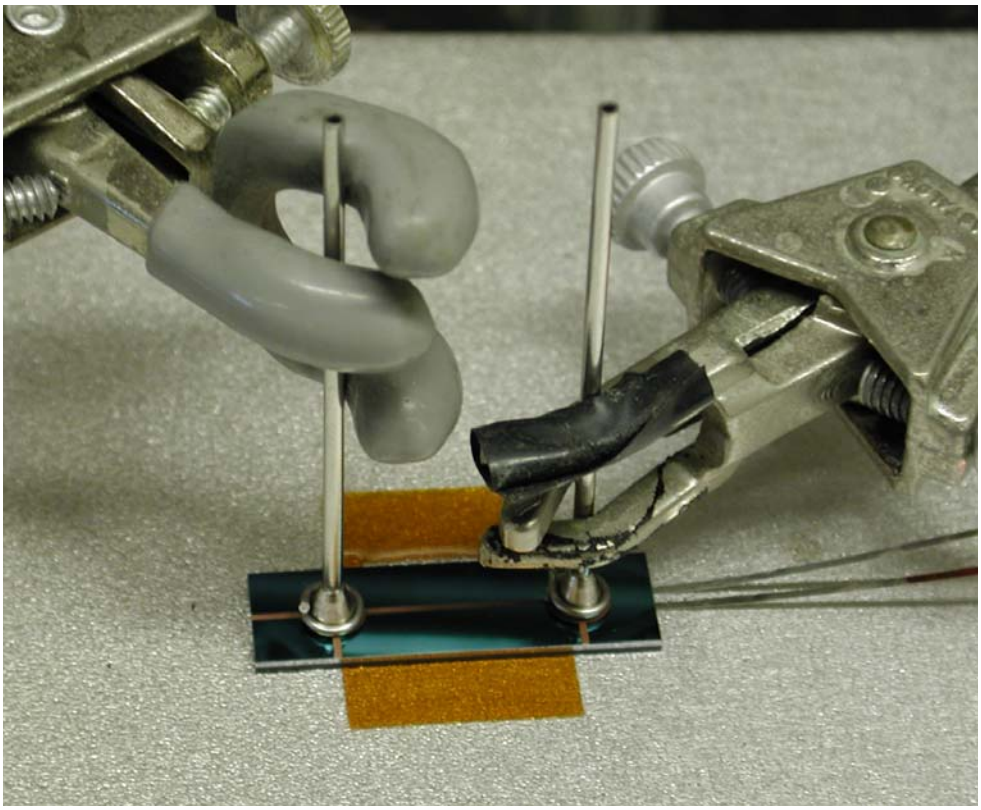

Figure 2-5: Hotplate Assembly for Solder Bonding

Bond Removal and Rebonding Procedure

Removal of the tubes from the device could be achieved via either the use of a soldering iron or reheating the device to 200°C on the hotplate. The removal of the solder bond was a more delicate process than the original attachment as the molten solder could reflow into the fluidic channel and plug the device. If too much solder had been applied in the initial bonding, or if the tubes were removed too quickly, the solder was found to either reflow into the fluidic channel or form a hemispherical dome capping the inlet port. When the tubes were removed slowly, the wetting characteristics of the solder led to the formation of a circular solder bead around the fluid port of the device to which additional tubing could be attached.

Reattachment was accomplished by positioning the tubing over the bead and heating the device either by soldering iron or on a hotplate. When the original tubing was removed, some of the solder remained on the brass ferrule. During rebonding, additional solder was added manually to compensate for this loss as well as to serve as a source of additional rosin flux to facilitate the reflow of the solder around the new bond. While copper devices could be rebonded 2 to 3 times, the brass ferrules on the tubing were found to be significantly less wetting upon reuse, possibly due to oxidation during the initial bonding process.

2.2.3 Test Device Chip-to-Chip Bonding

As an example of chip-to-chip bonding a fluid bridge was constructed. The fluid bridge, shown in Figure 2-6, was built on a base of four adjacent test devices diced from the device wafer. Onto this base, two tubes and another device diced from the same wafer were bonded. This device was positioned such that fluid introduced through the stainless steel tubes would travel through the channel in the base, enter the bridge and cross over a second channel before returning to the base and exiting from the second stainless steel tube.

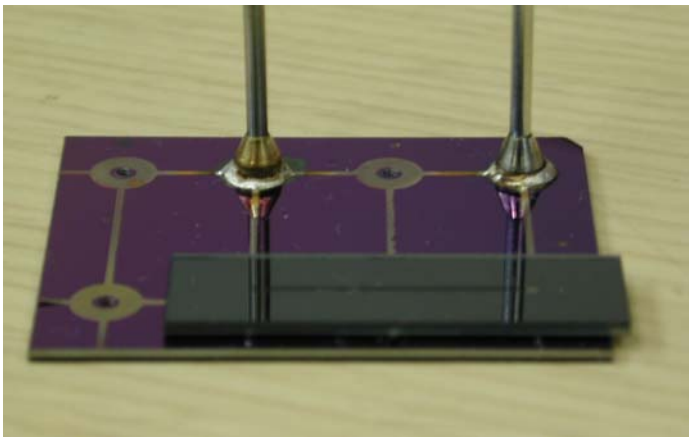

Figure 2-6: Fluid Bridge Formed by Chip-to-Chip Packaging

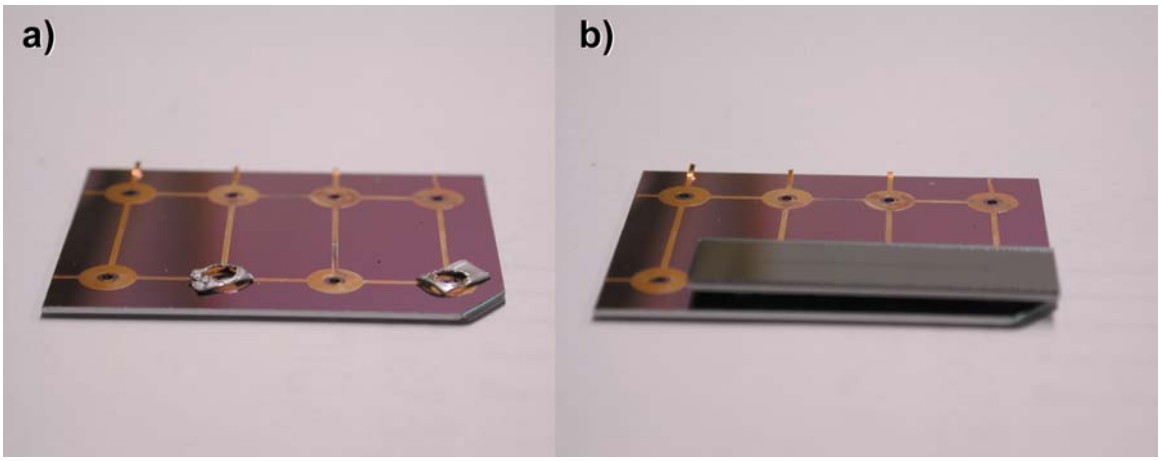

Figure 2-7: Fluid Bridge Assembly
a) Base with Solder Preforms b) Device Placement for Bonding

The assembly of this device required solder preforms that were flattened and shaped into squares with holes punched through the center using a 5/64" diameter leather punch. These preforms were placed over the solder bond pads on the base and the fluid bridge was positioned over them. The copper lines intended to serve as electroplating connections aided alignment as the through hole of the fluid bridge device could be positioned at the intersection of these perpendicular lines. The assembly is presented in Figure 2-7 with the placement of the prefoms and the fluid bridge device. Bonding was performed on a hotplate with the inlet and outlet tubes prepared and positioned as described in Section 2.2.2. As before, once the temperature was raised to 200°C, bonding of the tubes occurred within 1 to 2 minutes whereas bonding of the bridge device was

observed within 2 to 3 minutes. Again, the device was allowed to cool to 80°C before removal from the hotplate.

Once cool, a luer fitting (Upchurch P-628) connected by a Tefzel® nut and ferrule (Upchurch P-218 and P-200Nx) was attached directly to the inlet tube so that fluid could be delivered by syringe. The device was then rinsed with acetone to remove any residual rosin flux before performing a leak test with water. For the leak test, the device was filled with water and the outlet tube was capped with a Tefzel® cap (Upchurch P-755) connected to another Tefzel® nut and ferrule. No leaks were observed when the syringe was manually advanced through the fluid bridge against the capped tube.

Removal of the chip-to-chip bond was accomplished by the same techniques described for chip-to-tube bond removal. In this case however, heating the device on a hotplate was found to be much easier than reheating by soldering iron. Since the Pyrex® upper surface of the bonded chip was les conductive than the silicon bonding surface, the use of a soldering iron led to uneven heating during the bond removal process. Once heated to 200°C the device could be removed from the base using tweezers. Again, if the device was removed slowly, the solder would form a circular bead on the bond pads of both the base and the device that could be used for subsequent reattachment.

Reattachment of the same device could be accomplished by bringing the device in contact with the base and reheating to 200°C. Alignment of the device for rebonding was difficult as, after bond removal, both devices had rounded solder beads over the bond pads. Balancing the device over these rounded pads was difficult and best results were achieved when the device was held gently in place with tweezers during rebonding. To bond a new device to a previously used set of bond pads the additional solder required to complete the bond was applied to the fresh device by pre-tinning. This process required the application of a small amount of solder manually to each of the fresh bond pads. This had to be performed with a soldering iron as pre-tinning on the hotplate led to oxidation of the copper bond pads.

2.2.4 Bonding Process Improvements

Packaging tests were performed using devices fabricated and packaged as described in Sections 2.2.1 and 2.2.2. During the process of testing, additional fabrication

techniques and bonding materials were explored. Herein, alternate packaging methods and second generation improvements to the original bonding process have been outlined.

Alternate Fabrication Techniques

In the fabrication process outlined in Section 2.2.1, the metal bond pads were patterned using an acetone lift-off process. The lift-off process enabled the deposition of metal lines for compatibility with subsequent electroplating of thicker bond pads. Thicker pads were hoped to allow multiple attachment and reattachment at each solder joint. It was later found that thicker pads did not provide any noticeable improvement in this area. The cleanliness of the silicon surface prior to metallization was significantly more important than the layer thickness to the success of the bond. Insufficient development of the photoresist lift-off layer or inadequate cleaning after development caused organic residues to remain on the wafer surface greatly reducing the adhesion of the metal pads.

While careful processing provided good results using lift-off patterning, shadow mask processing eliminated the need for photolithography on the bonded wafer stack. Thus, where possible, shadow masks were was used to pattern the bond pads in subsequent designs. Shadow masks were fabricated either in silicon or in aluminum which were then aligned to the device wafer. Best results were obtained with shadow masks less than 1mm thick as corner shadowing on thicker shadow masks produced uneven metal deposition. The shadow mask was attached either by adhesive tape or by applying drops of AZ9260 photoresist to areas on the periphery of the device wafer and baking the stack at 90°C for 20 minutes.

In addition to the elimination of several processing steps, the use of a shadow mask allowed the wafers to be transferred to the deposition chamber directly from the anodic bonding step. This greatly increased the cleanliness of the deposition surface as the wafers had been cleaned in a piranha bath (hot 3:1 H_2SO_4, H_2O_2) immediately before bonding. One problem with shadow mask processing was the limitation on the metal layer design. Since the central portion of haloed structures, such as the doughnut shape used in the original test devices, would simply drop out during the shadow mask fabrication process, only filled shapes could be patterned. This caused all devices patterned by shadow mask to have a small amount of the bonding metal deposited at the

bottom of each of the fluid ports. In designs where haloed structures were required, or when electrical interconnects were simultaneously deposited, patterning was necessarily performed by lift-off.

A second alteration to the fabrication process was the addition of a thermal oxidation step before the anodic bond. By growing 2000Å to 5000Å of oxide on the silicon wafer, all of the surfaces in the fluid channels would be glass after sealing to the Pyrex® wafer with an anodic bond. This glass lined reactor had superior resistance to strong bases such as sodium hydroxide and sodium *tert*-butoxide.

Alternative Bond Materials

Copper was originally chosen as the bonding pad material as it was compatible with a wide range of organic solvents and the native oxide is easily removed with acetic acid prior to bonding. The copper pads are also well behaved when bonding to SnPb solder; however, these materials are incompatible with acids and fluorine gas. Additionally, for fabrication processes that required the deposition of the bond pads prior to anodic bonding, the conditions involved in the bonding process were found to oxidize the metal pattern.

To address these compatibility concerns, two additional bond pad materials were investigated. Gold pads, 5000Å thick on a 1000Å titanium adhesion layer, were the preferred choice to prevent oxidation during anodic bonding. Unfortunately, gold pads were only capable of a single bond. When the bonds were removed, only the titanium adhesion layer, with poor solder wetting characteristics, was observed to remain.

For a chemically resistant bond, capable of repeated bonding, nickel pads were found to be very useful, particularly in microfluidic devices for fluorination chemistry. The deposition of nickel required the use of chromium as an adhesion layer and the residual stress of the nickel-chromium stack exacerbated adhesion problems due to surface contamination. Successful bonds were formed with 2000Å nickel layers with a 100Å chromium adhesion layer. An indium solder (Indalloy 4 100%In, Indium Corporation of America®, Utica, NY) was used in this bond to demonstrate a bond with a less toxic and more fluorine compatible alternative to the lead based SnPb solder.

As an alternative to stainless steel, Teflon® tubing was tested in the solder interconnects. For this softer tubing, the ferrules were similarly swaged with a 1/16" Swagelok® bored-through union and excess tubing was trimmed back to the surface of the brass ferrule with a razor. Extra care was needed while swaging, for if the union was tightened beyond 1¼ turns past finger-tight, the soft tubing collapsed. Also, while the melting point of Teflon® is in excess of 300°C, the polymer was observed to soften at temperatures near 200°C. For this reason, Teflon® tube bonding was more successful when performed via soldering iron. When bonding was performed on a hotplate, the tubing deformed at the swaged ferrule causing leaks between the stainless steel top ferrule and the Teflon® tubing.

Bonding Process Improvements

Rosin-core solder purchased from Radio Shack® was highly successful in forming fluidic seals to tubing; however, when similar solder was purchased from other vendors, the rosin flux would often wick into the channels. This flux could be removed after bonding by either rinsing the device with acetone or, for devices with smaller channels, the bonded device could be immersed in a beaker of boiling acetone to loosen the clog.

In order to prevent excess flux from depositing into the fluid channels, the solder used for bonding was switched to a 0.03" diameter solder wire consisting of a solid 63%Sn 37%Pb alloy (Indalloy 106, Indium Corporation of America®, Utica, NY) and flux was applied manually. Best results were obtained when flux (5RA or 5RMA, Indium Corporation of America®, Utica, NY) was applied sparingly by lint-free swabs (VWR Critical Swab 10812-040) to both the bond pad and the brass ferrule. After the solder wire was formed into a ring, the preform was dipped into the flux and the excess was wiped off before placing the preform around the ferrule for bonding.

For chip-to-chip connections, a more precise application of 63%Sn 37%Pb solder was achieved by purchasing 0.001" thick square frame solder preforms 0.140" square with a 0.084" square cutout in the center from the Indium Corporation of America®. Flux was again applied manually to both bond pads. No flux was applied to the solder preform, as the preform is positioned between two fluxed surfaces and not exposed to the air during bonding.

2.3 Results

2.3.1 Joint Failure Tests

The pressure limits of the solder bond were tested by connecting the test devices to a nitrogen cylinder by stainless steel tubing and Swagelok® unions. Attaching the unions was done carefully as excess lateral force on the soldered tubes caused the device to break. It was noted that this point of failure in these cases was not at the bond, but within the silicon of the device. Once connected to the nitrogen cylinder, the device was submerged in a water bath behind a polycarbonate shield such that both the device and the unions connecting the device to the cylinder could be observed for leaks.

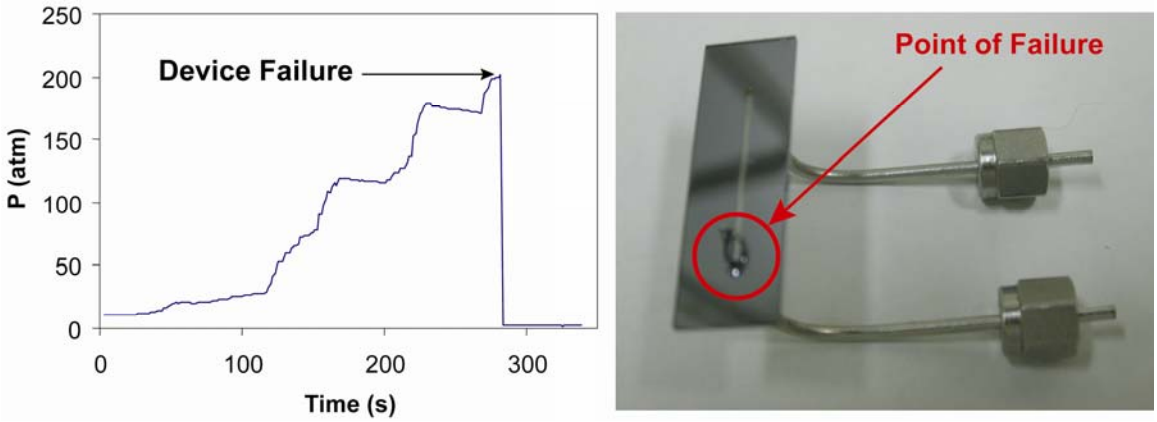

Figure 2-8: Pressure Test Results
Left) Pressure Trace Right) Observed Failure in Pyrex Wafer

On pressurization, some devices were observed to fail between 58.7 bar and 66.2 bar. Upon examination of the failed joint, delamination of the titanium adhesion layer was observed, suggesting organic contamination due to incomplete development of the lift-off pattern during fabrication. On other devices, no failure was observed up to 124.6 bar which was the maximum pressure possible with the regulator used. In order to determine the maximum pressure limit for these devices, the inlet of a test device was connected to an Eldex® high-pressure water pump and the outlet was connected to a dead-end tube. The pressure was monitored at the inlet with a pressure transducer connected to a LabView® enabled computer. Figure 2-8 shows the pressure data collected as water was pumped through the device to the dead-end tube. The pump was turned off at two points to monitor for leaks: 170-200seconds and 230-260seconds. The negative slope of the

pressure trace during these times suggests a leak, but no water was observed to leak from either of the solder joints during this process. Upon reaching a pressure of 200 bar, the device failed; however, as seen in the photograph of the failed device (Figure 2-8), this failure occurred in the Pyrex® wafer, indicating that, for a properly sealed device, the strength of the Pyrex® was limiting.

The chemical compatibility of these devices was tested by exposing both the interior and exterior of the joint to several organic and aqueous solutions. For the solvents tested (acetone, dichloromethane, dioxane, DMF, THF, and toluene) no degradation was observed. As expected, the fluidic connection disintegrated when exposed to concentrated acids. This disintegration was especially rapid in nitric acid and mixtures of sulfuric acid and hydrogen peroxide. While no visible signs of degradation were observed for several hours at sulfuric acid concentrations below 1.5M, atomic absorption tests of the effluent revealed copper, lead, and tin in the device effluent.

2.3.2 Near-Critical Emulsion View-Cell

The effect of acoustic emulsification of near critical carbon dioxide was under investigation as a method to enhance the rate of reactions including hydrolysis of benzoyl halides.[72] In order to separate mass transfer and kinetic effects, it was necessary to determine the droplet size of emulsions of both near-critical carbon dioxide in water and water in near-critical carbon dioxide. Due to the high-pressure capability of the solder joint, the test device used in joint failure tests was also useful as a sampling cell to examine high-pressure media. The Pyrex® wafer bonded to the fluid channels allowed visible microscopy of the samples collected such that the emulsions created in an external reactor could be transferred into the device for offline droplet characterization.

To reduce the strain on the device during repeated connections to the high-pressure emulsification reactor, the microdevice was connected to a stabilizing assembly. As shown in Figure 2-9, this assembly consisted of 5cm lengths of tubing anchored into an aluminum stabilizing block with epoxy. At each end, 1/16” Swagelok® unions were attached to allow connection to the soldered device on one end and the emulsification reactor on the other. To allow removal of the view-cell from the reactor without

depressurizing, both connections to the chuck were connected to valves that would be closed prior to removal.

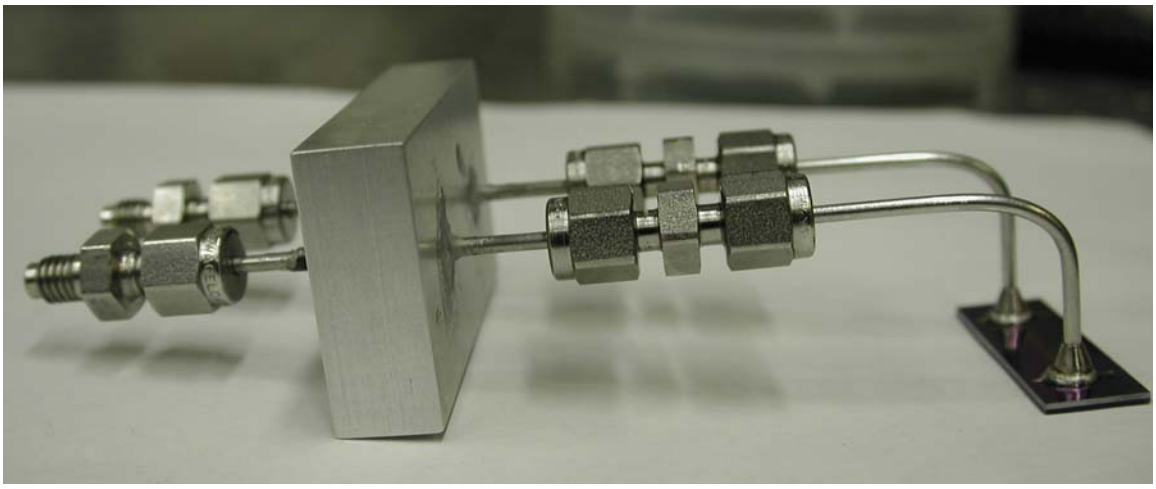

Figure 2-9: View-Cell Assembly and Tubing Connections

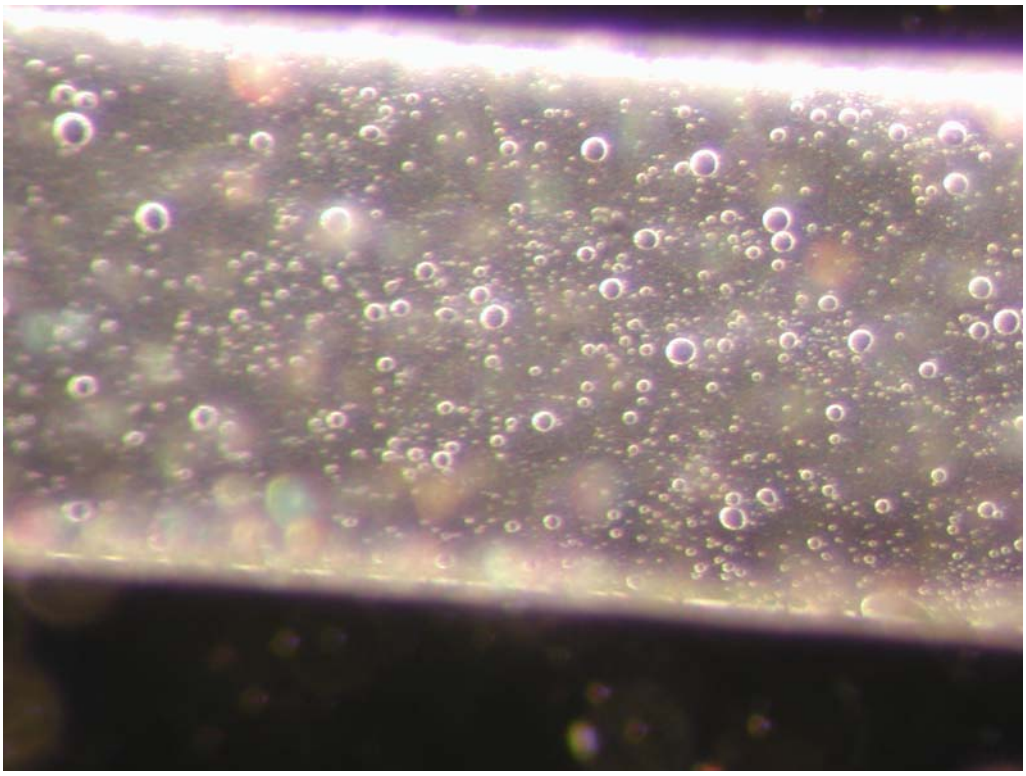

Figure 2-10: CO_2 Emulsion in Water at 80bar

Once connected to the reactor, the device was pressurized to 80 bar and maintained at that pressure overnight to ensure leak-free operation. Next, the emulsions to be tested were formed by sonication at 80 bar and 30°C before delivering the emulsion to the microdevice. The valves connecting the device to the system were then closed and the view-cell assembly was removed. Once removed, the device was placed onto a Zeiss Axiovert 200 optical microscope so that the contents of the channel could be imaged. Figure 2-10 is an image of an 80 bar emulsion of CO_2 in water. These images were then analyzed in the program ImageJ, available through NIH (http://rsb.info.nih.gov/ij/), to determine the droplet size distribution. The droplet size distribution was subsequently used to determine the specific interfacial areas for each emulsion. With this method, the interfacial areas were found to be 200 cm^{-1} for CO_2 in water and 600 cm^{-1} for water in CO_2.[73]

2.3.3 Microreactors & Integrated Microfluidic Devices

Individual Microreactors

In addition to the single channel test device previously described, the solder joint has been useful in the construction of several other microfluidic devices. Figure 2-11 shows a nickel coated device packaged with indium solder to brass ferrules swaged to stainless steel tubes. This packaging enabled the device to be used for hypofluorite chemistry at cryogenic conditions down to -30°C.[74]

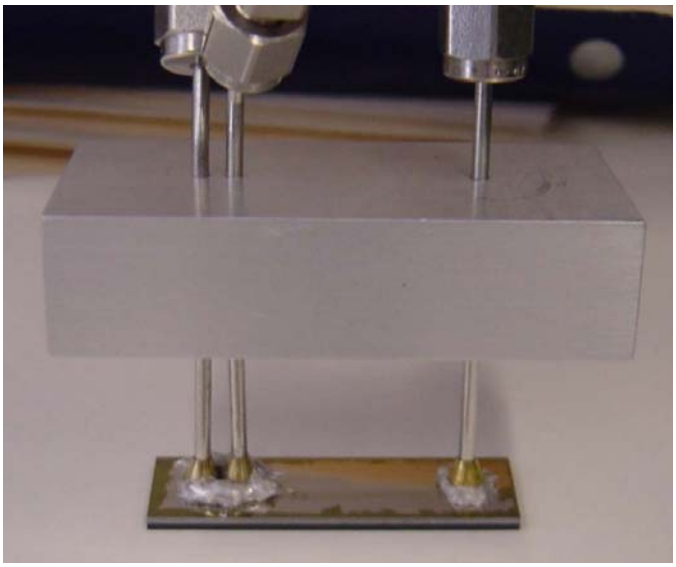

Figure 2-11: Nickel Coated Reactor for Cryogenic Hypofluorite Synthesis[74]

Solder packaging has also enabled the construction of a 5-port microreactor that is chemically compatible with strong organic solvents such as toluene and dichloromethane. These solvents had been incompatible with other packaging techniques, limiting the number of experiments that could be performed before the packaging failed. As described in Chapter 3 of this thesis, this packaging enabled oligosaccharide synthesis in dichloromethane and cryogenic conditions down to -78°C.[75] This packaging system also facilitated the exploration of the multi-phase reactions, discussed in Chapter 4 of this thesis, at temperatures up to 160°C and at pressures up to 14.8 bar. As the 183°C melting point of the SnPb solder was approached, softening of the solder was observed while operating at 14.8 bar. Operation at temperatures above 150°C was achieved with external reinforcement of the solder joint with epoxy (Loctite High Performance Epoxy 99393).

Figure 2-12: 5-port Silicon Microreactor with SnPb Solder Packaging
Photography by Felice Frankel

Integrated Microsystems

The solder packaging techniques developed for chip-to-chip bonding were also used in conjunction with the 5-port silicon microreactor. As shown in Figure 2-13, a UV-vis/NIR optical detector chip was connected via solder bonding to the outlet of the microreactor to enable on-line spectroscopy. Because these components could be fabricated separately, the fabrication of each component could be optimized independently. This was especially important for this pair of devices as the detector chip was fabricated by KOH wet etching to allow automatic alignment of the optical fibers to the device crystal planes. The reactor, on the other hand, consisted of serpentine channels that were most easily fabricated by DRIE processing. By separating the fabrication of these devices and bonding them afterward the fabrication for the integrated system was greatly simplified. Additionally, modular construction prevented the failure of one device from forcing the disposal of a possibly good reactor as only Known-Good devices were used for bonding.

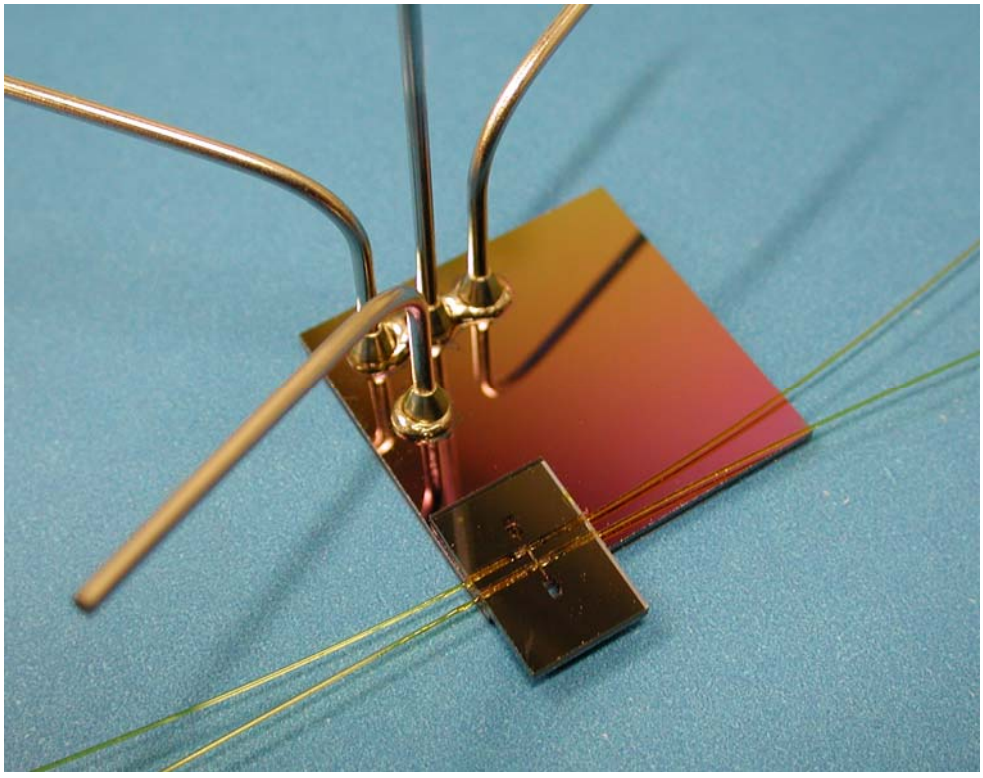

Figure 2-13: Chip-to-Chip Packaging, Reactor and Detector

A more advanced degree of integration is displayed in Figure 2-14. This board demonstrates the integration of three parallel reactor chains structured around the 5-port microreactor and on-line UV-vis/NIR detector chip shown in Figure 2-13. Each device was solder-bonded to the fluidic breadboard which provided connection between the reactors, detectors and 1/16" tubing. The flow through each inlet was also monitored by pressure drop measurements. Pressure drop channels were fabricated into the board and the pressure was monitored with Honeywell piezoresistive pressure sensors (26PC Series PK 80083) bonded to access holes drilled into the Pyrex® wafer.

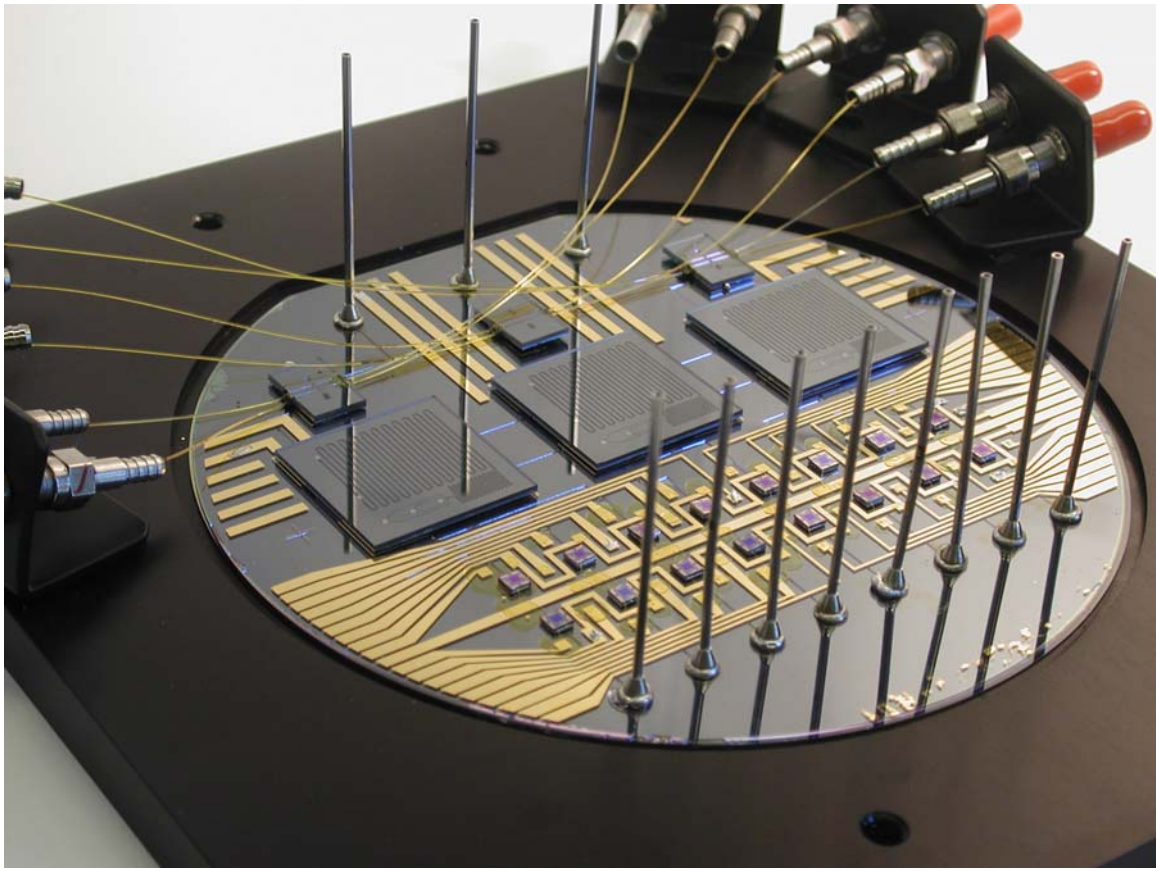

Figure 2-14: Integrated Microchemical System

In order to mount the pressure sensors, they were removed them from their original packaging and soaked for 24 hours in THF to remove polymer residues. The chips were subsequently cleaned in Nanostrip (Cyantek Corporation, Freemont, CA) and bond pads (1000Å Ti and 5000Å Cu) were deposited by e-beam evaporation. In order to provide a degree of thermal isolation for each of the reactor chains, the fluid ports and bond pad metallization were on a drilled Pyrex® wafer as opposed to the silicon wafer which

contained the fluid channels. Also, since electrical connections to the pressure sensors were also required, the electrical and fluidic connections were patterned on the same metal layer. Since this pattern could not be deposited using a shadow mask, the metal layer was patterned by lift-off. In order to use only Known-Good metal layers with adequate adhesion, the metal layer was patterned on the Pyrex® wafer before the anodic bond and, to accommodate this process, the metal layer was 1000Å Ti and 5000Å Au since only gold could survive the anodic bond and still produce viable bond pads.

Final assembly of this system was executed in four steps. First the reactors, detectors, and pressure sensors were bonded to the board on a hotplate using the 0.140" square frame solder preforms purchased from the Indium Corporation of America®. The stainless steel tubes could not be attached at this time as the second step was to wire bond the pressure sensors to the electrical interconnects. Third, the stainless steel tubes were attached by soldering iron with solder wire with manually applied flux. Finally, the optical connections were made to the detector chips with either Kapton® resin or high performance epoxy. After packaging, the board was tested for leaks and the electrical interconnects were connected to a separate LabView® system for calibration of the pressure sensors.

2.4 Conclusions

Solder-based packaging has been demonstrated to be a highly versatile alternative to existing microfluidic packaging techniques. This technique not only allowed the use of organic solvents, such as dichloromethane and toluene, that had been incompatible with previous epoxy and compression sealing techniques, but also proved robust over a wider range of conditions. Devices packaged with this method have been used at temperatures from -70°C to 160°C and at pressures up to 200 bar enabling the exploration of chemistries and conditions that had previously been impractical to pursue. Importantly, this packaging technique has also proven to be simple to execute. Intricate device packaging can easily be performed with standard laboratory equipment and chip-to-tube connections can be formed simply with a soldering iron and standard rosin-core solder wire.

Chapter 3

Oligosaccharide Synthesis[†]

As a demonstration of microreactors as a robust platform for rapid profiling of reaction conditions, the mannosylation of two different glycosyl acceptors were explored. The rapid optimization of oligosaccharide synthesis is of great interest due to the bottlenecks in the bench top synthesis of this diverse family of molecules. This chemistry is highly sensitive to both reaction and water contamination and has traditionally been carried out under argon, at cryogenic temperatures, and scrupulously dry conditions. The reagents used for these reactions are also particularly costly to produce and are rarely available in significant quantities for a full characterization of reaction conditions. Thus, it is desirable to minimize the amount of reagents used for optimization studies.

The low thermal mass and small volume of microreactors enabled a significant increase in the amount of data that could be collected from a single preparation of reagents. Additionally, the sealed microreactor system proved to be more resistant to water contamination than traditional synthesis methods since multiple reaction conditions could be explored without disconnecting any of the fluid lines. Up to 44 reaction conditions a day were explored consuming 2 milligrams of glycosyl donor per experiment, producing a reaction space profile which indicated the optimum conditions for the reaction.[75] Compared to traditional synthesis methods, this represents a 20 fold increase in the rate of data collection while halving the reagent consumption necessary to run the experiments.

[†] This chapter describes work done in close collaboration with Daniel M. Ratner who, at the time, was a doctoral student in the laboratory of Prof. Peter H. Seeberger in the Department of Chemistry at MIT.

3.1 Motivation

The synthesis of oligosaccharides is of great interest to chemists and biochemists alike. Oligosaccharides are involved in several biological processes including cell to cell communication, target recognition, and tissue organization.[76] In addition, the binding of oligosaccharides to proteins can dramatically alter protein stability, activity, and physical characteristics in solution.[77] Unfortunately, unlike proteins and nucleic acids, oligosaccharides are not produced in linear chains from a single information carrier. Oligosaccharides are instead produced by a large number of competing enzymatic reactions creating a large diversity of molecules. This diversity of reactions precludes the approaches used for the study of proteins through mutagenesis and instead requires a synthetic approach.

Although glycosylations have been carried out for more than a century, the union of glycosylating agent and nucleophile to form a glycosidic linkage is notoriously challenging.[78] The difficulty in this synthesis arises from the fact that the donors and acceptors contain similar functional groups and, in order to form the glycosidic linkage at only the desired site, the other functional groups must be protected.[79] Thus, even before performing the glycosylation, several synthetic steps are required to produce the saccharide building blocks for the reaction of interest and, after the saccharide molecules are linked, the protecting groups must be removed before continuing on to the next linkage. The overall yield of such a sequence of n synthetic steps, drops rapidly with increasing number of reactions according to Equation (3.1).

$$Y_{Overall} = \prod_{i=1}^{n} Y_i \tag{3.1}$$

The glycoside formation itself depends on the conformation, sterics, and electronics of both reaction partners. Challenges in accurately predicting the reactivity of the coupling partners make it difficult to foresee the outcome of the reaction. In addition, the role of reaction variables such as concentration, stoichiometry, temperature, reaction time, and activator must also be considered.[80] This complexity is shared by many other organic transformations in which multiple factors determine the outcome of the reaction. In both academic and industrial settings, much of the effort spent by synthetic organic chemists is consumed searching for optimal reaction conditions to achieve a particular

transformation. Method optimization frequently requires significant commitments of both time and large quantities of starting material.[81] In glycosylation, the value of these staring materials are assessed not only by the cost of the materials but also the time required to follow the long chain of protection and deprotection reactions. The ability to find ideal reaction conditions quickly and with minimal waste therefore has a major impact on the practice and pace of research and development in oligosaccharide synthesis.

3.2 Description of Oligosaccharide Synthesis

The reactions involved in the mannosylation reactions investigated in this study are represented in Figure 3-1. In this synthesis, the glycosyl donor is activated to form a carbocation intermediate. This intermediate is highly reactive and the synthesis must be carried out in scrupulously dry conditions to prevent the decomposition of the intermediate to the undesired lactol. Nucleophilic attack by the acceptor on the carbocation produces the desired product. One of the major side products of this reaction are orthoesters. This side product is frequently found in glycosylations involving a glycosyl donor with a C2 ester.[82] This ester is believed to cause the carbocation to undergo internal rearrangement causing the nucleophillic attack of the acceptor to form the othoester. This orthoester can be converted to the desired product under appropriately acidic conditions.

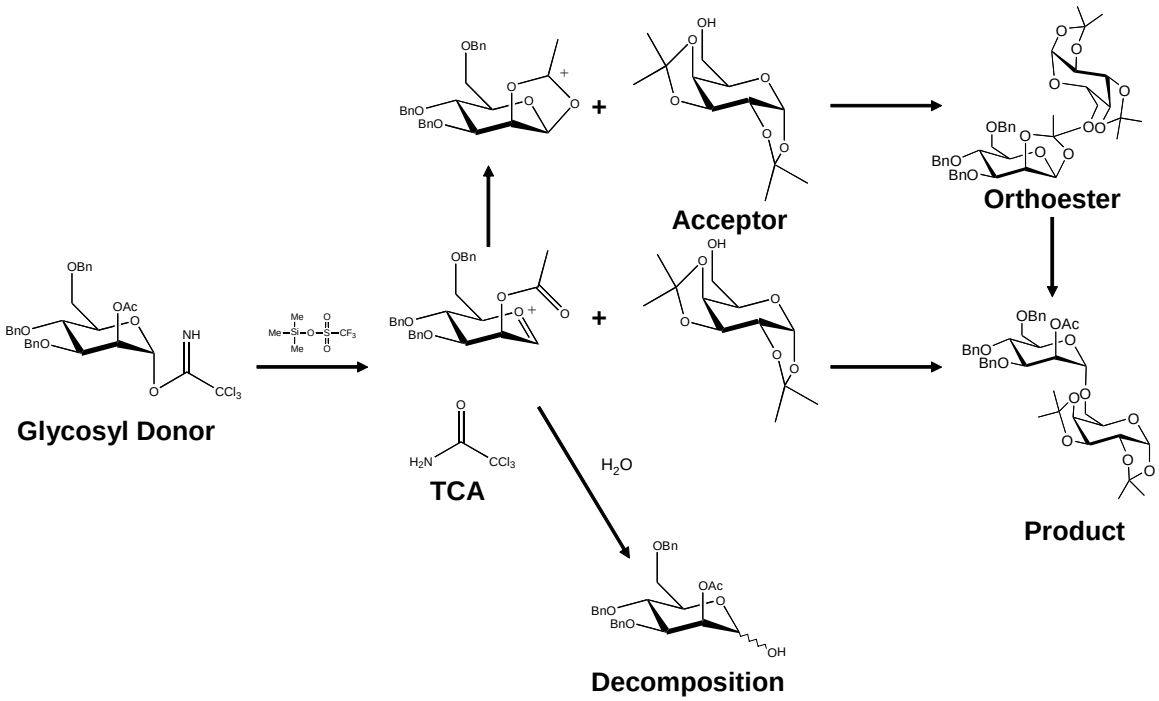

Figure 3-1: Oligosaccharide reaction pathways

Two reactions were examined in this study. The first reaction is presented in Scheme 3.1. In this reaction, the glycosyl donor mannosyl trichloroacetimidate **3-1** is activated by Trimethylsilyl trifluoromethanesulfonate (TMSOTf) and reacts with the glycosyl acceptor diisopropylidene galactose **3-2** to form the desired product **3-3** and orthoester **3-4**. The second reaction, presented in Scheme 3.2, reacts the same glycosyl donor with 2,3,4 tri-*O*-benzyl mannoside **3-5** to produce the disaccharide **3-6** and the orthoester **3-7**. This acceptor is more sterically hindered than **3-2** and was expected to cause the reaction to progress more slowly. The UV absorbing functional groups allowed 2,3,4 tri-*O*-benzyl mannoside **3-5** to be measured by HPLC analysis unlike **3-2**. The TMSOTf activator was quenched by a solution of 75vol% triethylamine in dichloromethane. The triethylamine quench solution also contained the HPLC internal standard methyl 2,3,4,6-tetra-*O*-benzyl-α-D-mannopyranoside **3-8**[83] (Figure 3-2). The standard was selected for high UV/Vis absorbance, and compatibility with the reacting species. The HPLC standard normalized the output stream for HPLC analysis by compensating for solvent evaporation and variability in the volume of collected sample.

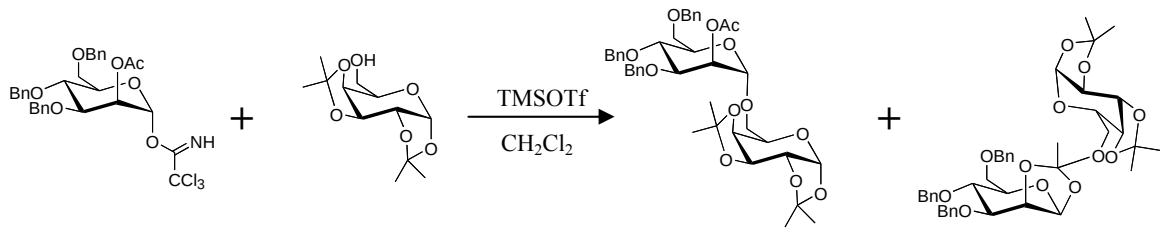

3-1 **3-2** **3-3** **3-4**

Scheme 3.1: Glycosylation of diisopropylidene galactose (3-2)

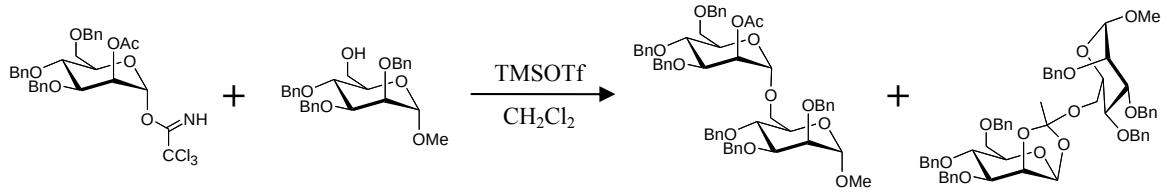

3-1 **3-5** **3-6** **3-7**

Scheme 3.2: Glycosylation of 2,3,4 tri-*O*-benzyl mannoside (3-5)

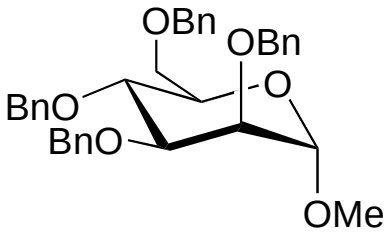

Figure 3-2: HPLC internal standard
methyl 2,3,4,6-tetra-*O*-benzyl-α-D-mannopyranoside (3-8)

3.3 Microchemical System Design

The primary challenges in developing a microsystem for oligosaccharide synthesis arise from the choice of solvents and reaction conditions. On the benchtop, this synthesis is typically performed in aggressive solvents such as dichloromethane and diethyl ether.[80] These solvents present challenges in traditional batch synthesis as the amount of reagent used in a synthesis is often limited by the difficulty in maintaining accurate

concentrations in small volumes of volatile solvents. This typically limits a chemist to running two batch reactions simultaneously as each reaction requires constant monitoring.[84] These solvents are also incompatible with both the gaskets and most epoxies used to seal microreactors to external tubing. The use of dichloromethane in particular also greatly limits the choice of system materials as this solvent will cause most polymers, including PEEK®, to swell. Furthermore, the microchemical system must tolerate reaction temperatures down to -78°C.

3.3.1 Reactor Design

The reactor used in this study was fabricated in silicon due to its compatibility with a wide range of chemical reagents, as well as its high thermal conductivity facilitating rapid thermal equilibration and temperature control.[30] The reactor was fabricated in silicon with copper bond pads according to the process outlined in Chapter 2 and fabrication details are provided in Appendix A. Microfluidic channels and flow ports were etched into a <100> double side polished silicon wafer using deep reactive ion etching. This wafer was subsequently oxidized and capped by a Pyrex® wafer via an anodic bond producing a microreactor with glass surfaces. All ports were directly connected by soldering 5 cm lengths of stainless steel tubing (1/16" OD, 0.02" ID) pre-swaged with brass ferrules to e-beam deposited copper bonding pads. This created an entirely metallic seal compatible with organic solvents such as CH_2Cl_2. The ductility of the solder in the joint also allows reliable seals at the reduced temperatures required despite the differences in the various material coefficients of thermal expansion.

In order to ensure adequate mixing and long residence times, the 5-port silicon microreactor, shown in Figure 3-3, is split into a mixing zone and reaction zone. The mixing zone has three primary inlets to mix the glycosylating agent, nucleophile (acceptor), and activator before entering the reaction zone. The reaction zone terminates at a secondary inlet from which a quenching agent is introduced to halt the reaction. The quenched reaction stream then exits the reactor for collection and analysis.

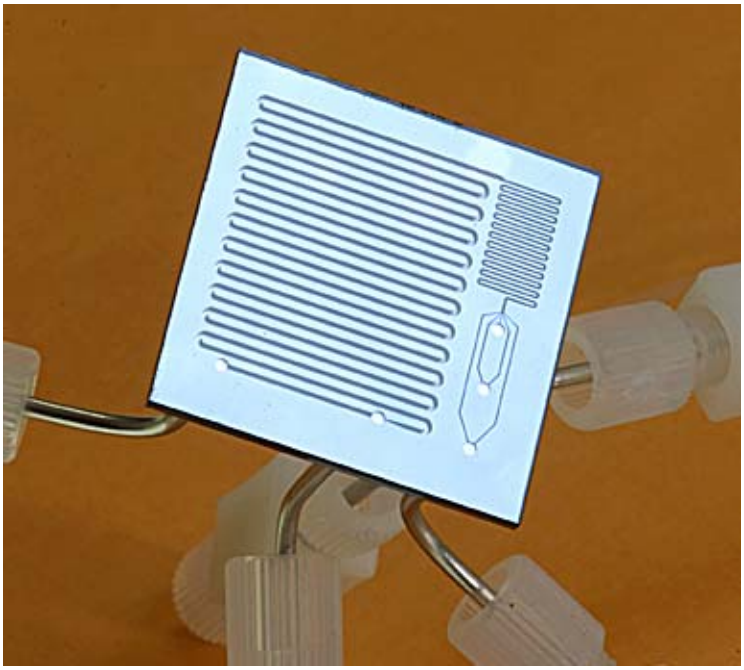

Figure 3-3: Packaged Microreactor
Photography by Felice Frankel

The mixing zone channel for this device is 200µm wide and 119 mm in length (Figure 3-4a). This channel was etched to a depth of 400µm giving a volume of 9.5 µL. For this synthesis, it was necessary to control the order of mixing. Once activated, the glycosyl donor could rapidly react with water to form undesired decomposition products. In order to maximize the possibility for desired product formation, the mixer was designed to split the first two inlet streams and stack them as shown in Figure 3-4b. This geometry ensures that the activator would diffuse through the acceptor lamina before reaching the donor lamina. The splitting of these streams also makes the concentration profile across the channel symmetric, reducing the diffusion width to half that of the channel. Since, the flow is laminar, each fluid stream forms a stable stream that mixes with the adjacent layers by diffusion. The time required to mix laminae can be estimated by $t = w/D$ where w is the width to diffuse and D is the diffusivity of the component of interest. For compounds with a diffusivity of $2 \cdot 10^{-9}$ m^2/s this results in a mixing time of 5 seconds. The maximum flow rate of for this mixer is thus 114 µL/min. At flow rates above this maximum, mixing continues in the reaction zone.

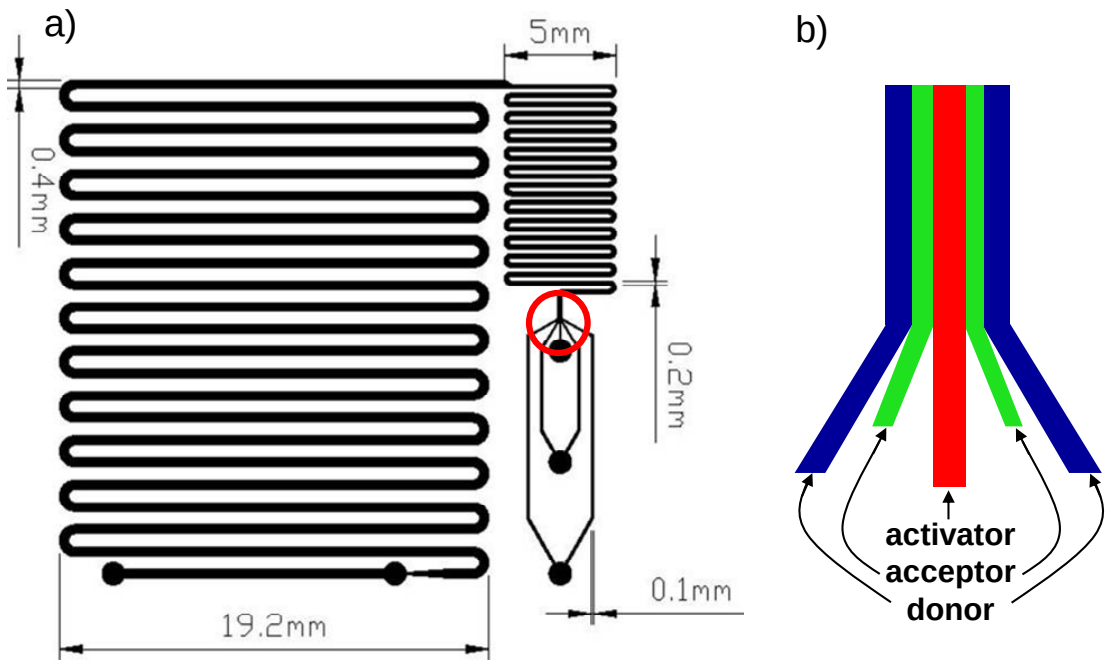

Figure 3-4: Microreactor Schematic
a) Reactor pattern with dimensions etched 400µm deep
b) Expansion of mixer inlet with anticipated lamina stacking

The reaction zone of this device is a 400µm wide channel 430 mm in length and is etched 400µm deep. This section has a much larger volume (68.8 µL of the 78.3 µL total) than the mixing zone and is intended to increase the residence time of the device. The reaction zone terminates at the secondary inlet where the quenching agent and HPLC internal standard is introduced.

3.3.2 Microsystem Setup

In order to rapidly scan reaction temperatures and residence times the microreactor was submerged in a temperature controlled bath and connected to a Harvard Apparatus PHD 2000 Infuse/Withdraw syringe pump as shown in Figure 3-5. To minimize contamination, Hamilton Gastight® syringes were used to introduce the reagents. The syringes used were fitted with 22 gauge removable needles with flat tips (point style 3). These needles allowed for the same syringe to be used for withdrawl of reagents from argon purged flasks and subsequent insertion into to Teflon®-lined stainless steel fill ports (Valco VISF-2). These fill ports were connected to 1/16 inch OD, 0.01 inch ID PFA

Teflon® tubing (Upchurch Scientific) via stainless steel unions (Valco ZU1) with Teflon® ferrules (Valco ZF1TF-10). These Teflon® inlet lines were connected to the solder bonded stainless steel tubes by Tefzel® unions (Upchurch P-630). Due to the incompatibility of the solvent with polyethylene syringe filters, reagent filtering was attempted with Teflon® syringe filters. However, the flexibility of the Teflon® coupled with the elevated pressure drop across the filter caused the assembly to expand under pressure. As an alternative, one of the ferrules in each of the Tefzel® unions was replaced by stainless steel frit ferrules (Upchurch P-272x) for in-line filtering.

Figure 3-5: Experimental Setup

In order to use a single syringe pump, relative flow rates of each component were controlled by varying the internal diameter of the syringe barrels. The syringes used were Hamilton Gastight models: 1001 (1mL, 4.608mm ID), 1002 (2.5mL, 7.285mm ID) and 1005 (5mL, 10.3mm ID). The flow rate of a given material stream is calculated according to Equation (3.2) where Q is the volumetric flow rate, r is the syringe internal radius, and $\dot{h}$ is the linear speed of the syringe plungers.

$$Q = \pi r^2 \dot{h} \tag{3.2}$$

As the plunger speed ($\dot{h}$) is the same for all of the syringes, it is possible to calculated the concentration of reagents within the reactor. The total flow rate through the reaction zone is given by Equation (3.3) and the total flow rate after the quench has been added is given by Equation (3.4) where r_i is the radius of syringe i (i.e. r_{p_1} is the radius of the syringe attached to primary flow port 1 and r_q is the radius of the syringe attached to the secondary, quench inlet).

$$Q_{react} = \pi\left(r_{p_1}^2 + r_{p_2}^2 + r_{p_3}^2\right)\dot{h} \tag{3.3}$$

$$Q_{total} = \pi\left(r_{p_1}^2 + r_{p_2}^2 + r_{p_3}^2 + r_q^2\right)\dot{h} \tag{3.4}$$

Thus the initial concentration of any component inside the reaction zone can be determined by:

$$C_{i,react} = C_{i,syringe}\frac{r_i^2}{r_{p_1}^2 + r_{p_2}^2 + r_{p_3}^2} \tag{3.5}$$

The use of an HPLC standard to normalize the data compensated for collection errors and solvent evaporation. This inert species was added to the quenching syringe. To calculate the outlet concentration of the inert species, the dilution due to the addition of the quench stream had to be included, thus the HPLC standard concentration was determined by:

$$C_{q,out} = C_{q,syringe}\frac{r_q^2}{r_{p_1}^2 + r_{p_2}^2 + r_{p_3}^2 + r_q^2} \tag{3.6}$$

3.4 Reaction Space Profiling and Optimization

3.4.1 Experimental Procedure

General Methods

All chemicals were reagent grade and used as supplied. Trimethylsilyl trifluoromethanesulfonate (TMSOTf) was purchased from Acros Chemicals. Dichloromethane (CH_2Cl_2) was distilled over fresh calcium hydride prior to use. All compounds were previously described in the literature. ^{13}C NMR was used to identify orthoester-containing mixtures by monitoring for peaks at ~120-125 ppm. ^{1}H NMR

spectra were obtained on a Bruker (400 MHz) or a Varian VXR-500 (500 MHz) and ^{13}C NMR spectra were obtained on a Bruker (100 MHz) or a Varian VXR-500 (125 MHz). HPLC standards were purified by chromatography over a Silicycle Inc. silica gel (230-400mesh) using forced flow of ethyl acetate and hexanes. Chromatography fractions were characterized by analytical thin-layer chromatography was performed on E. Merck silica gel 60 F_{254} plates (0.25 mm). Compounds were visualized by dipping the plates in a cerium sulfate-ammonium molybdate solution followed by heating. These fractions were then dried and the neat samples were diluted in dichloromethane to produce solutions used for HPLC peak identification. High-performance liquid chromatography was performed using a Waters Nova-pak© silica column (3.9 x 150 mm) with ethyl acetate and hexanes as the mobile phase, monitoring at 257.9 nm.

Reagent and Reactor preparation

Reagents were prepared by azeotroping the glycosylating agent and acceptor separately, and drying overnight on vacuum. Samples were diluted with freshly distilled dichloromethane to the desired concentrations: 0.04M for mannosyl donor **3-1**, 0.033 M for the nucleophile (acceptor) **3-2** or **3-5**, and 0.033M for the activator TMSOTf. The triethylamine quench contained 0.066M internal standard **3-8** and 25 vol% dichloromethane to prevent crystallization of the trichloroacetimidate byproduct at temperatures below -60°C. The glycosyl donor and nucleophile were each placed in separate 5.0mL Hamilton gas-tight syringes. A 2.5mL syringe was used for the quench/internal standard mixture, and a 1.0mL syringe was used for the TMSOTf activator. This produced reaction zone concentrations of 18mM for the glycosylating agent **3-1,** 15 mM for the acceptor **3-2** or **3-5**, and 3mM for the activator TMSOTf.

Prior to the introduction of reagents, the microchemical device was manually rinsed with 3mL of anhydrous dichloromethane. Immediately before priming the device with reagent, 500µL of 0.025M TMSOTf in CH_2Cl_2 were flushed through the activator port and throughout the device. This procedure ensured that the activator tubing line was fully primed and free from air bubbles, and simultaneously deactivated the surfaces of the microreactor by silylation.

The device priming had to be performed carefully as backflow of reagents through the inlet lines could cause premature activation of the donor. To prevent backflow, the syringes were loaded with reagents and placed on the syringe pump without connecting to the fill ports. The rear plate of the syringe pump was then brought forward to contact the syringe plungers. The syringe pump was subsequently run at 50-70 μL/min with a tissue held to the syringe needles until material was observed flowing from all syringes. At this point the syringes were connected to the fill ports and the device was primed with 400-500 μL of material until all bubbles were expelled from the reactor.

Sample Collection and Analysis

Once primed, the reactor was immersed in a stirred dewer containing acetone. The temperature of this bath was dropped to -78°C using dry ice. The temperature was monitored by an Omega HH21 digital thermometer with a K-type thermocouple and maintained manually by the addition of dry ice or room temperature acetone as needed. This technique enabled the bath temperature to be maintained to ±0.5°C. For data collected at 0°C the device was immersed in a stirred ice water bath and for temperatures above 0°C the water bath temperature was maintained by the addition of room temperature water or ice as needed. Again this bath was maintained to ±0.5°C.

The heat transfer coefficient for the stirred temperature bath was calculated by the correlation in (3.7) for impeller stirred tanks where h is the heat transfer coefficient, d_{tank} is the diameter of the stirred tank, L_P is the impeller diameter, N_r is the rotational speed of the impeller, and μ, ρ_f, k_f, and $C_{P,f}$ are the viscosity, density, thermal conductivity, and heat capacity of the surrounding fluid respectively.[85]

$$\frac{hd_{tank}}{k_f} = 0.87\left(\frac{L_P N_r \rho_f}{\mu}\right)^{0.62}\left(\frac{C_{P,f}\mu}{k_f}\right)^{1/3} \tag{3.7}$$

The heat transfer coefficients for the water and acetone baths were calculated to be 1456 W/m^{2}K and 596 W/m^{2}K respectively. From the parallel resistances to heat transfer through the Pyrex and silicon halves of the reactor, an average thermal conductivity for the reactor was found to be 83 W/mK. The thermal response of the silicon/Pyrex® microreactor was characterized by the Biot number given as:

$$Bi = \frac{hL}{k} \tag{3.8}$$

Using the device thickness L and the values of h and k calculated above gives Biot numbers of 0.02 for the water bath and 0.01 for the acetone bath. Since these Biot numbers are small, the lumped capacitance model can be used to determine the time required for the device to equilibrate to the bath temperature. From Equation (3.9), where A_s is the surface area of the device and ρ, V, and C_P are the density, volume and heat capacity of the device respectively, the time required for the device to equilibrate to 99% of the temperature difference between device and bath are calculated to be 1.6 s for the water bath and 3.9 s for the acetone bath.

$$\frac{T - T_\infty}{T_{initial} - T_\infty} = e^{-\frac{hA_s}{\rho V C_P}t} \tag{3.9}$$

Following equilibration of the temperature, the reagent flows were set to the desired reaction conditions and allowed to run until 220 µl of material were flushed through the device. Following the flush, 44 µl of material was collected for analysis, diluted with 20 µl hexanes. Thus each experiment consumes a combined 264 µl of material translating to 2mg of glycosyl donor per data point. The reaction temperature was varied from -78°C to 20°C, with glycosyl donor stream flow rates of 10, 20, 40 and 80 µl/ml, that resulted in reactor residence times of 27, 53, 107, and 214 seconds. After each sample was collected, the device was again flushed with 220 µl of material to ensure that no reactor contents from the previous sample remained in the reactor or outlet tubing to contaminate the following data point. After completing the runs at each temperature, flow was halted and the bath temperature was raised for the next set of conditions.

Collected samples were loaded into a Waters 717+ Autosampler and analyzed using a Waters Nova-pak© silica column (3.9 x 150 mm) with EtOAc/hexanes as the mobile phase driven by a Waters 1525 binary pump. The eluent was monitored on a Waters 2996 Photodiode Array Detector at 257.9 nm. Sample traces for Scheme 3.1 and Scheme 3.2 are shown in Figure 3-6 and Figure 3-7 respectively. For analysis of the products of Scheme 3.1, the mobile phase was ramped linearly from 5% ethyl acetate to 32.5% over 30 minutes. For samples from Scheme 3.2, the method ramped from 5% to 30% ethyl acetate over 10 minutes in a concave gradient (Waters Empower™ instrument method

curve #10). This concentration of ethyl acetate was held for an additional 25 minutes. The peak areas from these traces were then normalized to the area corresponding to the standard.

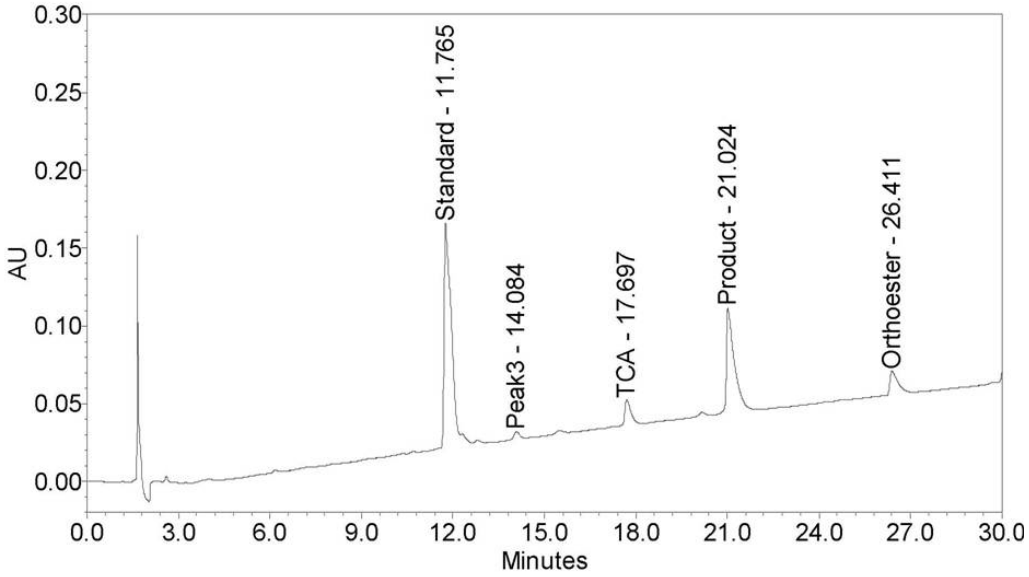

Figure 3-6: Sample HPLC trace for Scheme 3.1

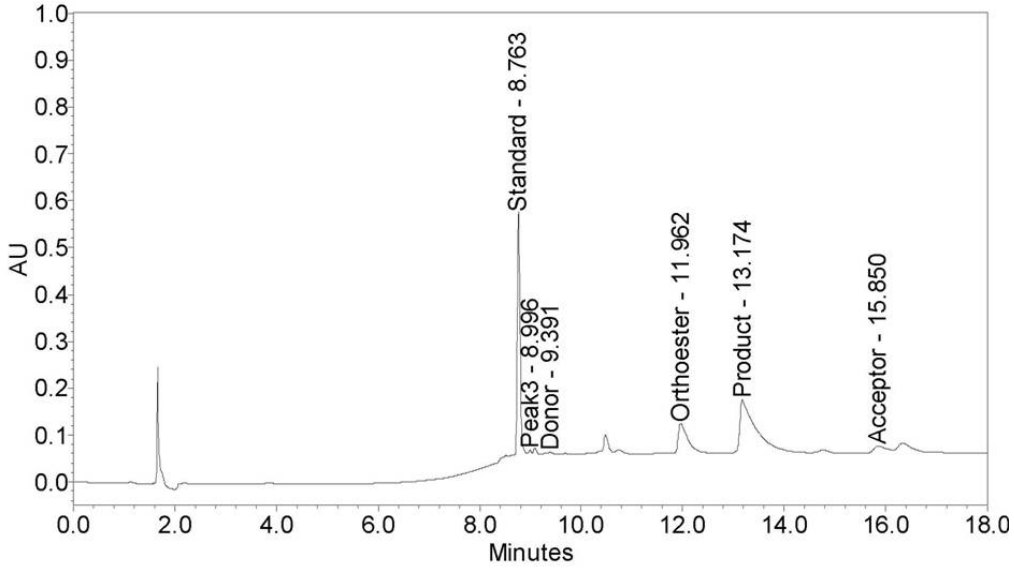

Figure 3-7: Sample HPLC trace for Scheme 3.2

3.4.2 Results

The first reaction explored was the mannosylation of diisopropylidene galactose **3-2** with 1.2 equivalents of mannosyl trichloroacetimidate **3-1** upon activation with 0.2 equivalents TMSOTf in anhydrous dichloromethane (Scheme 3.1). Figure 3-8a shows the data assembled from HPLC analysis of samples collected in a single afternoon from one preparation of reagents. These data, normalized by the internal standard, span the reaction space of operable conditions and show the effects of temperature and residence time. As expected, for a given reaction time, the yield of product increases with temperature until maximum conversion is achieved. Correspondingly, at temperatures lower than the optimum, yield increases with increasing reaction time (*i.e.* decreasing flow rate). Importantly, we were able to observe the formation of orthoester **3-4** as a major product at lower temperatures. The maximum production was observed at -70°C and a residence time of 53 seconds. It is notable that as both temperature and residence time increased, the reaction became more selective toward the primary product **3-3** suggesting that the orthoester **3-4** is an intermediate and not a side product under these conditions.

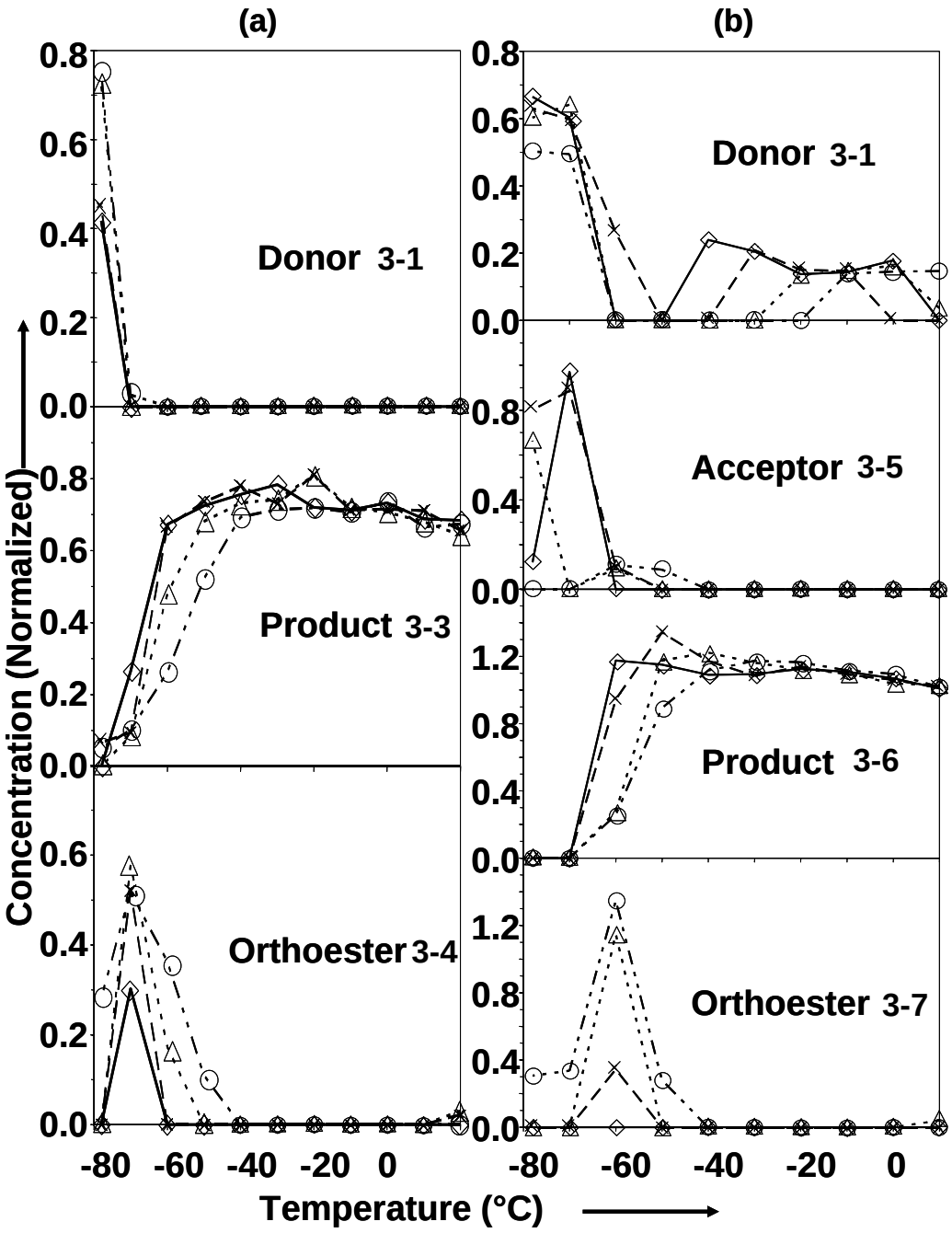

Figure 3-8: Gycosylation Reaction Space Data
a) Scheme 3.1 b) Scheme 3.2 Legend:◇214s, ×107s, △53s, O27s

Following the success with the initial glycosylation, 2,3,4-tri-*O*-benzyl-methyl mannoside **3-5** was mannosylated with **3-1** (Scheme 3.2). While this nucleophile is more sterically hindered, the additional phenyl rings allowed the acceptor to be analyzed on the HPLC traces. The reaction profile for Scheme 3.2 is presented in Figure 3-8b. Due

to the more complex reaction with the sterically hindered acceptor, the optimal operating window for this chemistry is much narrower than for Scheme 3.1. There is a maximum in desired product yield at -50°C and a residence time of 107 seconds. From this data the orthoester again appears to be an intermediate as the yield of **3-7** decreases with increased temperature and residence time from its optimum at -60°C and 27 seconds.

3.5 Conclusions

This study serves as an example of the increased versatility of the microreactor and illustrates the advantages of using a microreactor to scan reaction conditions. With a solder-based packaging scheme the microreactor can now be used with chemistries requiring aggressive solvents and cryogenic temperatures. With a microreactor capable of oligosaccharide synthesis, it was possible to reduce reagent consumption to 2mg of glycosyl donor per experiment. These savings are particularly advantageous for this chemistry, as the products of glycosylation are the reagents for the next glycosylation along the oligosaccharide synthesis. With less consumption, there is less fear of losing valuable material permitting the exploration of conditions that may have been considered unlikely to work in the past such as temperatures above -20°C. Additionally the use of the microreactor greatly accelerates the process of collecting data. The microreactor system serves to rapidly obtain comprehensive information about a given reaction. In a single afternoon, 44 reactions were completed over a wide range of temperatures and reaction times. This is a significant improvement over traditional glycosylation methods which are typically limited to two simultaneous reactions over the course of several hours.

With the reduced reagent consumption and increased speed of data collection, the microreactor system enabled a much more detailed study than would have previously been feasible. By expanding the breadth of reaction conditions and the ability to collect large amounts of data, new insights into these glycosylation reactions were found. Surprisingly, for both Scheme 3.1 and Scheme 3.2 no significant lactol decomposition products were observed, even at temperatures above -20°C, as had been observed in batch reactions. Operation within the sealed microreactor system allowed for multiple experiments without opening the fluid path to the atmosphere and levels of water and

oxygen contamination were expected to be significantly lower than found in traditional methods of argon purged flasks with rubber septa. This would suggest that the decomposition of the donor is more a function of the presence of these contaminants such as opposed to spontaneous thermal decomposition. Furthermore, the yield of desired product did not significantly degrade as the temperature increased. Even at 0°C similar conversions to those found at -40°C were observed. Thus, the microreactor makes it possible to run these reactions at much higher temperatures, and therefore much faster rates, than previously possible.

The success of this study raises the possibility that the microreactor could be used not only for reaction space analysis, but also small scale production. Therefore the microreactor system outlined here could be used for both rapid optimization of a glycosylation step and subsequent operation of the same reactor system at the optimum conditions to produce preparative amounts of reagent for the next reaction step. From the perspective of developing a method for semi-preparative or preparative scale, significant advantage can be found from the results of this continuous-flow study, over a much more cumbersome and costly batchwise optimization and synthesis.

Chapter 4

Palladium Catalyzed Syntheses[†]

In addition to accelerated data collection, reduced waste, and reduced contamination, microsystems enable the exploration of reaction conditions that are too hazardous or too difficult to attempt via traditional means. As an example of how microreactors can increase safety and expand the range of accessible reaction conditions, palladium catalyzed amide synthesis from aryl iodides and aryl bromides were profiled and optimized.

This synthesis was performed in the same reactor as that used for oligosaccharide synthesis, demonstrating that a single microreactor design can be adapted to multiple chemistries. Additionally, significant advantages were realized in performing these reactions in the microreactor. On the benchtop, this synthesis was limited to atmospheric pressure, and therefore by the atmospheric boiling points of the solvents. High-pressure experiments previously required the use of complex autoclaves or pressure vessels that made reaction monitoring and sampling difficult. The use of a solder-sealed microreactor enabled the manipulation of the higher reaction pressures and thus greatly increased the operating temperature range for this reaction in a simpler system that allowed rapid sample collection and analysis. By manipulating both the reaction pressure and temperature, the product ratio of single CO insertion amide and the more difficult dual CO insertion α-ketoamide have been profiled for multiple substrates.

[†] This chapter describes work done in close collaboration with Joseph R. Martinelli who, at the time, was a doctoral student in the laboratory of Prof. Stephen L. Buchwald in the Department of Chemistry at MIT.

4.1 Motivation

Palladium catalysts have been shown to be useful in the synthesis of carbon-nitrogen[86,87] and carbon-carbon bonds[88] from aryl halides as well as the synthesis of both esters and amides in the presence of carbon monoxide.[89,90] These reactions are of great interest both academically and industrially for the total synthesis of natural products and for the synthesis of pharmaceutically active compounds.[91-93] In addition, the optimization of these reactions depend on the synthesis of improved palladium ligands that can also be synthesized via these reactions.[94] Recent research into these reactions has focused on the moderation of reaction conditions through increased catalyst activity and the discovery of alternatives to hazardous and toxic intermediates such as organostannanes and cobalt carbonyl complexes.[95,96] Of particular interest to industry is the extension of palladium catalyst systems from the aryl iodides and aryl bromides, prevalent in academic research, to the more difficult aryl chlorides that are significantly more cost effective.[96,97]

One of the primary difficulties in optimizing palladium catalyzed syntheses is the fact that these reactions run very slowly for unactivated substrates and aryl chlorides. While increasing the temperature accelerates the reaction rates, the reaction temperature is limited by the boiling point of the solvent for these reactions, typically toluene (110.8°C) or tetrahydrofuran (65°C).[98] Also, for the Heck carbonylation reactions involving the formation of esters and amides with carbon monoxide, carbon monoxide pressures are limited by the common laboratory technique shown in Figure 4-1 where the reagent gas is introduced through a septum from a balloon attached to a syringe needle. This setup is undesirable not only because the reagent gas is limited to near atmospheric pressures and low mass transfer area but also because this delivery method involves several balloons of toxic gas in close proximity to needles and heat sources. Both of these limitations on reaction conditions are mitigated through closed systems capable of higher pressures; however, this has typically been attempted through the use of either Parr® bombs or autoclaves both of which are unwieldy to set up.[99] Additionally, maintaining the inert atmosphere required to prevent catalyst degradation requires that these systems must remain closed while the reaction is running. This complicates reaction control and requires elaborate sampling techniques for on-line composition monitoring.

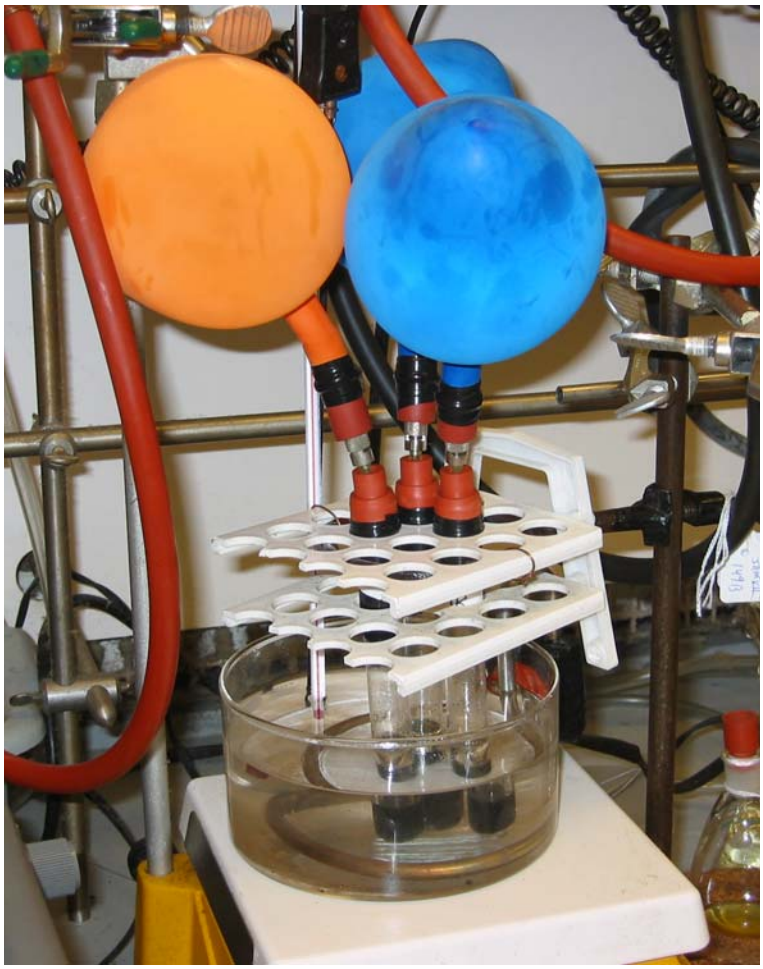

Figure 4-1: Typical Set of Batch Carbonylation Reactions

As described in Chapter 3, the use of microsystems greatly accelerated data collection enabling rapid profiling of the effects of reaction conditions on production rate. Furthermore, the enhanced heat transfer, reduced reaction volumes, and the ability to run several experiments within a sealed fluidic system (minimizing oxygen and water contamination) increased the quality of the data collected, enabling improved insight into the reaction mechanism. These advantages make the microreactor highly attractive for the investigation and optimization of palladium catalyzed syntheses. Another advantage of microsystems, specifically applicable to the multiphase esterification and amidation reactions, is the ten-fold to fifty-fold increase in multiphase mass transfer area over a conventional bench-top apparatus. With enhanced mass transfer as a motivation, carbonylation of two aryl iodides and bromopyridine was recently attempted in a glass microfluidic device; however, the short residence times, atmospheric pressures, and batch

extraction methods required for sample preparation resulted in poor yields and limited selectivity data.[100]

The solder-based packaging method outlined in Chapter 2 raised the possibility of performing high-pressure carbonylation reactions. Elevated pressures would not only increase the concentration of dissolved carbon monoxide, but also increase the range of operable temperatures as the boiling point of the reaction solvent increases according to Equation (4.1) where T_b is the boiling point in °C, P is the pressure in mmHg and A, B, and C are the Antoine constants for the solvent.[101] Additionally, the solder-based packaging method has been designed to directly interface to fluidic connectors used in high pressure liquid chromatography applications enabling the use of commercially available 6-way valves for convenient sampling of the reactor effluent during operation without disturbing the reaction conditions.

$$T_b = \frac{B}{A - \log_{10} P} - C \tag{4.1}$$

Carbonylation reactions have also been useful in the synthesis of carbon-11 labeled radiopharmaceuticals. [^{11}C]Carbon monoxide has been readily formed from the reduction of $^{11}CO_2$ in a zinc furnace at 400°C which, in turn, was formed via the $^{14}N(p,\alpha)^{11}C$ reaction in a cyclotron.[102] The incorporation of ^{11}CO into drug molecules has produced high specific radioactivity in the range of $1.5 \cdot 10^{11}$ to $6.4 \cdot 10^{11}$ Becquerels/μmol making these drugs particularly useful for non-invasive *in-vivo* studies in combination with positron emission tomography (PET).[103,104] Rapid optimization of these reactions, as well as acceleration of the reaction rate are of particular importance to this synthesis as the β^+-particle emitting ^{11}C has a half life of 20.3 minutes and much of the ^{11}C has decayed during the conversion of $^{11}CO_2$ to ^{11}CO.[105] In fact it has been estimated that, to be useful, the ^{11}C labeled drug must be synthesized, purified, and dissolved in a physiological vehicle within one hour from the initial radionuclide production.[106] So far, attempts at addressing the issues of poor mass transfer, low ^{11}CO concentrations, and slow reaction rates have focused on the use of autoclaves at elevated pressure and temperature which can be detrimental to the drug molecules.[107] The enhanced gas-liquid contact area within a microreactor as well as the possibility of synthesis at elevated pressures without the use

of an autoclave could provide a milder and more efficient platform for synthesis of ^{11}C-labeled compounds.

4.2 Description of Palladium Catalyzed Syntheses

The carbonylation reaction described in Scheme 4.1 was chosen as an example to demonstrate the microreactor benefits of increased pressure and enhanced mass transfer. In this reaction, the aryl halide and amine are mixed with palladium (II) acetate, ligand, and base under carbon monoxide. The aryl halide and carbon monoxide undergo oxidative addition to the palladium-ligand complex and the base deprotonates the amine. This deprotonated amine attacks the palladium complex, forming the final aryl amide. While running this reaction under high pressure, the production of a double CO insertion product, the aryl α-ketoamide, is also observed.

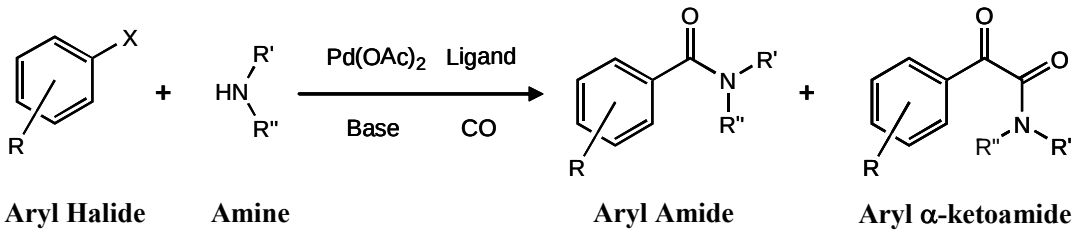

Aryl Halide **Amine** **Aryl Amide** **Aryl α-ketoamide**

Scheme 4.1: Palladium Catalyzed Aryl Halide Carbonylation

In addition to the carbonylation reaction, the palladium-ligand complex is also capable of catalyzing the amination of an aryl halide as shown in Scheme 4.2. As in the carbonylation, the aryl halide undergoes oxidative addition to the palladium-ligand complex and reacts with the amine that was deprotonated by the base. The mechanism for both the carbonylation and amination reactions, as they are currently understood, is presented in Figure 4-2.[108] The reagents used in this study are identified in Table 4.1. The desired products have been similarly listed in Table 4.2.

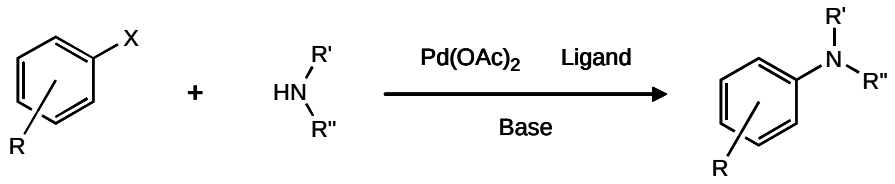

Aryl Halide **Amine** **Aryl Amine**

Scheme 4.2: Palladium Catalyzed Aryl Halide Amination

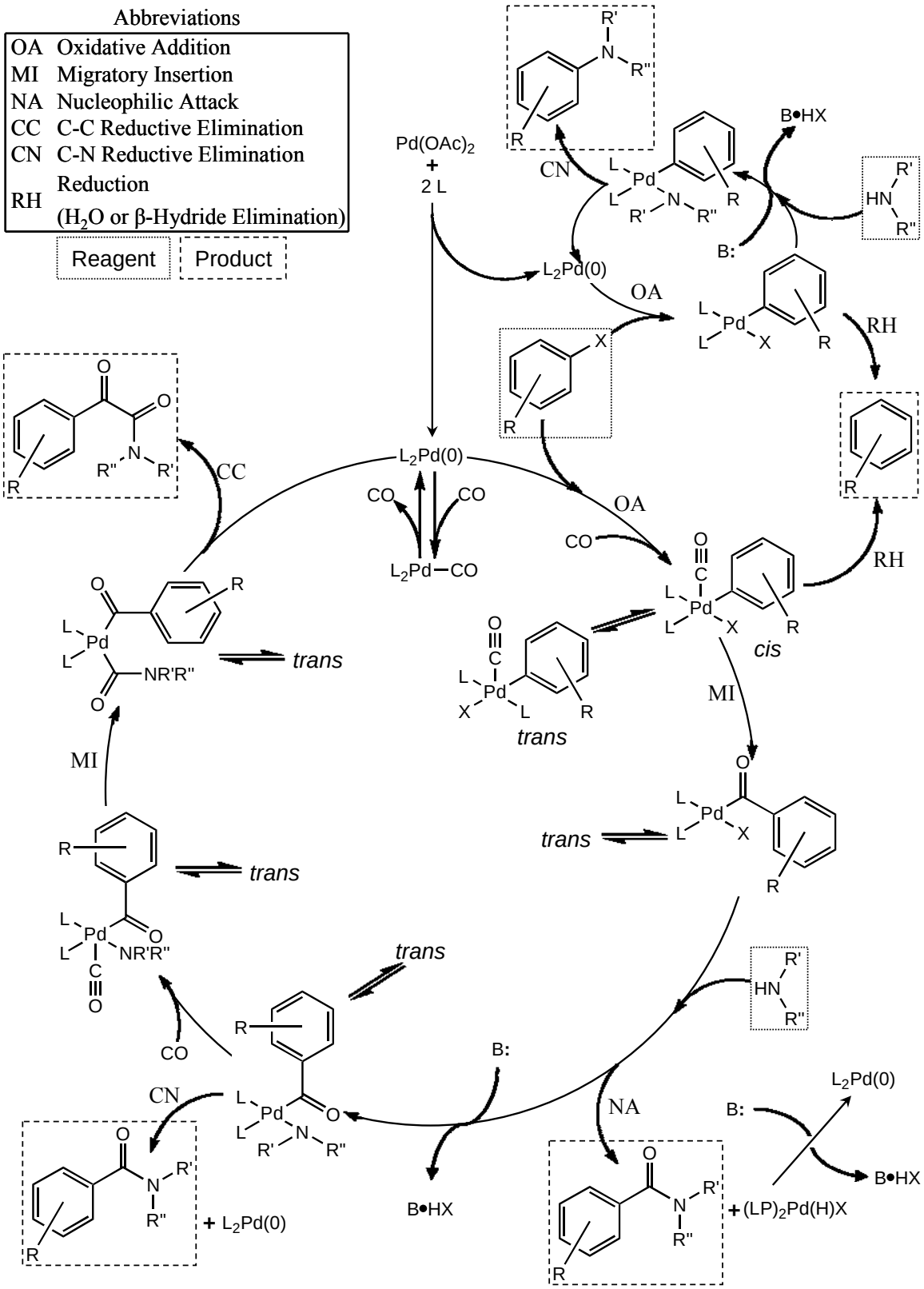

Figure 4-2: Possible Mechanism for Scheme 4.1 and Scheme 4.2[108]

Table 4.1: Palladium Catalyzed Carbonylation and Amination Reagents

Reagent Name	Role (Product)	Structure
Morpholine **4-1**	Amine (**4-8** through **4-13**)	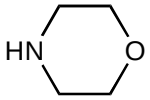
3-Iodoanisole **4-2**	Aryl Halide (**4-8**, **4-11**)	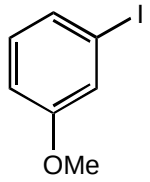
3-Bromoanisole **4-3**	Aryl Halide (**4-8**, **4-11**)	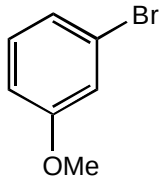
4-Bromoanisole **4-4**	Aryl Halide (**4-9**, **4-12**)	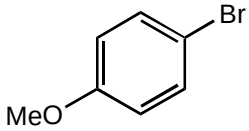
4-Bromobenzonitrile **4-5**	Aryl Halide (**4-10**, **4-13**)	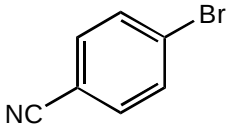
1,8-Diazabicyclo [5.4.0] undec-7-ene (*DBU*) **4-6**	Base (**4-8** through **4-13**)	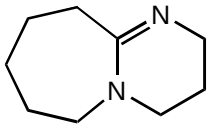
9,9 Dimethyl 4,5 bis (diphenyphosphino) xanthene (*Xantphos*) **4-7**	Ligand (**4-8** through **4-13**)	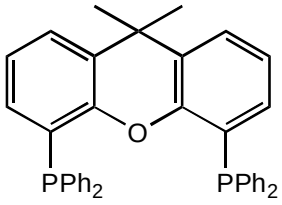

Table 4.2: Palladium Catalyzed Carbonylation and Amination Products

Product Name	Role (Reagents)	Structure
4-(3-Methoxybenzoyl)morpholine **4-8**	Amide (**4-2** or **4-3** with **4-1**, **4-6, 4-7**)	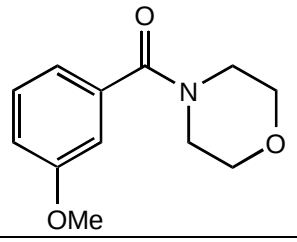
4-(4-Methoxybenzoyl)morpholine **4-9**	Amide (**4-1**, **4-4, 4-6**, **4-7**)	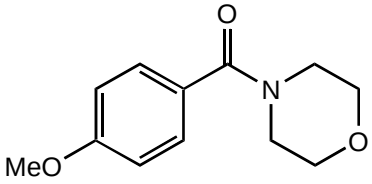
4-(4-Cyanobenzoyl)morpholine **4-10**	Amide (**4-1**, **4-5, 4-6**, **4-7**)	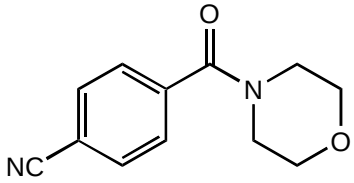
4-(Oxo-3-methoxybenzoyl)morpholine **4-11**	α-ketoamide (**4-2** or, **4-3** with **4-1**, **4-5, 4-6**, **4-7**)	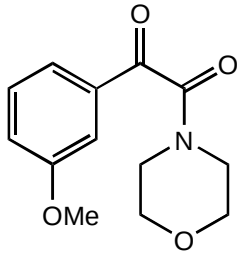
4-(Oxo-4-methoxybenzoyl)morpholine **4-12**	α-ketoamide (**4-1**, **4-4, 4-6**, **4-7**)	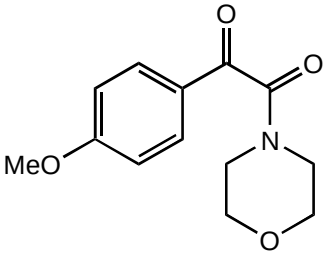
4-(Oxo-4-cyanobenzoyl)morpholine **4-13**	α-ketoamide (**4-1**, **4-5, 4-6**, **4-7**)	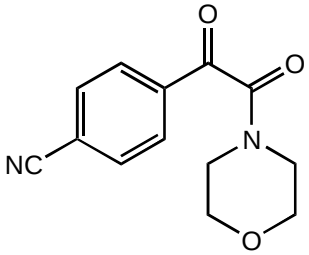

4.3 Microchemical System Design

The requirements for the reactor in this study are similar to those of the oligosaccharide synthesis study in Chapter 3. Both the solvent resistance of the solder-based packaging and the rapid thermal response of this basic design are well suited to the conditions required for the conditions required for this study. Additionally, the capability of the solder joint to withstand elevated pressures as demonstrated in Chapter 2 enables the use of a wider range of both pressure and solvent temperature.

The challenges encountered with this study were primarily in the design and implementation of the peripheral fluid handling and pressurization equipment. The fluid delivery method had to be capable of not only delivering liquid reagents at high pressure, but also controlling the flow of reagent gas. Since this was a multiphase system, the back pressure at the reactor outlet also had to be controlled. This control had to be precise to ensure both that the flow rate of reagent gas was stable and that the reaction partial pressure of reagent gas did not fluctuate during a run. Finally, a method for sample collection and dilution for analysis had to be devised that would not disturb the operation of the reactor.

4.3.1 Reactor Modifications

Initial studies on carbonylation used the microreactor designed for oligosaccharide synthesis as described in Chapter 3. It was known that during the course of the carbonylation reaction that several species could precipitate. The small dimensions of the reactor channels required that the generation of these particles be controlled and their potential to clog the reactor minimized. The solid byproducts that were of chief concern were the precipitation of palladium(0) metal (palladium black) and the formation of carbon monoxide/palladium complexes. Neither of these species was soluble in the reaction solvents, and it was anticipated that both of these species could be generated during the course of the reaction.

Another concern was that, despite the elevated temperatures and pressures of the microreactor environment, the required reaction time for the carbonylation reaction was significantly longer than those required for the oligosaccharide syntheses for which the

reactor was originally designed. This was further compounded by the higher flow rates of both gas and liquid required to maintain a steady slug flow. Thus, in order to accommodate the longer reaction times, a larger reactor volume was also needed. Table 4.3 compares the types of microreactors used in this study.

Table 4.3: Reactor Designs

Reactor Name	Mask Version	Reactor Volume	Notes
Original	Original	78μL	Used for the production of **4-8** and **4-11** from **4-1** and **4-2**
Extended	Original	400μL	Used for the production of **4-10** and **4-13** from **4-1** and **4-5**
Revised and Extended	Revised	400μL	Used for the production of **4-9** and **4-12** from **4-1** and **4-4**

Alternate mask design

Since the generation of particles could not be avoided, an alternate microreactor layout was designed and fabricated. In order to minimize the possibility of clogging the reactor, all flow restrictions were removed such that all feature sizes smaller than 100μm were opened to the size of channel that preceded them. In the original design (Figure 4-3a), flow contractions occurred at two locations: at the quench port flow focuser, where the flow channel narrowed from 400μm to 50μm to improve the mixing with the incoming quench stream; and at the mixer inlet where the inlet channels narrowed from 100μm to 50μm, again to enhance mixing. Since the carbonylation reactions were carried out at elevated temperatures and the mixing would be achieved by recirculation within liquid slugs, as opposed to laminar mixing, neither of these mixing structures was needed. Thus, for the revised design (Figure 4-3b), the reaction zone outlet was widened to 400μm and the mixer inlets were widened to 100μm.

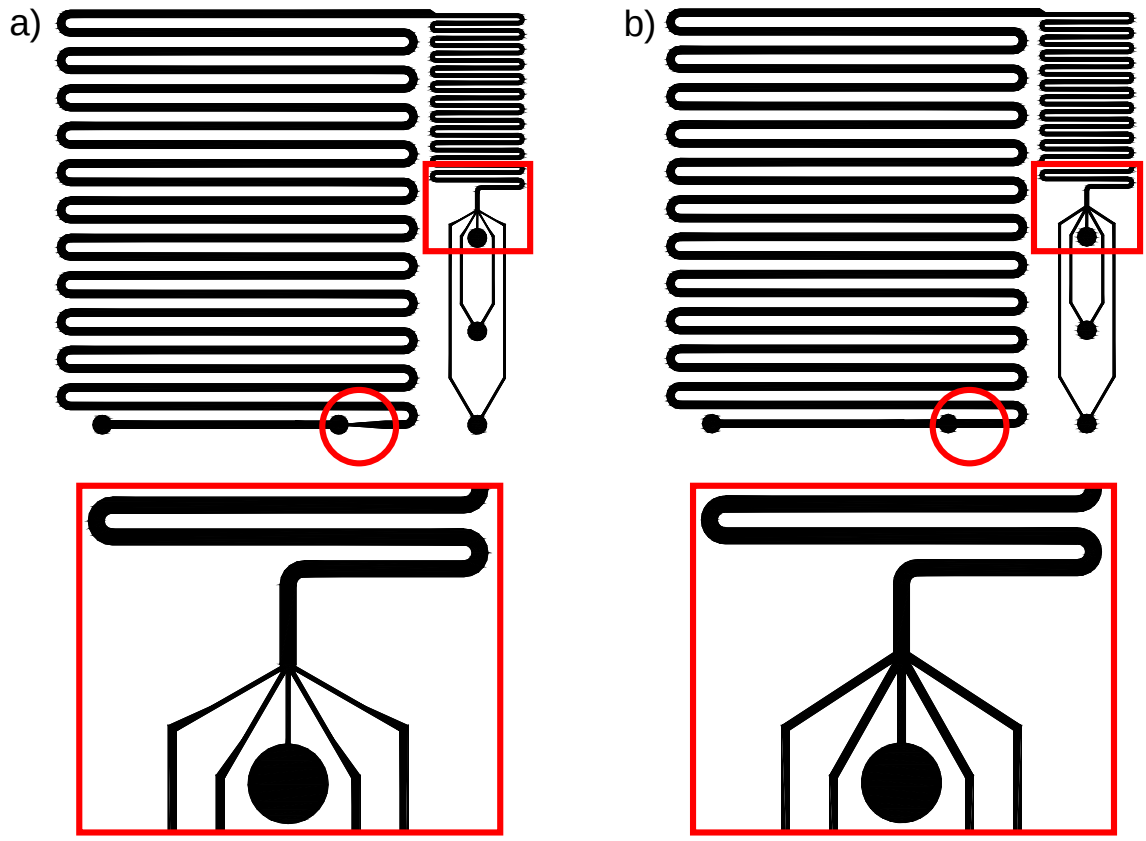

Figure 4-3: Microreactor Mask Revision for Particle Control
a)Original design b)Revised mask

Both the revisions to the reaction zone outlet and the mixer inlets were adjusted on the second mask of the fabrication process and did not require alterations to any processing steps. These revised reactors were fabricated and packaged using the same methods outlined in Appendix A and Chapter 2. Both the original design of the reactor and the revised design were used in this study. While palladium black precipitation was observed, the formation of precipitates within the reactor was found to be less of a concern than initially feared. The original design did clog if sufficient particulates accumulated in the system; however, the quantity of these side products was minimal and the precipitation was observed to occur primarily along the side walls and did not block the flow if the reactor was cleaned daily. This coating of palladium species was cleared from the reactor by rinsing the system with methanol. Occasional clogs from excessive buildup were cleared by either rinsing the reactor backwards with methanol or sonication.

Reactor volume extension

In order to extend reactor volume, a 30cm length of stainless steel tubing with a 0.046" internal diameter was connected to the quench port and the original reactor outlet was sealed. Thus the reagents were introduced through the 3 inlet mixer and exited through the quench port into the stainless steel tubing extension. The volume extension was connected to the reactor via the same solder bonding technique used for the other reactor tubes and described in Chapter 2. After cooling, the tubing extension was coiled such that both the silicon reactor and tubing could be submerged in a temperature controlled oil bath. The volume of the silicon microreactor from the mixer inlet to the quench port was 78μL and the additional tubing has a volume of 322μL, giving a total reactor volume of 400μL.

4.3.2 Reagent Delivery and Sample Collection

Reactor Secondary Packaging

While the reactor and tubing are capable of withstanding high pressures, the fittings used for the oligosaccharides study were composed of Teflon® and Tefzel® neither of which were rated for use at the carbonylation reaction conditions. In order to construct a more compatible connection to the device, an aluminum chuck was used to connect the directly soldered stainless steel tubes to inlet and outlet tubing. As shown in Figure 4-4 the microreactor is connected to the chuck by compressing a Tefzel® ferrule (Upchurch P-200Nx) around the stainless steel tubing between the two aluminum plates. This compression seals the tube to the chuck which has female 1/4"-28 threaded ports that can either be connected to tubing with a Delrin® nut (Upchurch P-301x) and Tefzel® ferrule or closed with a plug made either of Teflon® (Upchurch P-316) or Delrin (Upchurch P-309x). To ensure that these connections withstand the operating pressures, all fittings were tightened using a tightening tool (Upchurch P-299).

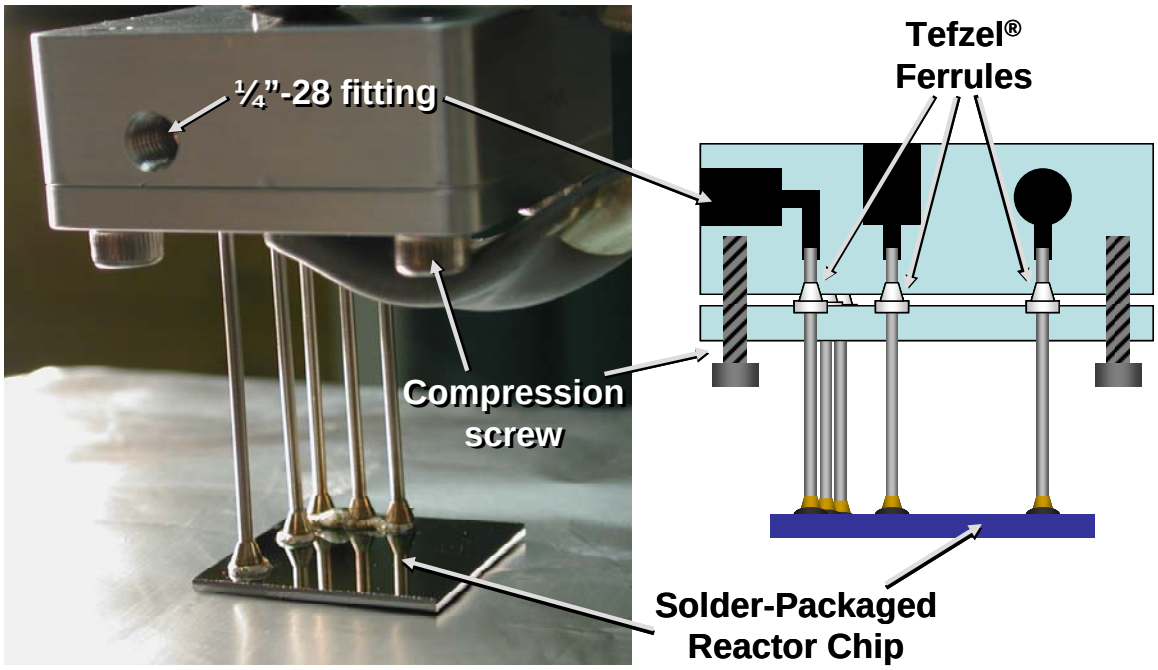

Figure 4-4: Reactor Compression Chuck

Relocating the inlet line connections to the chuck greatly reduced the force exerted on the device during sealing. Additionally, the tubes were often inserted into the chuck prior to solder bonding, such that the reactor joints would never be exposed to any force in excess of that due to thermal expansion. The fluidic connections on the chuck also made cleaning the device much simpler as the fluid lines could be easily removed and cleaned without risking damage to the device due to careless handling.

Use of the compression chuck greatly improved reactor handling and reduced breakage but an additional reinforcement was found to be necessary when operating the reactor at elevated temperatures. While the solder joints have proven to be quite robust to pressure at room temperature, the melting point of the 63%Sn 37%Pb solder used for this packaging was 183°C and the joint was observed to soften above 150°C. While no melting was observed during the course of this study, the solder joints would bulge and leak when exposed to pressures in excess of 8 bar when the temperature was above this softening point. It was found that by reinforcing the joints with epoxy (Loctite High Performance Epoxy 99393), the reactor could withstand temperatures up to 160°C at pressures of 14.8 bar.

Gas Delivery and Pressure Control

The construction of a system to control not only the flow rates of liquid and gas but also the reactor pressures required specialized equipment. While fluid delivery could be controlled by a Harvard Apparatus PHD 2000 Programmable syringe pump, the Hamilton glass syringes would not withstand the necessary pressures. Thus, liquid reagents were loaded into high pressure stainless steel syringes (Harvard Apparatus 702267). To ensure that the Viton® O-rings would not degrade due to the solvents used, the plunger tips were wrapped tightly in Teflon® thread seal tape (DuPont™) and coated with a thin layer of high vacuum grease (Dow Corning®). These syringes were connected to the reactor chuck with 1/16" OD, 0.009"ID stainless steel tubing.

In order to control the pressure in the reaction zone, the outlet of the reactor was connected to a pressure bomb. As shown in Figure 4-5 and Figure 4-6, the system pressure was controlled by three needle valves (Upchurch P-445). The cylinder outlet was split and each branch was connected to a needle valve. One branch was connected to the microreactor gas inlet and the second branch was connected to the bomb makeup inlet. In order to maintain sufficient pressure within the system, the cylinder regulator was set to a pressure 5% higher than the desired system pressure as measured by the pressure gauge on the bomb. Operating with an excess cylinder delivery pressure enabled both valves to be operated in a partially opened state, facilitating the control of the system. The third needle valve was connected to the bomb outlet tubing such that there was a controlled constant leak from the headspace of the pressure bomb. The leak was monitored by immersing the end of the Teflon® outlet tubing in 2mL of dichloromethane in a graduated cylinder.

Unless the bomb pressure fell below the desired operating pressure, the bomb inlet valve was fully closed during operation. The gas flow rate through the reactor was primarily controlled by adjusting the magnitude of the leak from the bomb. Increasing the leak slightly increased the overall pressure drop across the reactor and increased the flow rate, while closing the leak valve fully allowed the pressure to build up in the bomb, thus slowing the flow. When larger manipulation was required, coarse adjustments were made by adjusting the microreactor reactor gas inlet valve.

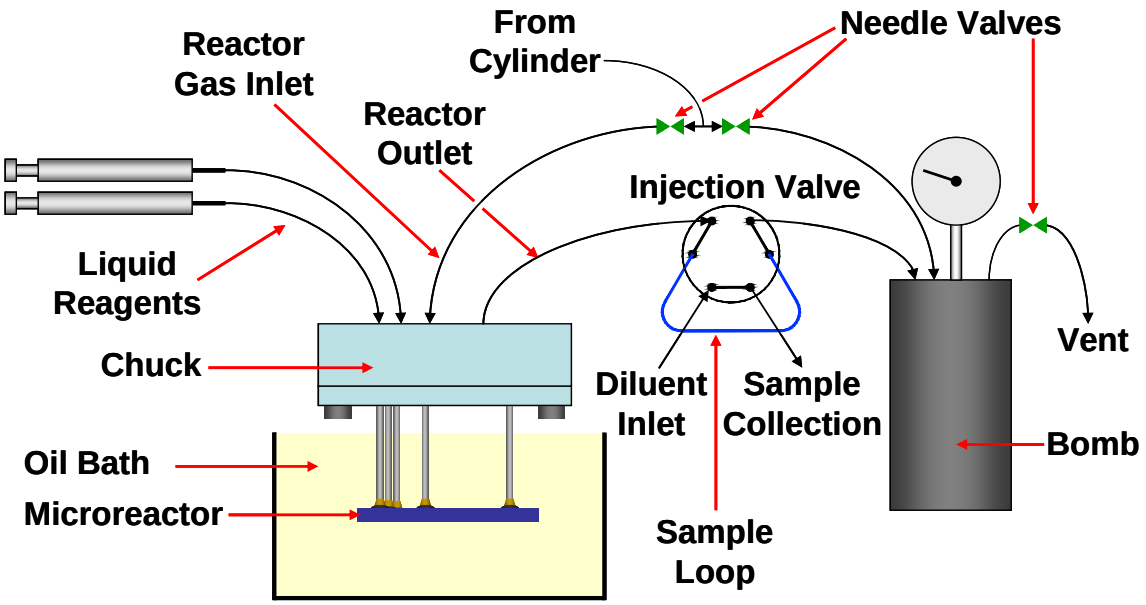

Figure 4-5: Schematic of High-Pressure Multiphase Microreactor System

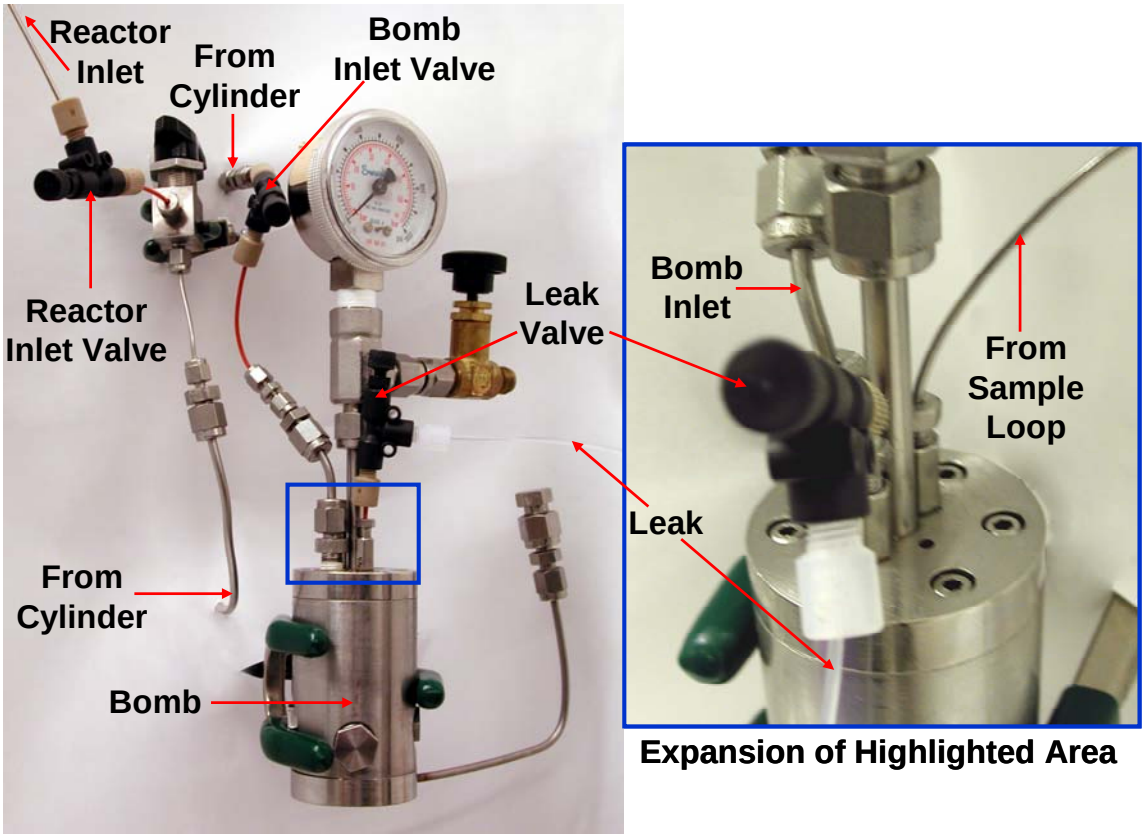

Figure 4-6: Pressure Control Apparatus
Pressure Bomb and Valves

Sample Collection Valve

To operate the system in slug flow large changes in the pressure drop across the system had to be avoided. In addition to destabilizing the slug flow, large fluctuations in pressure could force reagents backwards into the reactor gas inlet. In order to facilitate sampling of the system without interrupting the flow through the reactor, an HPLC injection valve (Upchurch V-451) was connected to the reactor outlet.

The injection valve was plumbed such that it operated in reverse of that on a standard HPLC system. This reverse plumbing was necessary, because samples were to be removed from a high pressure flow instead of the normal operation of injecting into a pressurized stream. Thus, when the valve was in the "Load" position (the position illustrated in Figure 4-5), flow from the reactor outlet proceeded through the sample loop before flowing into the pressure bomb. When the valve was turned to the "Inject" position, the reactor outlet flow bypassed the sample loop and proceeded directly into the bomb, the sample loop would then be connected to the diluent inlet and sample outlet ports.

Turning the valve to the "Inject" position immediately exposed the sample loop to atmospheric pressure, causing a rapid expansion of the gas slugs in the sample loop. To prevent back-flow into the diluent supply, a check valve (Upchurch CV-3301) was installed to the diluent inlet. Thus, upon decompression, the sample would flow into a collection vial, placed at the outlet of the injection valve.

The diluent was a 50 vol% mixture of dichloromethane and isopropanol. This choice of solvents was compatible with the sample and analysis method and the viscosity of this mixture approximated the apparent viscosity of the slug flow through the sample loop. By matching the viscosity, disturbances to the reactor flow were minimized when the injection valve was returned to the "Load" position to begin collection of the next sample.

Combinatorial Reagent Delivery

When collecting detailed data on conversion and selectivity for a single compound, the liquid reagents were loaded directly into the stainless steel syringes. For the latter part of this study, it was desirable to explore multiple compounds at similar reaction

conditions. To enable such a study, two additional injection valves were installed to the liquid reagent inlet lines. For combinatorial studies, the stainless steel syringes were loaded with filtered toluene as a carrier liquid and reagents were loaded into 1mL loops. This loading allowed reagents to be rapidly switched without depressurizing or disassembling the system. As an additional guard against cross-contamination, alternating tracer compounds (dodecane or pentadecane), which also served as internal chromatography standards, were added to the reagent mixtures. By monitoring for these tracers, it was possible to determine if there was any sample contamination from the previous reagent loading.

Syringe Driven Gas Delivery

The gas delivery for the synthesis of 4-(Oxo-3-methoxybenzoyl)morpholine **4-11** and 4-(3-methoxybenzoyl)morpholine **4-8** from 3-Iodoanisole **4-2** and morpholine **4-1**was accomplished by a third stainless steel syringe. This syringe was mounted into a second syringe pump (KD Scientific 200 series) so that the gas flow could be manipulated independently of the liquid flow. In this system, a 3-way valve (Swagelok SS-41XS1) was installed such that the syringe could be connected either to the reactor or directly to the cylinder, which was also connected to the bomb. During reactor charging, liquid flow was initiated and the 3-way valve was opened to the cylinder and both the syringe and pressure bomb were charged simultaneously. The cylinder outlet pressure was slowly raised by the regulator such that the syringe and bomb pressures remained equal. This technique also ensured that the liquid reagents were not aspirated through the reactor. Once pressurized to the desired operating pressure, flow from the gas syringe was initiated. The 3-way valve was then turned to connect the syringe to the reactor and the gas flow was controlled by the syringe pump.

The high reactivity of the 3-Iodoanisole **4-2**, meant that only short reaction times were necessary and the reaction was well behaved. Unfortunately, when exploring the carbonylation of aryl bromides, the increased reactor volume required and increased precipitation observed, coupled with the intrinsic pulsing of the syringe pump, precluded achieving stable gas flows via this delivery method. Additionally, when exploring pressures above 7.9 bar, the KD Scientific syringe pump would either stall or, more

disturbingly, the syringe advancing plate would release from the drive screw and snap to the rear of the syringe pump. Thus it was decided that the use of needle valves would enable a more reliable and, more importantly, safer mode of operation.

4.4 Selectivity Profiling and Optimization

4.4.1 Experimental Procedure

General Methods

All chemicals were reagent grade and used as supplied. 1,8-Diazabicyclo [5.4.0] undec-7-ene (DBU) 98% was purchased from Acros Organics (New Jersey). Pentadecane 99%, 4-Bromobenzonitrile 99%, and 3-Bromoanisole 98% were purchased from Sigma-Aldrich in St. Louis, MO. Morpholine 99% and 3-Iodoanisole 98% were purchased from Alfa-Aesar Lancaster in Pelham, New Jersey. 9,9-Dimethyl-4,5-bis (diphenyphosphino) xanthene 98% (Xantphos) was purchased from Strem Chemicals in Newburyport, Massachusetts. Palladium (II) acetate was obtained from the Engelhard Corporation in Iselin, New Jersey and n-dodecane 99% was purchased from Avocado Research Chemicals Ltd. in Heysham, Lancashire UK. Carbon monoxide cylinders were purchased from Airgas Inc in Radnor, PA. Toluene was purchased in CYCLE-TAINER® solvent delivery kegs from Malinckrodt Baker Inc. in Phillipsburg, New Jersey. Before use, the toluene was vigorously purged with argon for two hours. The toluene was further purified by passing it under argon pressure through two packed columns of neutral alumina.[109]

^{13}C and ^{1}H NMR was used to identify α-ketoamide compounds and to confirm the purity of compounds for gas chromatography standards. ^{1}H NMR spectra were obtained on a Varian (300 MHz) and ^{13}C NMR spectra were obtained on a Varian (75 MHz). GC standards were purified by chromatography over a Silicycle Inc. silica gel (230-400mesh) using forced flow of ethyl acetate and hexanes. Chromatography fractions were characterized by analytical thin-layer chromatography performed on E. Merck silica gel 60 F_{254} plates (0.25 mm) observed under a UV lamp.

Reagent Preparation

Liquid reagent mixtures were prepared under argon in oven-dried glassware. The first reagent mixture was 0.65M aryl halide, 1.30M base, and 0.65M internal standard dissolved in neat amine. The catalyst solution was 0.02M palladium(II) acetate and 0.02M ligand dissolved in neat toluene. Since the amine was used as the solvent for the aryl halide solution, the mixture had to be filtered before loading. Filtration was performed by syringe over glass wool inserted into the luer end of an 18 gauge needle. This filtered solution was transferred to a second dried flask under argon from which the mixture was drawn into the stainless steel syringe.

Reagent Loading and Reactor Pressurization

Once loaded, the syringes were placed into the syringe pump and the rear plate of the pump was advanced into contact with the syringe plungers. The syringe pump was then run at 500µL/min with a tissue held to the tip of the syringes until material was observed to flow from both syringes. At this point, the syringes were attached to the 1/16" stainless steel inlet tubing and the reactor was primed with 100µL to 150µL of material at a flow rate of 70µL/min. Next, the carbon monoxide cylinder was opened and the delivery pressure adjusted to the desired reactor pressure. The reactor gas inlet valve was opened slightly to allow gas flow into the reactor. The bomb inlet valve was then opened to allow pressurization of the bomb. The flow through the reactor was monitored and both the bomb and reactor inlet valves were adjusted to ensure that the reagent flow progressed forward during pressurization.

When the bomb reached the desired pressure, all needle valves were closed and the cylinder delivery pressure was raised an additional 5%. The liquid reagent flow rate was next set to the desired reaction conditions and the reactor gas inlet was partially opened to allow gas flow and begin slug flow equilibration. Additionally, the leak valve was slightly opened to allow the microsystem to come to steady state. During operation, these two valves were used to maintain the desired flow rate as observed in the reactor by measuring the speed of the slugs on a stopwatch (VWR Traceable® 4-Channel Alarm Timer). The bomb inlet valve remained fully closed unless the pressure in the bomb

dropped below the desired operating pressure, in which case the valve was opened to allow repressurization.

Sample Collection and Analysis

After a stable slug flow had been achieved, the temperature of the oil bath was raised. The temperature was controlled by a temperature controller with a K-type thermocouple and the actual bath temperature was measured by an alcohol thermometer. Once equilibrated to the desired operating point, the reactor was allowed to run until a full reactor volume had flowed through (78μL or 400μL combined flow). The sample loop was then flushed with diluent and set to the "Load" position to begin collecting a sample. Sample sizes were collected in a 322μL sample loop at liquid volumes between 100μL and 160μL as determined by the liquid flow rate from the syringe pump. Samples were collected by turning the sample valve to "Inject" and delivering 1.5mL of diluent through the sample loop into the collection vial, thus collecting properly diluted GC samples and rinsing the sample loop simultaneously. The valve was then returned to the "Load" position to collect the next sample. Multiple samples were collected at each set of reaction conditions before adjusting the temperature to the next data point. After the oil bath reached the next temperature, the reactor was again flushed with a reactor volume of slug flow before collecting the next set of samples.

The samples were analyzed by gas chromatography on an Agilent 6890 Series gas chromatograph with an FID detector. The samples were injected by an Agilent 7683 automatic liquid sampler, onto a 10 meter Agilent HP-1 capillary column (200μm I.D. 0.11μm film thickness) with a 1mL/min flow rate of nitrogen. The oven temperature was raised from 70°C to 240°C over 6.5 minutes. Sample peak areas were normalized to the peak area of the internal standard and multiplied by the response factor for the compound divided by the response factor for the internal standard to determine the sample concentrations.

4.4.2 Results

3-Iodoanisole 4-2 Carbonylation

The first carbonylation reaction explored was the synthesis of 4-(3-Methoxybenzoyl)morpholine **4-8** and 4-(Oxo-3-methoxybenzoyl)morpholine **4-11** from 3-Iodoanisole **4-2** and morpholine **4-1** catalyzed by Xantphos **4-7** ligated palladium with dodecane as the internal standard. The carbonylation was performed in the original reactor design and the carbon monoxide was delivered by syringe pump at 100 psig (7.9 bar). While there was some variability in the residence times due to the pulsation of the syringe pump delivering the gas, average reaction times could be calculated from the reactor volume (78μL) divided by the averaged volumetric flow rate observations. The reaction conversions obtained at each temperature are listed in Table 4.4 with the measured conversion of 3-Iodoanisole **4-2**.

Table 4.4: 3-Iodoanisole (4-2) Results at 7.9 bar (Averaged)

Measured Temperature	96°C	106°C	116°C	126°C	137°C	146°C
Average Reaction Times (min)	7.0	7.5	3.9	3.3	2.9	3.5
Measured Conversion	94%	95%	98%	100%	100%	100%

The measured yields of amide **4-8** and α-ketoamide **4-11** are shown in Figure 4-7. Yields were calculated according to Equation (4.2) and, since all the data was collected from samples with greater than 90% conversion, the data were not normalized for conversion.

$$Yield = \frac{[Product]_{outlet}}{[3\text{-}Iodoanisole]_{initial}} \tag{4.2}$$

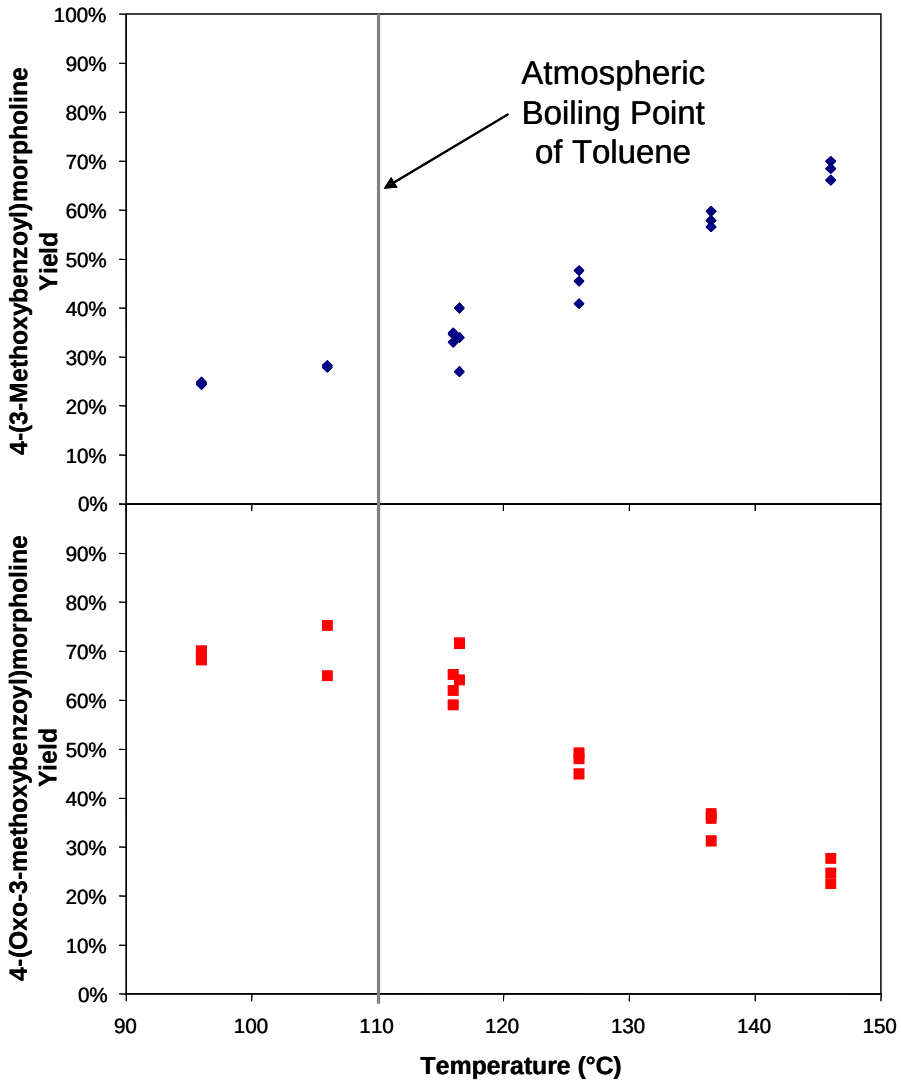

Figure 4-7: Yields for the Carbonylation of 3-Iodoanisole (4-2) at 7.9 bar CO

From the yield data it can be seen that, as temperature increases, more amide **4-8** is produced. The results presented in Figure 4-7 suggest that the production of α-ketoamide **4-11** and amide **4-8** are parallel reactions and that the rate limiting step for amide **4-8** formation has a higher activation energy than that for the formation of α-ketoamide **4-11**. This is consistent with the mechanism presented in Figure 4-2 since the nucleophilic attack of the amine is believed to be rate limiting in the mechanism. Thus, if the rate of nucleophilic attack increases, less of the single insertion intermediate will be able to undergo a secondary migratory insertion of carbon monoxide. It is also important to note that, at the temperatures possible with standard experimental techniques, very little effect on the product yields is observed.

4-Bromobenzonitrile Carbonylation

To demonstrate the flexibility of the microreactor to rapidly scan both pressure and temperature, the selectivity of the carbonylation of 4-Bromobenzonitrile **4-5** to 4-(Oxo-4-cyanobenzoyl)morpholine **4-13** was profiled. While the carbonylation of aryl bromides are more challenging than reactions involving aryl iodides, such as 3-Iodoanisole **4-2**, aryl bromide reactions are also more interesting due to the greater diversity of available substrates as well as the reduced cost of the compounds.[91] To accommodate the longer reaction times required for aryl bromide chemistry, as well as to allow greater stability in the reaction times, the selectivity study was performed in the original microreactor design with a reactor volume extension and carbon monoxide delivery was controlled via needle valves.

Reaction data was collected at temperatures between 98°C and 160°C and carbon monoxide pressures from 50 psig to 200psig (4.5 to 14.8 bar). For each sample, overall selectivity for the α-ketoamide **4-13** was calculated according to Equation (4.3) and plotted in Figure 4-8.

$$Selectivity = \frac{\left[\alpha\text{-}ketoamide\right]_{outlet}}{\left[Amide\right]_{outlet}} \tag{4.3}$$

From the selectivity data, the expected increase in amide **4-5** selectivity was again observed. Additionally as the pressure of carbon monoxide was increased, additional selectivity for the α-ketoamide **4-13** was observed. This shift in selectivity could be caused by the increase in dissolved carbon monoxide with increased pressure as shown by Equation (4.4) where x_{CO} is the mole fraction of carbon monoxide in solution, f_{CO}^{G} is the fugacity of the carbon monoxide gas, $f_{pure,CO}^{L}$ is the fugacity of the hypothetical liquid carbon monoxide at the solution conditions, and $\delta_{solvent}$ is the Flory-Huggins solubility parameter of the solvent.[110] Since $\delta_{solvent}$ was dependent on the concentration of carbon monoxide, Equation (4.4) was solved by iteration. The predicted dissolved carbon monoxide concentrations for the reaction conditions tested were plotted in Figure 4-9.

$$\frac{1}{x_{CO}} = \frac{f_{pure,CO}^{L}}{f_{CO}^{G}} \exp\left[\frac{32.1\dfrac{cm^3}{mol}}{RT}\left(\delta_{solvent} - 6.4\frac{J^{1/2}}{cm^{3/2}}\right)\right] \tag{4.4}$$

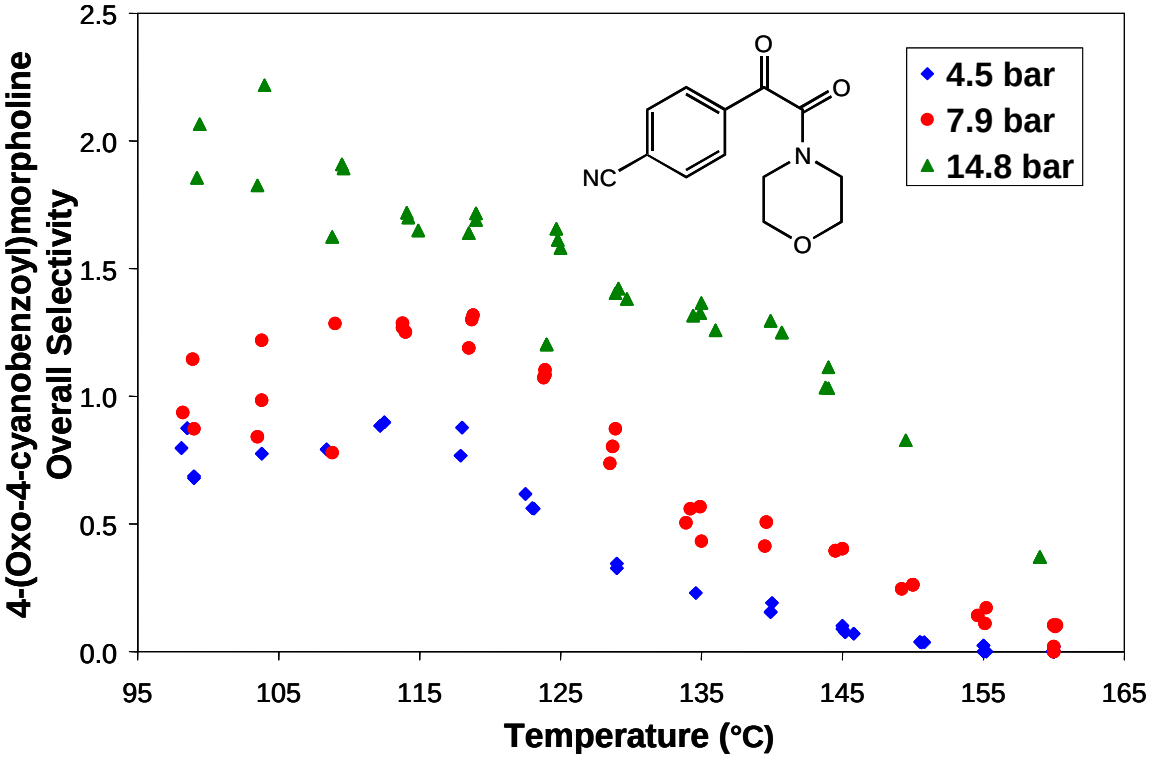

Figure 4-8: Selectivity profile of 4-(Oxo-4-cyanobenzoyl)morpholine (4-13) Temperature and pressure dependence

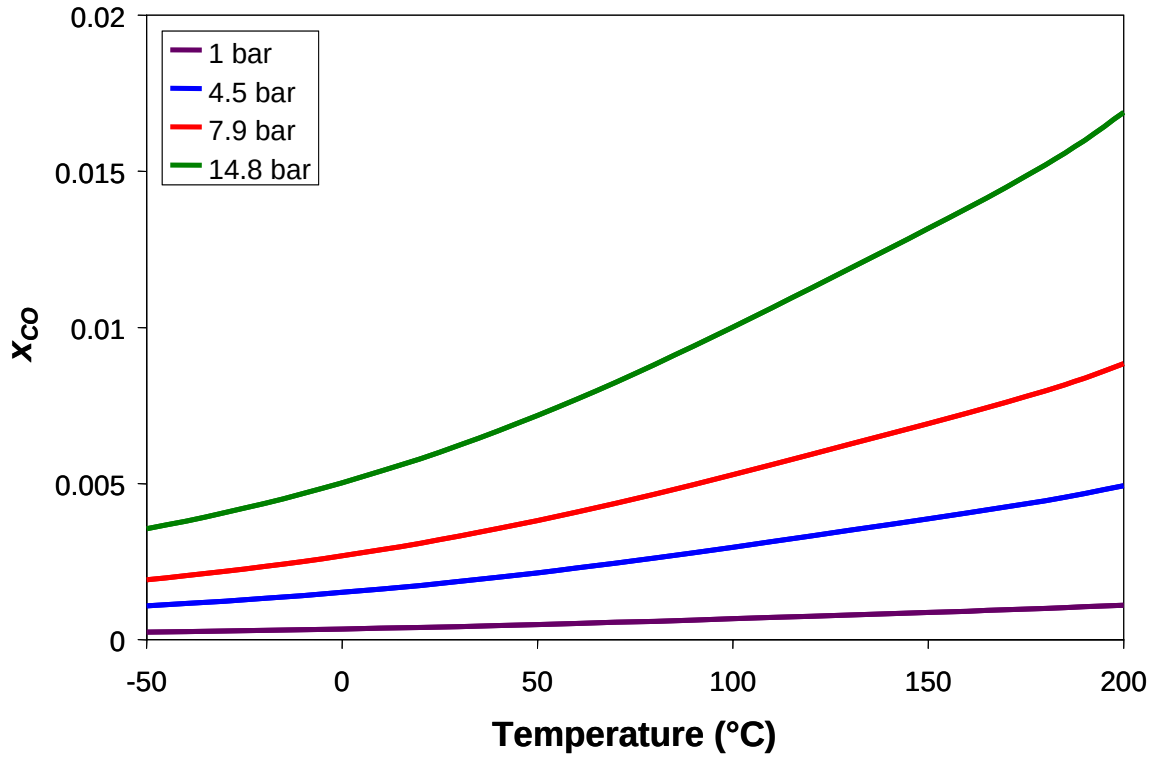

Figure 4-9: Predicted Carbon Monoxide Solubility

4.5 Rapid Reagent Screening

In addition to using the microreactor to rapidly scan the effect of reaction conditions on production and selectivity, the system was also used to test multiple reagent variations at the reaction conditions previously profiled. By installing injection valves to the liquid reagent inlet lines, several reagent solutions could be tested in rapid succession. In this way, the effects on reaction performance of not only reaction conditions, but also chemical variables such as substrate functional groups, ligand and base selection, or amine reactivities could be rapidly screened. Table 4.5 summarizes the conditions where the maximum amide and α-ketoamide yields for each reaction were observed. Conversion was calculated as the moles of aryl halide consumed divided by the initial moles fed and product yields were calculated as the total moles of product formed divided by the initial moles of aryl halide fed. All conversions and yields were determined by GC analysis.

Table 4.5: Conditions for Maximum Amide and α-ketoamide Yields (Averaged)

Halide, Amine	Ligand, Base	Amide, α-ketoamide	Conditions	Conversion	Amide Yield	α-ketoamide Yield
4-2, **4-1**	**4-7**, **4-6**	**4-8**, **4-11**	7.9bar, 146°C, 3.5min	100%	68%	25%
4-2, **4-1**	**4-7**, **4-6**	**4-8**, **4-11**	7.9bar, 96°C, 7.0min	94%	25%	69%
4-5, **4-1**	**4-7**, **4-6**	**4-10**, **4-13**	14.8bar, 109°C, 6.6min	99%	32%	57%
4-5, **4-1**	**4-7**, **4-6**	**4-10**, **4-13**	4.5bar, 160°C, 7.1min	100%	83%	0%
4-4, **4-1**	**4-7**, **4-6**	**4-9**, **4-12**	4.5bar, 150°C, 12.7min	48%	35%	0%

4.6 Conclusions

The use of a pressurized microreactor system greatly expands the range of reaction conditions available to a bench chemist. In this study, pressures up to 14.8 bar and temperatures up to 160°C were able to be tested with much more flexibility in terms of loading and sampling than traditional high pressure chemical equipment such as a Parr® bomb or autoclave. Furthermore, with the microreactor system, the reaction conditions themselves are improved, the significantly greater mass transfer area resulting from slug flow enables very rapid reaction times due to accelerated mass transfer.

The microreactor as a chemical tool shows great promise, particularly in the areas of determining optimum reaction conditions and investigating reaction mechanisms. By

increasing reaction speed, many more data points can be collected in a brief period of time. For instance, in the selectivity study for the cross coupling amidation of 4-Bromobenzonitrile **4-5** and Morpholine **4-1**, 135 samples were collected and analyzed in 8 days to profile the effects of pressures and temperatures over the ranges of 4.5-14.8 bar and 98°C-160°C. This ability to rapidly scan a wide range of reaction conditions in addition to the flexibility to test multiple reagents can greatly accelerate chemical research.

Chapter 5

Diazonium Kinetics & Production[†]

As a demonstration of how microsystems can enable quantitative study and improved production of chemistries that have been too hazardous to pursue via traditional means, the kinetics of direct sodium nitrotetrazolate (NaNT **5-3**) synthesis were characterized and a microsystem for its commercial production has been constructed. Sodium nitrotetrazolate **5-3** is an energetic compound used in the synthesis of propellants for fire control systems on military and commercial aircraft.[111] The safety concerns involved in the synthesis of this material limit production to small batches and require the use of a copper salt to stabilize the diazonium intermediate **5-2** to prevent detonation.[112,113]

A PDMS modular microreactor system capable of both multi-step synthesis and rapid scale-out was constructed. This system minimized the necessary volume of unstable intermediate enabling the kinetic study of the direct synthesis of NaNT that was previously unfeasible to test with traditional techniques. The gas generated during the process was more easily controlled in the continuous flow microreactor which prevented deposition and subsequent drying of diazonium intermediate **5-2** or NaNT **5-3** crystals on the reactor sidewalls. These crystals are shock sensitive and have led to explosion in batch vessels.[114] The modular design of this system also enabled the same set of modules used in the characterization of the reaction kinetics to be rearranged as parallel reactor chains for small scale production. A second generation microsystem for the on-demand synthesis of NaNT was fabricated in silicon to allow higher throughput and longer operational lifetimes as a full-scale production platform.

[†] This chapter describes work done in collaboration with Jason G. Kralj who, at the time, was a doctoral student in the laboratory of Prof. Klavs F. Jensen in the Department of Chemical Engineering at MIT.

5.1 Motivation

One of the more promising uses of microreactors is the possibility to perform on-demand synthesis of hazardous intermediates.[25,30] With reduced thermal mass and rapid mixing, conditions within a microreactor can be more tightly controlled than those in a traditional reactor or storage tank. Furthermore, the use of a microreactor limits the quantity of reactive intermediate to only that which is required for immediate processing thus simplifying containment in the event of a reactor failure. The enhanced heat and mass transfer within microreactors has also been shown to reduce reagent consumption, accelerate reaction optimization, and grant access to reaction conditions that would be impractical to pursue by standard laboratory techniques.[23,84]

A challenge with microfluidic systems is that, for multi-step syntheses, it is difficult to optimize reaction steps independently as reactors are often fabricated in a single, monolithic device. In such a system, it is not possible to either alter the ratio of reaction times between reaction steps or isolate intermediate species without using multiple reactor designs. Additionally, a device designed for the characterization of a reaction may not have sufficient volume for increased production at higher flow rates. A microfluidic system consisting of interchangeable mixing and reaction modules makes it possible to size the reaction zone such that the initial reaction step in a multi-step sequence can be studied independently. Subsequent reaction steps can then be explored by adding mixers and reaction zone modules for each step in the reaction sequence. If the modules are also designed such that they can be easily disconnected and reconnected for direct probing of reaction conditions, such as pH, at various points along the reactor chain, kinetic studies of multi-step syntheses become feasible. Finally, a modular system would allow for rapid scale out of the reactors into parallel streams enabling the microsystem used for characterization of the reaction to be transferred to full-scale production.

Tetraamine-*cis*-bis(5-nitro-2*H*-tetrazolato-N^2) cobalt(III) perchlorate (BNCP) is an example of a commercial product that would benefit from on-demand synthesis. As shown in Figure 5-1, each molecule of BNCP requires two molecules of the high explosive, sodium nitrotetrazolate (NaNT) **5-3**.[115] NaNT **5-3** is synthesized through a Sandmeyer type reaction that involves an even more reactive diazonium intermediate **5-2**. The instability of the diazonium intermediate **5-2** not only rules out commercial

production by direct synthesis but also makes a kinetic study of the NaNT **5-3** reactions too hazardous to pursue in batch vessels.

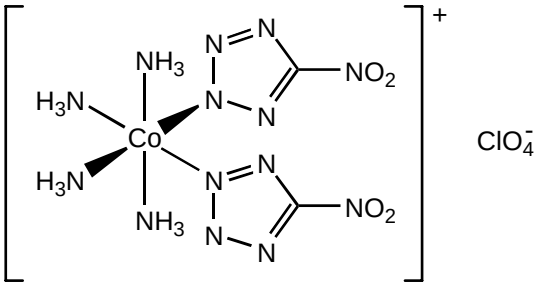

Figure 5-1: BNCP Structure[115]
Tetraamine-*cis*-bis(5-nitro-2*H*-tetrazolato-N^2) cobalt(III) Perchlorate

5.2 Description of Tetrazole Synthesis

Reactions involving diazonium intermediates, such as the synthesis of azo dyes, have been of great interest in the microreactor community for some time due to the microscale safety advantages. However, these reactions were not optimized due to the difficulty in optimizing the initial diazotization step on monolithic devices.[116,117] Additionally, combinatorial synthesis of azo dyes in immiscible liquid slugs has also been demonstrated but this technique was not ideal for characterizing the effects of reaction conditions such as temperature and pH on conversion and selectivity.[118]

The direct synthesis of NaNT **5-3** is shown in Scheme 5.1 where 5-aminotetrazole **5-1** (5-AT) reacts with nitrous acid to produce the diazonium intermediate **5-2**. It is imperative that while processing, the diazonium intermediate **5-2** remain in solution. In batch synthesis, the evolution of nitrogen and nitrogen oxides must be closely monitored to prevent reaction with dried intermediate **5-2**. Upon raising the pH of the solution, the diazonium intermediate **5-2** undergoes a Sandmeyer type reaction that displaces the diazonium group by the nitrite ion.

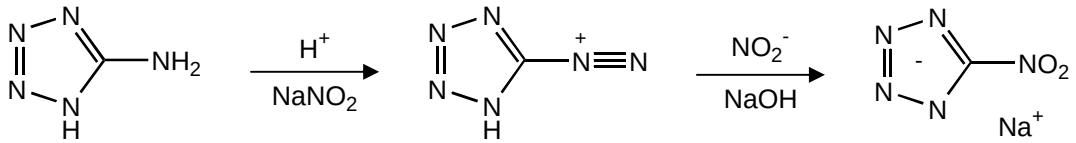

5-1 **5-2** **5-3**

Scheme 5.1: Direct Synthesis of Sodium Nitrotetrazolate (5-3)

5.2.1 Diazotization

For moderate acidities (0.1M to 6.5M [H_3O^+]) the rate law for the diazotization of aromatic amines is given by Equation (5.1) where h_0 is the Hammett acidity function.[119] Since h_0 is constant and amines less basic than p-nitroaniline are mainly present in the protonated form in acidic solutions (0.5M acid or greater), the rate equation can be expressed as the stoichiometric Equation (5.2).[120-122] The integrated form for Equation (5.2) is solved for the rate constant in Equation (5.3) where M_d is the initial concentration of nitrous acid divided by the initial concentration of 5-Aminotetrazole **5-1** and X_d is the fractional conversion of 5-Aminotetrazole **5-1**.[123] For the diazotization, the concentration of sodium nitrite was considered equivalent to the concentration of nitrous acid (HNO_2) as the *pKa* of nitrous acid is 3.25 and nitrous acid would be the predominant form at the sulfuric acid concentrations used for the diazotization.[124] This assumption would be revisited in the substitution part of this study.

$$Rate = k_{diazo,1}\left[ArNH_2\right]\left[HNO_2\right]h_0 + k_{diazo,2}\left[ArNH_3^+\right]\left[HNO_2\right]h_0 \tag{5.1}$$

$$Rate = k'_{diazo}\left[ArNH_2\right]\left[HNO_2\right] \tag{5.2}$$

$$k'_{diazo} = \frac{1}{\left[ArNH_2\right]_0 t}\frac{1}{1-M_d}\ln\frac{M_d\left(1-X_d\right)}{M_d - X_d}, \qquad M_d = \frac{\left[HNO_2\right]_0}{\left[ArNH_2\right]_0} \tag{5.3}$$

5.2.2 Nitrite Substitution

It was found during the course of this study that the second reaction step of Scheme 5.1 is highly sensitive to the pH of the solution. In initial experiments, when the diazonium intermediate **5-2** containing reaction mixture was rapidly quenched with sodium hydroxide, the reaction yielded no NaNT **5-3**. HPLC analysis of these solutions revealed only an unreactive hydroxydiazonium/nitrosylamine **5-4** compound with a peak absorbance at 261.5±0.5 nm as opposed to the NaNT peak at 256.7±0.5 nm. When these reaction solutions were reacidified and the nitration was carried out between pH 4 and pH 6 complete conversion of hydroxydiazonium **5-4** to NaNT **5-3** was observed. This suggested that a pH dependent equilibrium exists between the intermediate **5-2** and the more stable hydroxydiazonium **5-4**.

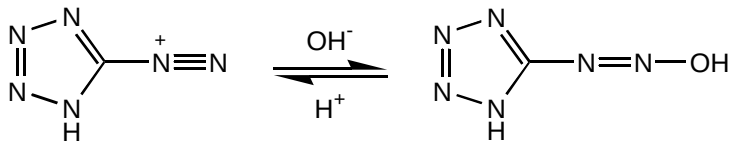

5-2 **5-4**

Scheme 5.2: Diazonium (5-2) and Hydroxydiazonium (5-4) Equilibrium

The nitration of the diazonium intermediate **5-2** involves the replacement of the diazonium group by the nitrite anion in a Sandmeyer type reaction. As such, the kinetics were expected to be second order. Due to the equilibrium between the nitrous acid (HNO_2) and the dissociated nitrite ion (NO_2^-) if the reaction is carried out below pH 3 the concentration of nitrite ion calculated by Equation (5.4) is insufficient to perform the substitution. Thus it is necessary to run the substitution reaction at a higher pH than that used for the diazotization. Unfortunately, under more basic conditions, the equilibrium shown by Equation (5.5) between the reactive diazonium ion and diazohydroxide **5-4** favors the non-reactive form. By solving these opposing equilibria with the material balances described by Equation (5.6), the product of the concentrations of the reactive species can be expressed as the product of the initial concentrations of sodium nitrite and diazonium **5-2** multiplied by the function of pH described by Equation (5.7).

$$10^{\left(pH-pK_{a,NO_2}\right)} = \frac{\left[NO_2^-\right]}{\left[HNO_2\right]} \tag{5.4}$$

$$10^{\left(pH-pK_{diazo}\right)} = \frac{\left[Diazohydroxide\right]}{\left[Diazonium^+\right]} \tag{5.5}$$

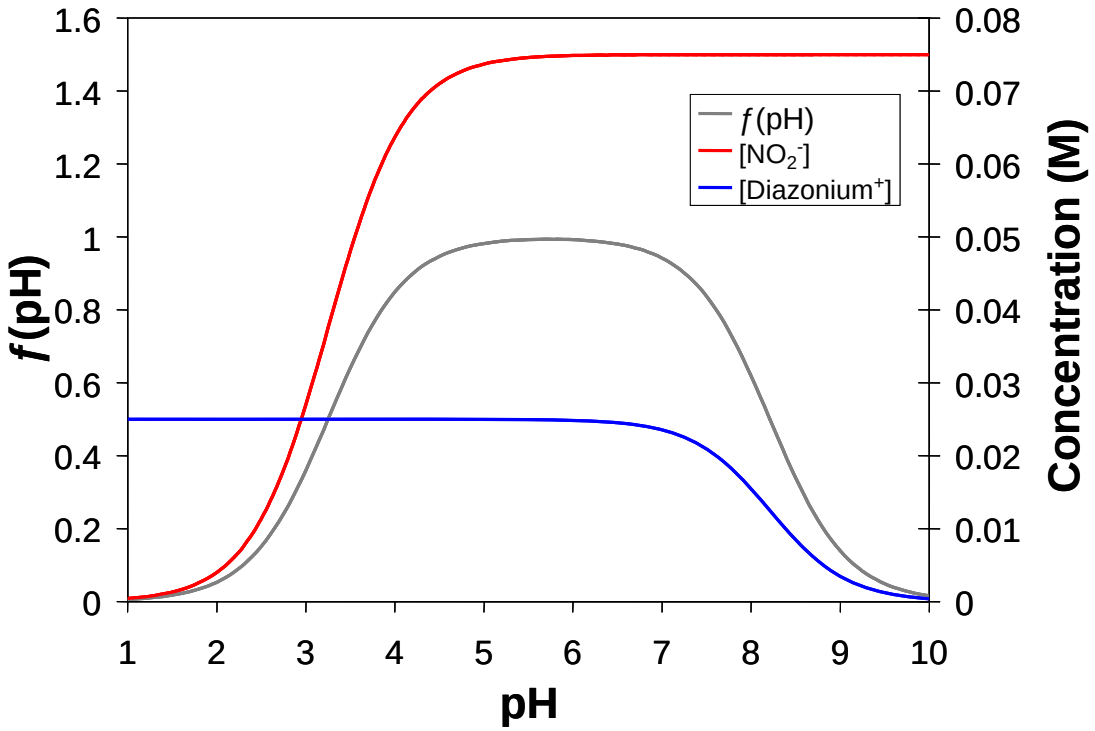

Figure 5-2: Reactant Concentration pH Dependence

$$\begin{aligned}\left[NaNO_2\right]_0 &= \left[HONO_2\right] + \left[NO_2^-\right], \\ \left[Diazonium^+\right]_0 &= \left[Diazonium^+\right] + \left[Diazohydroxide\right]\end{aligned} \tag{5.6}$$

$$f\left(pH\right) = \frac{10^{pK_{diazo} - pK_{a,NO_2}}}{\left(1+10^{pK_{diazo}-pH}\right)\left(1+10^{pH-pK_{a,NO_2}}\right)} \tag{5.7}$$

As illustrated in Figure 5-2, the effect of pH on the reactive species concentrations predicts an optimum pH range in which NaNT **5-3** can be effectively produced. Incorporating the pH effect into the kinetic expression yields the rate law presented in Equation (5.8). This combined form is preferable for the kinetic study as it is expressed in terms of measurable concentrations. The integrated form of Equation (5.8) can then be solved for $k_{sub}f(pH)$ as shown in Equation (5.9) where M_s is the initial concentration of sodium nitrite divided by the initial concentration of diazonium intermediate **5-2** and X_s is the fractional conversion to NaNT **5-3**.

$$Rate = k_{sub} f\left(pH\right)\left[Diazonium\right]_T\left[NaNO_2\right]_T \tag{5.8}$$

$$k_{sub} f(pH) = \frac{1}{[Diazonium]_T} \frac{1}{t} \frac{1}{1 - M_s} \ln \frac{M_s (1 - X_s)}{M_s - X_s}, \qquad M_s = \frac{[NaNO_2]_0}{[Diazonium]_0} \quad (5.9)$$

Due to the instability of the diazonium salt **5-2**, the direct synthesis of NaNT **5-3** in batch vessels is not the preferred method of preparing this compound. As such, the kinetics of Scheme 5.1 and the equilibrium described in Scheme 5.2 have not been previously determined. The commercial production of NaNT **5-3** has therefore had to rely upon alternative syntheses such as the use of copper(II) sulfate ($CuSO_4$).[112] The presence of copper salt in the reacting solution successfully stabilizes the diazonium intermediate **5-2** but has the disadvantage of reducing reaction yields.[125] An additional difficulty with the $CuSO_4$ mediated synthesis is the precipitation of copper oxide (CuO) which leads to additional processing difficulties such as solids handling and purification. The use of a microsystem to increase the safety of the direct synthesis of sodium nitrotetrazolate **5-3** has economic advantages over $CuSO_4$ mediated production. Furthermore, the potential for an on-demand synthesis of NaNT **5-3** eliminates the need for storing this explosive material, thereby reducing the hazards associated with BNCP production.[111]

5.3 Microchemical System Design

In order to allow detailed analysis of the multi-step synthesis of NaNT **5-3** a modular microsystem was designed. As opposed to a monolithic design, the same micromixer could be used for each reaction step changing only the reaction zone volume attached to it. Further saving on fabrication costs, only the micromixer was microfabricated as 1/16" OD Teflon® tubing with reliable internal diameters was commercially available and could be used to form the reaction zone. This had the advantage of increasing the flexibility of the microsystem while also decreasing the costs of construction by reducing the number of components that require microfabrication.

5.3.1 PDMS Prototype

For the kinetic studies and initial production capacity estimates a prototype system was fabricated from polydimethylsiloxane (PDMS). The micromixer modules, shown in

Figure 5-3, were molded in degassed PDMS over a 100mm diameter silicon wafer patterned with the photodefinable epoxy SU-8 2050. PDMS was chosen as the mixer material due to the compatibility of this material with aqueous systems as well as the ease in fabricating multiple, interchangeable micromixers.[126] Additionally, the enhanced gas permeability of PDMS prevented significant bubble formation within the channels during kinetic studies, enabling more reliable residence times. After initial tests with devices bonded to glass substrates, oxidized silicon was chosen as the bonding substrate due to its higher thermal conductivity.

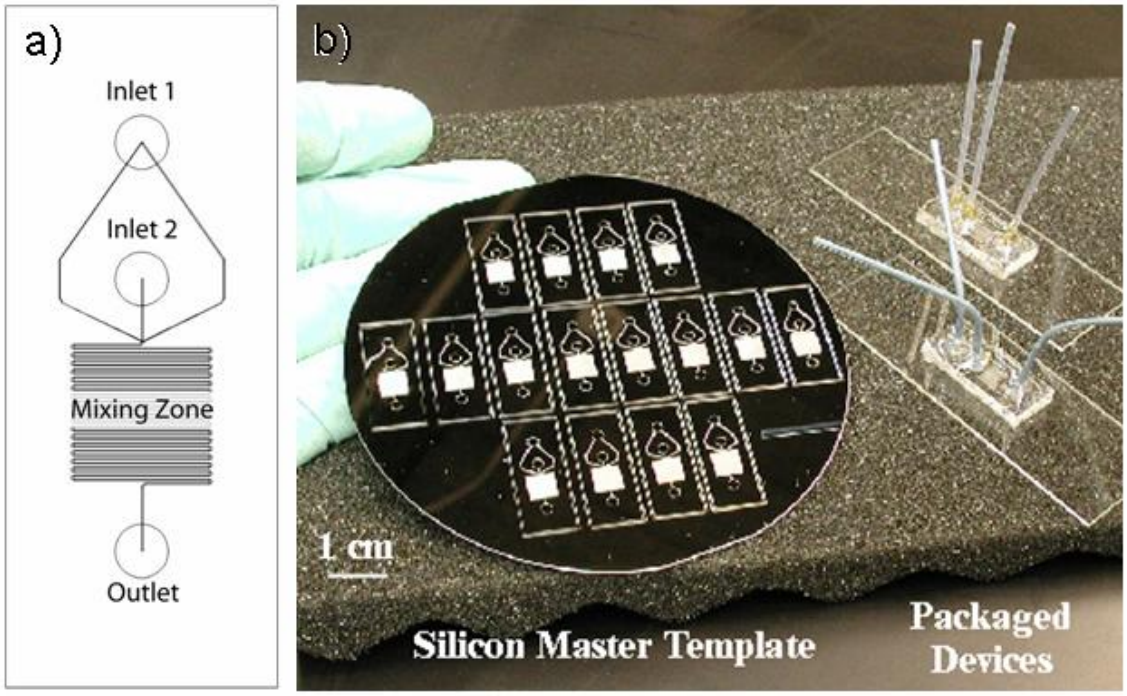

Figure 5-3: PDMS micromixer design
a) Micromixer diagram b) Silicon master and sealed devices

The silicon master was formed by dispensing 3 to 4 mL of SU-8 2850 onto the silicon wafer. The silicon wafer was then spun at 750 rpm for 15 seconds followed by 1000 rpm for 60 seconds. After baking at 65°C for 1 min the temperature was raised to 95°C and held at that temperature for 30 minutes. This process was repeated a second time to produce a double layer of SU-8 170µm thick. The photomask, a transparency printed by Pageworks in Cambridge, MA, was placed directly onto the SU-8 coated wafer and compressed with a 5-inch square quartz plate. This stack was then exposed to UV light for 9 intervals of 5 seconds each with a 2 second wait between exposures on an

Electronic Visions EV620 mask aligner. The exposed wafer was subsequently developed in PGMEA developer for 30-60 minutes. Once developed, the SU-8 master was placed in a vacuum chamber at 0.11 bar and exposed to open vials of n-octyltriethoxysilane or (tridecafluoro-1,1,2,2-tetrahydrooctyl)-1-trichlorosilane purchased from United Chemical Technologies Inc. in Bristol, PA. Silanization of the SU-8 master for 3-6 hours deactivated the surface and prevented the PDMS from tearing during release from the mold.

The PDMS was prepared by mixing Dow Corning Sylgard 184 with its activator in the ratio of 10:1 by weight. This mixture was degassed and cast onto the SU-8 master. Curing of the PDMS was performed in a VWR model 1410 vacuum oven at 70°C and 1 bar for 3 hours. After curing, the PDMS was allowed to cool before peeling the micromolded mixers from the master wafer. The devices were cut from the molded PDMS slab and fluid ports were formed with a 5/64" leather punch. The devices were rinsed with isopropanol and cleaned of dust and PDMS scrap with adhesive tape. The 11mm by 26mm PDMS die and a 12mm by 30mm piece of oxidized silicon wafer were then placed into a Harrick PDC-32G oxygen plasma chamber and ashed for 60s to remove residual organics. The silicon slab was from a 500μm thick silicon wafer with a 5000Å thermal oxide. The PDMS and silicon pieces were then removed from the plasma chamber and non-bonding surfaces were covered in adhesive tape. Once protected, both pieces were again exposed to oxygen plasma for 35 seconds, after which, the PDMS device was immediately placed on the oxidized silicon forming a covalent bond between the PDMS and silicon oxide.

The mixer consists of one bifurcated inlet surrounding a second inlet. This design reduces the mixing length to half the width of the channel. The mixing channel is 50μm wide giving a mixing time of 0.3s for small molecules in aqueous solution. To ensure complete mixing within the mixer for flow rates up to 290 μL/min, the mixing channel was sized to be 170 μm deep by 178 mm long for a total volume of 1.5 μL.

The micromixers were packaged with 5cm lengths of 1/16" OD 0.01" ID Teflon® tubing with swaged stainless steel ferrules were inserted into the inlet and outlet ports of the mixer and sealed with Devcon 5 minute epoxy. In order to produce the desired residence time in the reaction zone, additional 1/16" OD Teflon® tubing with inner

diameters of either 0.02" or 0.03" was attached to the device outlet using Tefzel® unions (Upchurch P-630). The multi-step reaction system was constructed by attaching the outlet of one reactor chain to the inlet of the next PDMS micromixer. As shown schematically in Figure 5-4, the modular design of the system using interchangeable units allows for rapid scale out for either simultaneous experiments with different concentrations or identical reaction chains to accelerate data collection and maximize production. Each reactor chain, whether single step or multi-step, was terminated by a PEEK™ tee union or Y-connector (Upchurch P-712 or P-512 respectively) into which a sodium hydroxide solution was added to quench the reaction and stabilize the collected samples. The microreactor system was then submerged into water and reaction temperatures were controlled using a Neslab Endocal recirculating bath.

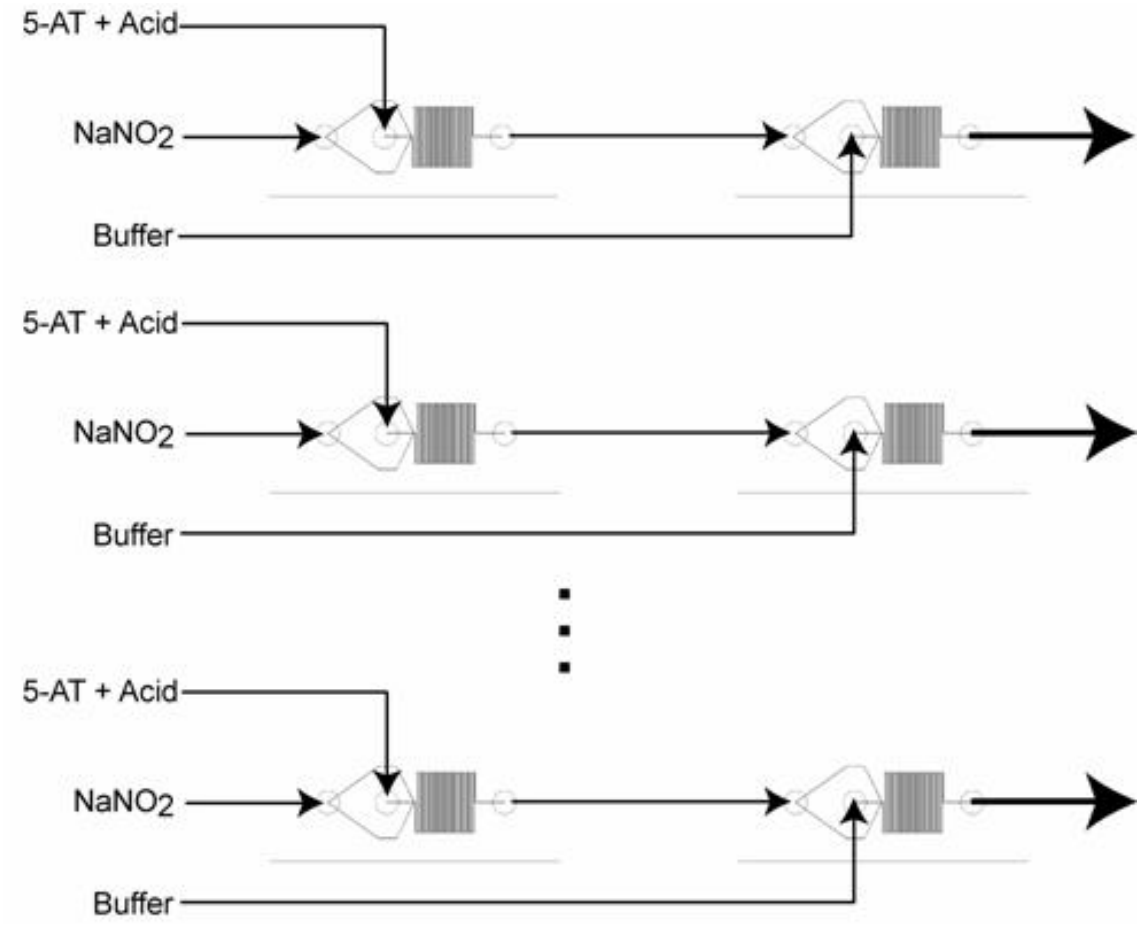

Figure 5-4: Modular Microsystem
Serial and Parallel Micromixer Modules

Fluid delivery was managed through the use of Harvard Apparatus PHD 2000 Programmable syringe pumps. In order to allow pH scanning, reagents and pH buffer flow had to be independently manipulated. To simplify this manipulation, one syringe pump was dedicated to the delivery of reagent and sodium hydroxide quench solutions while the second delivered pH buffer solutions. The reagents were delivered by Hamilton Gastight® syringes model 1005 (5mL, 10.3mm ID). These syringes were fitted with either Teflon® luer locks or luer tips and connected to 1/16" OD 0.01" ID Teflon® inlet tubing by Tefzel® luer fittings (Upchurch P-628, P-245x, and P-200Nx).

5.3.2 Silicon Production System

Since the kinetic study required only low flow rates and concentrations, the heat transfer and pressure drop of the PDMS devices were adequate. In order to accommodate the higher flow rates and more concentrated reagent streams required of an on-demand NaNT microsystem, an improved micromixer module was required. To this end, a second generation micromixer, shown in Figure 5-5, was fabricated in silicon which had both a higher thermal conductivity (148 W/m K vs. 0.15 W/m K) and was significantly more robust than PDMS. Thus, the production micromixers would be able to accommodate a considerably higher heat load and have longer operational lifetimes than the PDMS devices.

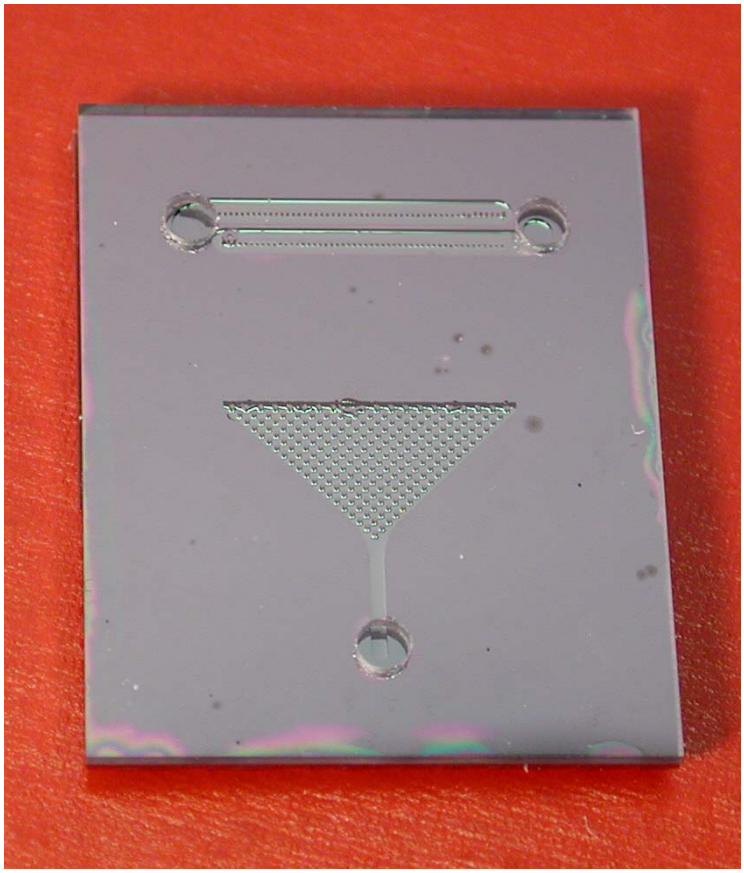

Figure 5-5: Silicon Micromixer Module

Like the PDMS design, the silicon micromixer utilizes laminar mixing; however, as opposed to one bifurcated inlet stacked around a second (Figure 5-3a) the silicon micromixer, splits the two inlet streams into 101 interdigitated lamina. As shown in Figure 5-6, the top side of the device consists of the fluid manifolds and mixing channel while the back side contains the back-pressure channels. A double sided device was necessary since the fluid paths from the uppermost manifold in Figure 5-6a must cross the lower manifold in order to produce alternating fluid streams in the mixer. Fluid is introduced to the device through the inlet manifolds and is distributed among the back-pressure channels (51 for the uppermost manifold and 50 for the lower). These back-pressure channels were designed to generate a tenfold higher pressure drop than throughout the rest of the device such that the flow rate through each channel is identical when the fluid enters the mixing channel.

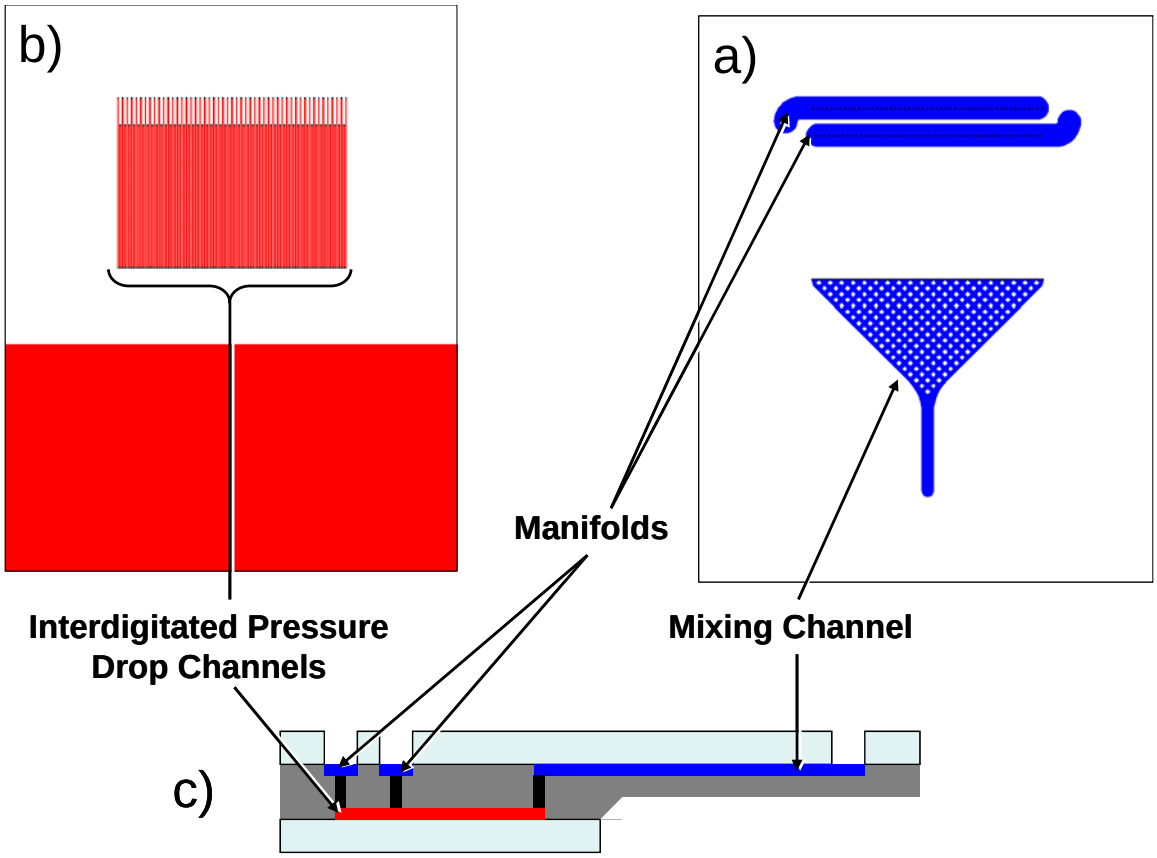

Figure 5-6: Silicon Micromixer Schematic
a) Top view b) Bottom view c) Side view

In order to fabricate the mixer, three etch steps were necessary. First the back-pressure channels and Pyrex® release trench (solid red area on Figure 5-6b) were etched by potassium hydroxide wet etch to a depth of 50µm using a 5000Å thermal oxide as a hard mask. Next, the wafer was re-oxidized at 1050°C for 3 hours and 20 minutes to cover the exposed silicon and thicken the protective oxide for nested deep reactive ion etching (DRIE). The manifold and mixing channel pattern (shown in blue on Figure 5-6a) were then defined by 7:1 buffered oxide etch (BOE). The top side was then coated with photoresist and the holes connecting the top and bottom of the device (shown in black on Figure 5-6) were exposed by photolithography. These holes were then etched through the wafer by DRIE. The photoresist was subsequently stripped from the wafer, exposing the nested (blue) pattern for etching to a depth of 200µm. The wafer was then stripped of all oxide by a second BOE and finally oxidized to a thickness of 2000Å. The fluid channels were then hermetically sealed by two 710µm thick Pyrex® wafers. External fluid ports

were drilled into the top Pyrex® wafer before bonding. After bonding the Pyrex® wafer, the back of the device was scored to a depth of 700μm over the Pyrex® release trench. This scoring was performed on a die saw (Disco Abrasive System Model DAD-2H/6T) immediately before final wafer dicing on the same machine. Once diced, the scored Pyrex piece over the release trench was easily removed to expose the silicon directly underneath the mixing channel thus enhancing the heat transfer to the device. A more detailed description of the fabrication of the micromixer can be found in Appendix A.

Due to the incompatibility of solder bonding with the extreme pH necessary for NaNT synthesis, the silicon micromixers were packaged in the same manner as the PDMS devices. In order to prevent the Devcon epoxy from wicking into the device and clogging it, the holes in the Pyrex® wafer were drilled to a diameter of 1.6mm. This diameter is sufficient to insert 1/16" tubing directly into the device. As an additional protection against wicking, and to allow the use of Teflon® tubing, stainless steel ferrules were swaged onto the tubing. Thus, the device could be packaged by applying epoxy only to the exterior of the device and the ferrules. Once packaged, the silicon mixer modules were incorporated into the microfluidic system via the same fittings and peripheral equipment used for the PDMS devices.

5.4 Kinetic Study

5.4.1 Experimental Procedure

Reagents were used as received and prepared in deionized water that was filtered through a Millipore Academic Milli-Q water purifier. 5-Aminotetrazole **5-1** was purchased from Lancaster Synthesis, Inc. in Pelham, NH. Analytical reagent grade sulfuric acid, sodium hydroxide, and citric acid monohydrate were supplied by Mallinckrodt Chemicals (Phillipsburg, NJ). Sodium nitrite (97%) was purchased from Alfa Aesar in Ward Hill, MA.

The modular design of the microsystem allowed the independent investigation of each of the reaction steps. In characterizing the first step of Scheme 5.1, a single micromixer connected to a 36mm length of 0.01" ID Teflon® tubing was used yielding a 3.32μL combined reactor volume terminated by a sodium hydroxide quench. The

substitution step of the synthesis was performed in a multi-step system in which the diazotization reaction volume was increased to 62µL and directly connected to a second micromixer with a 230µL reaction zone. The sodium hydroxide quench was introduced at a tee junction at the end of this second reaction zone. The reversible fittings on the tee junction allowed the reactor to be disconnected from the quench to measure the pH of the reacting solution with either EM Science colorpHast® indicator strips or Baker-pHIX pH papers before reconnecting the quench to collect samples for HPLC analysis.

Collected samples were loaded into a Waters 717+ Autosampler and analyzed using a Waters Nova-pak© C18 column (3.9 x 150mm). The mobile phase was an aqueous solution of 0.1M monobasic phosphate buffer pumped isocratically at 1 ml/min by a Waters 1525 binary pump. The eluent was monitored on a Waters 2996 Photodiode Array Detector. Elution of all compounds was complete after 5 minutes. Peak absorbance of NaNT **5-3** was observed at 256.7 ± 0.5nm while peak hydroxydiazonium **5-4** absorbance was 261.5 ± 0.5nm.

5.4.2 Results

Diazonium Formation

Reagents were delivered to the reactor from two syringes. The first syringe contained a solution of 5-AT **5-1** (0.025M) in 1.5M sulfuric acid. The second syringe contained an aqueous solution of sodium nitrite (0.025M of 0.05M). A third syringe contained 2M sodium hydroxide to quench the reaction at the reactor outlet. All three syringes were driven by the same syringe pump such that the three flows remained equal. Since the total volume of the reactor was known to be 3.32µL, reaction times were controlled by varying the flow rates of the syringes. The reaction zone flow rate was varied from 20 to 100µL/min corresponding to residence times of 10 seconds 2 seconds respectively. Four or five flow rates were tested at each of the temperatures investigated from 5°C to 30°C and each set of conditions were repeated at both concentrations of sodium nitrite.

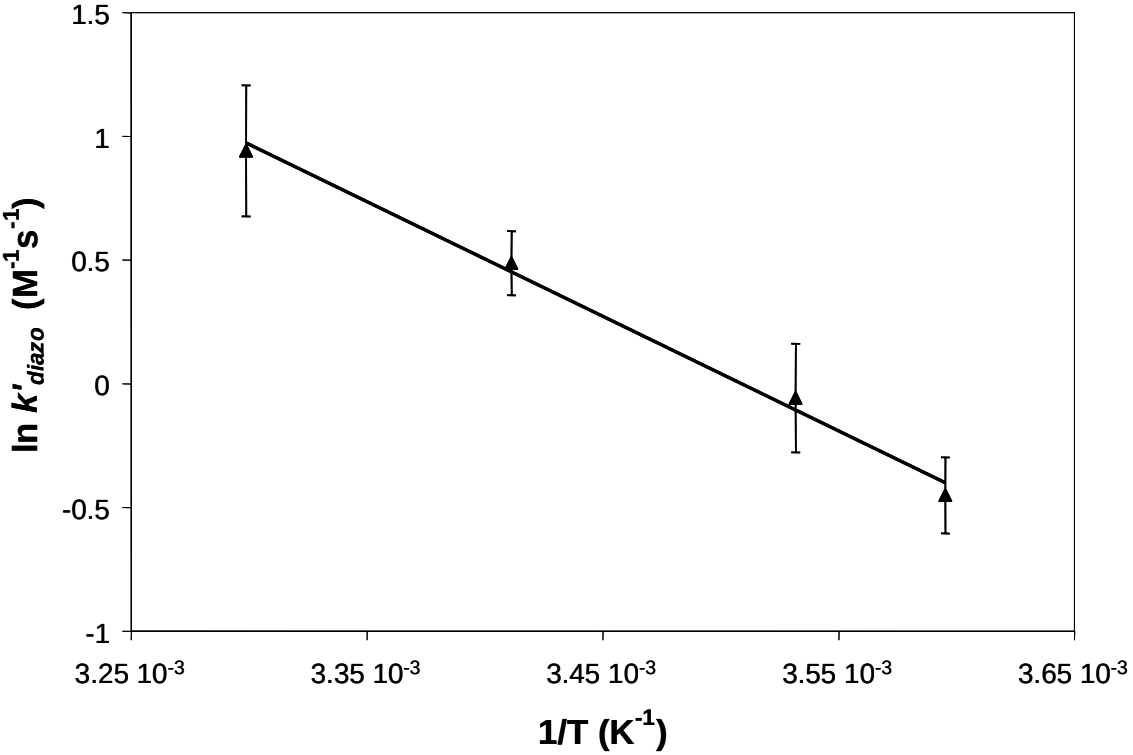

Figure 5-7: Diazonium (5-2) Formation Kinetics
With 95% confidence intervals

After quenching, samples were collected and analyzed by off-line HPLC. Because of the instability of the diazonium intermediate **5-2**, the reaction conversion was measured indirectly by measuring the concentration of the hydroxydiazonium **5-4** that is in equilibrium with the diazonium salt. The excess sodium hydroxide in the quench ensured a quantitative conversion to the hydroxydiazonium **5-4** and, as a result, no NaNT **5-3** production was observed in this portion of the study. The Arrhenius pre-exponential factor and activation energy are reported in Table 5.1. The observed rate constant data (Figure 5-7) showed good agreement with the expected second order kinetics. In addition, these data are within the range of typical values for secondary amines at similar conditions.[122]

Table 5.1: Diazonium (5-2) Formation Kinetic Parameters

	ln(A) ($M^{-1}s^{-1}$)	E_A (kJ/mol)	k_{298K} ($M^{-1}s^{-1}$)
Diazonium Formation $Rate = k'_{diazo}[5-AT][NaNO_2]$	16.2 ± 2.7	38.5 ± 6.5	2.0

Sodium Nitrotetrazolate Formation

In order to determine both the kinetic parameters of the substitution reaction as well as to identify the diazonium equilibrium constant, a multi-step system was used. The outlet of the first reactor was connected to additional tubing, increasing the total volume of the diazotization reaction zone to 62μL before connecting directly to a second micromixer. This increased reaction zone volume ensured complete conversion of 5-aminotetrazole **5-1** to the diazonium intermediate **5-2**. In the second micromixer, this stream was contacted with a citric acid monohydrate buffer solution and reacted in a 230 μL reaction zone. The outlet of this second reaction zone was quenched with sodium hydroxide.

The 0.2M sodium nitrite, 0.05M 5-aminotetrazole **5-1** in 1.5M sulfuric acid, and 4M sodium hydroxide quench solutions were driven by one syringe pump at the same flow rate (5μL/min or 10μL/min each). The 0.4M citric acid and 2M sodium hydroxide buffer solution was delivered by a second syringe pump and the buffer flow rate was adjusted between 0.5 and 3 times the flow rate of sodium nitrite solution. This change of flow ratio allowed the adjustment of the reaction zone pH. The pH was monitored by disconnecting the end of the substitution reaction zone from the quench and applying drops of the reaction media to pH indicator strips and pH papers. The reaction zone was then reconnected to the quench for sample collection and off-line HPLC analysis.

Using Equation (5.9), the combined term $k_{sub}f(pH)$ was obtained from the results of HPLC analysis of NaNT production for each data point over the temperature range of 5°C to 40°C and pH range of 3 to 8. Least squares regression was then used to fit the data to Equation (5.10).[127] The results of this analysis provided the values of the Arrhenius parameters as well as the value for pK_{diazo} listed in Table 5.2.

$$\ln\left(k_{sub}f\left(pH\right)\right)=\ln\left(A_{sub}\right)-\frac{E_{a,sub}}{RT}+\ln\left[\frac{10^{pK_{diazo}-pK_{a,NO_2}}}{\left(1+10^{pK_{diazo}-pH}\right)\left(1+10^{pH-pK_{a,NO_2}}\right)}\right] \quad (5.10)$$

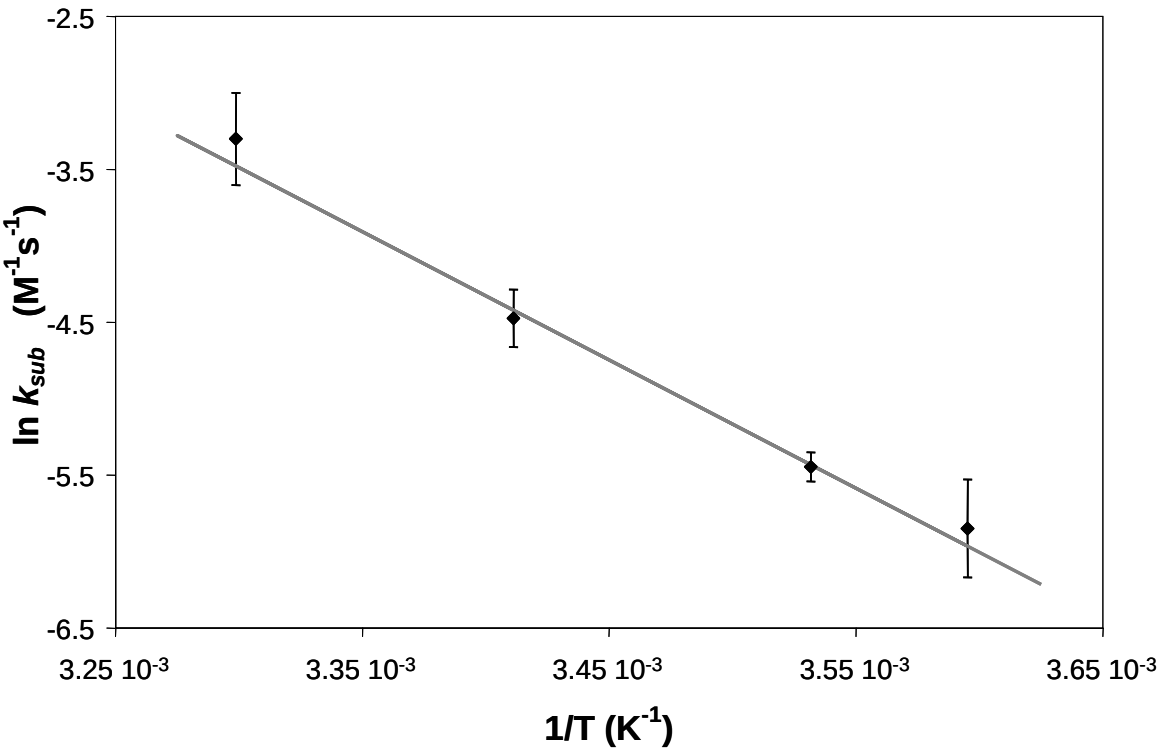

Figure 5-8: Nitrite Substitution Kinetics
With 95% confidence intervals

Table 5.2: Nitrite Substitution Kinetic Parameters

	ln(A) ($M^{-1}s^{-1}$)	E_A (kJ/mol)	k_{298K} ($M^{-1}s^{-1}$)
NO_2 Substitution $Rate = k_{sub}\left[\text{Diazonium}^+\right]\left[NO_2^-\right]$	24.2 ± 3.6	69.7 ± 8.8	$1.9 \cdot 10^{-2}$
pK_{diazo}= 7.9 ± 1.0			

The kinetic model for the diazonium substitution suggests that the effects of pH and temperature are separable. Thus, once the parameters were determined, the individual values of k_{sub} and $f(pH)$ could be calculated. The values for k_{sub} were derived by dividing the measured $k_{sub}f(pH)$ by the value of $f(pH)$ for the measured pH and the value of pK_{diazo} obtained by regression. These extracted rate constant data are plotted in Figure 5-8. Comparison with the predicted temperature dependence (gray line in Figure 5-8) calculated by the parameters in Table 5.2, showed good agreement to the expected second order kinetics.

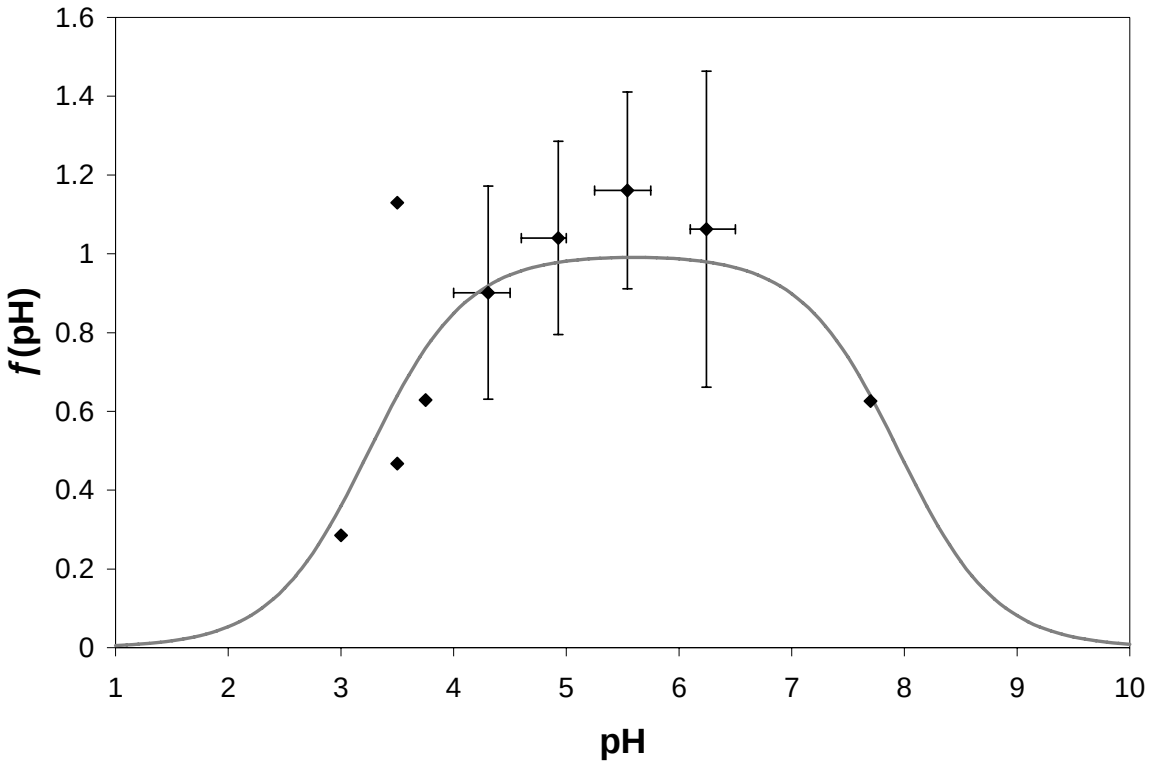

Figure 5-9: Nitrite Substitution pH Dependence
With 95% confidence intervals

To confirm the accuracy of the pH model, values for $f(pH)$ were extracted for each data point by dividing the measured $k_{sub}f(pH)$ by the value of k_{sub} predicted by the obtained Arrhenius parameters. The effect of pH on the conversion of diazonium **5-2** to NaNT **5-3** is shown in Figure 5-9. While the data to verify the model were limited to the region of high conversion, the data does reflect the predicted optimum conditions (gray line in Figure 5-9) between pH 4.0 and pH 7.0. Due to the fact that pH was measured and not explicitly controlled, the data between pH 4.0 and pH 6.5 were grouped in 0.5 pH increments and plotted with 95% confidence intervals. Data collected at or below pH 4.0 and above pH 6.5 were plotted as individual data points.

5.5 Reactor Scale Out

5.5.1 PDMS Based Reactor

The operation of multiple reactor chains in parallel, as illustrated in Figure 5-4, greatly accelerated data collection for the kinetic study allowing the collection of up to three data points simultaneously. In addition, the on-demand synthesis of the reactive intermediate enabled the entire kinetic study to be performed without having to store or manipulate the hazardous diazonium salt **5-2**. After characterizing the reaction, the next step was to explore the possibility of using these modules in a larger microsystem consisting of more parallel reactor chains to be used as a production platform.

Initial experiments used the same configuration of micromixers as used in the kinetic study but with increased reagent concentrations from those used in the kinetic study (0.025M 5-AT, 0.1M $NaNO_2$) to production levels (0.38M 5-AT, 0.75M $NaNO_2$). It was predicted that these concentrations would enable the same reactor chain that was used for the characterization of the substitution reaction to produce a maximum of 7 mg/min at a total flow rate of 150μL/min. With this production rate, a system of ten parallel reaction chains could supply sufficient NaNT **5-2** to feed current BNCP processes.[114]

Under these conditions, increased gas evolution was observed which exceeded the permeability of the PDMS micromixers. This gas appeared to be a combination of both the expected nitrogen evolution and NO_x products from the decomposition of the sodium nitrite. The evolving gas was not considered to present a safety hazard as these slugs easily advanced through the reactor tubing precluding the possibility of local drying on the reactor tubing walls. While the gas slugs did not change the overall behavior of the system, the reaction times were shorter than those seen in the characterization experiments due to the increase in volumetric flow rate as compared to the single phase operation during the characterization of the reaction. The decomposition of the sodium nitrite and the reduced reaction times combined to prevent the complete conversion within the PDMS devices. In addition, the PDMS devices themselves appeared to degrade under these more aggressive conditions. Within three hours the devices began to appear cloudy as NO_x gases permeated the polymer and, after several hours, the PDMS could delaminate from the oxidized silicon substrate.

5.5.2 Silicon Based Reactor

In order to construct a more robust system, the silicon micromixer shown in Figure 5-5 was constructed. This device was designed not only to better withstand the production of NO_x gases, but also to accommodate complete mixing at higher flow rates. In this way the microsystem could be operated at production concentrations by increasing the reaction zone volumes and replacing the PDMS micromixer modules with the silicon micromixer. Alternatively, at the higher flow rates capable with this new mixer, the microsystem could accommodate the desired production levels using the low concentration, single phase operation from the kinetic study. The concentration of the exiting NaNT **5-2** stream would be reduced, but the overall flow rate through the reactor could be increased to the desired production levels.

Mixing Tests

While diffusive mixing models predict that the silicon mixer is capable of complete mixing at up to 2mL/min, the results of the substitution kinetic study highlight the necessity of rapid mixing. If the mixing is incomplete, variations in local pH values lead to incomplete reaction or decomposition of sodium nitrite. In order to ensure complete mixing within the silicon device a stream of phenolphthalein indicator in 1M acetic acid was mixed with a 1M aqueous sodium hydroxide solution in the device. The indicator solution was prepared in a 10mL volumetric flask as 1M acetic acid, diluted from glacial acetic acid supplied by Mallinckrodt Chemicals (Phillipsburg, NJ) to which two drops (33μL to 50μL per drop) of phenolphthalein indicator supplied by the Thermo Electron Corporation (Beverly, MA) was added. Upon mixing, the two solutions have a pH of 8.7 triggering a color change in the phenolphthalein.

Transparent tubing was connected to the outlet such that the color of the reactor effluent could be monitored as the solutions were driven at flow rates from 200μL/min to 2mL/min total flow through the device. At all flow rates, the reactor effluent appeared colored. Since the color of phenolphthalein changes when the solution pH is greater than 8.2, and this pH corresponds to an acetic acid to sodium hydroxide ratio of 1.003:1, this indicated at least 99% mixing by volume at 2mL/min.

The mixing efficiency of the both the silicon micromixer and PDMS micromixer used in the kinetic study were further tested by the Villermaux/Dushman method. In this test the micromixer contacted a 15mM sulfuric acid solution with a boric acid and iodide solution containing 250mM sodium hydroxide, 246.5mM boric acid, 31.9mM potassium iodide, and 6.35mM potassium iodate (EMD Chemicals Inc. Gibbstown, NJ) at various flow rates. Upon mixing, two competing reactions occurred. The faster of these two reactions was the neutralization of the sulfuric acid. The second reaction, as shown in Scheme 5.3 was significantly slower than the neutralization reaction but is fast when the reaction mixture contains excess acid.

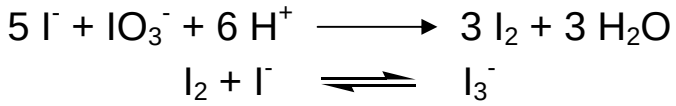

Scheme 5.3: Villermaux/Dushman Iodide Production

Among the products of this reaction was the triiodide ion that has an UV absorbance spectrum with peaks at 286nm and 353nm.[128] When the streams were initially contacted, areas of high acid concentration favored triiodide formation but, as the streams mixed, the acid was diluted and quenched, halting this reaction. Thus, when mixing occurred rapidly, more acid was quenched and little triiodide was formed. The triiodide concentration was measured by connecting the micromixer outlet to a UV spectrometer (Waters 2996 Photodiode Array Detector) and monitored at 353nm (ε_{353nm} = 26400 AU/M cm). The measured concentration of triiodide was plotted against the total flow rate for both the silicon and PDMS micromixers as shown in Figure 5-10.

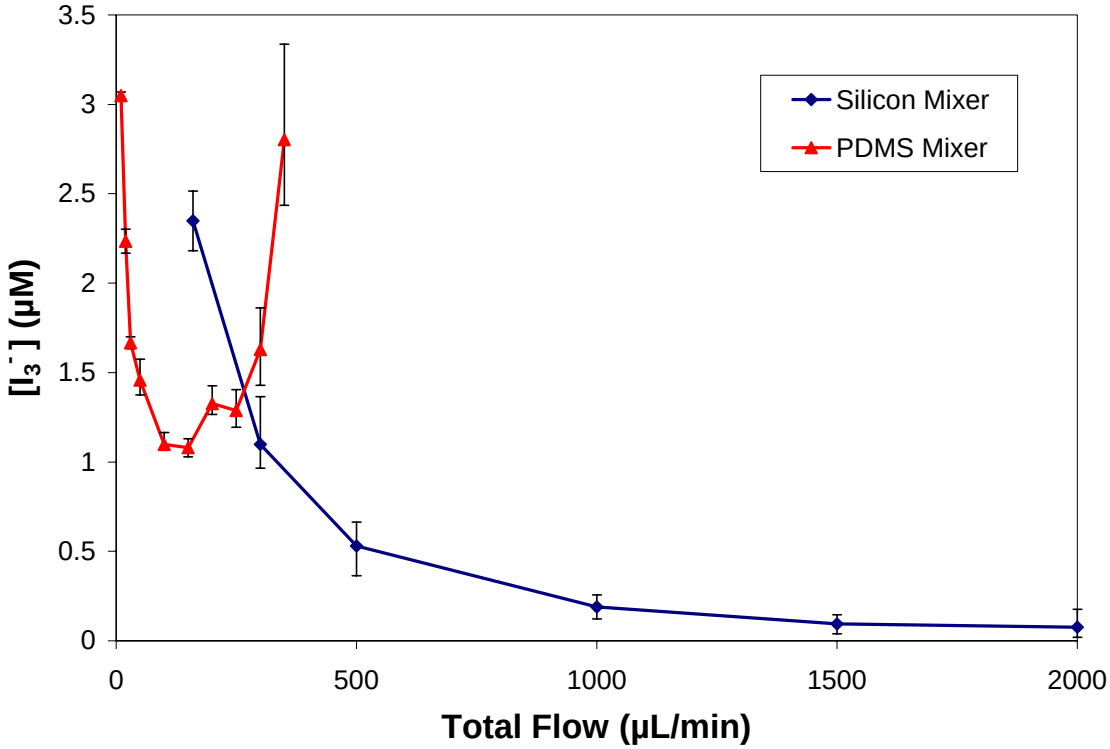

Figure 5-10: Micromixer Efficiency Results
Villermaux/Dushman Method

The results of the mixing tests showed that both micromixers provide excellent mixing when compared with other micromixers.[129] Both micromixers showed an initial improvement in mixing efficiency with increased flow rate. By accelerating the flow through the focusing region of the micromixer the reduction in the width of the mixing lamina occurred faster and thereby increased the overall mixing rate. However, when the PDMS micromixer was operated in excess of 300µL/min, mixing efficiency declined. This corresponds to the design limit of 290µL/min at which point mixing would continue downstream of the 50µm wide mixing channel. The silicon mixer, when compared to the PDMS device, showed superior mixing efficiency at flow rates above 300µL/min and easily accommodated the desired 2mL/min. Additionally, since the mixing channel in the silicon mixer was much wider than that of the PDMS device and similar to the diameter of the reaction zone tubing, less degradation in mixing efficiency was expected at flows in excess of the 2mL/min design limit.

Reaction Tests

The silicon micromixers were installed into a modular microsystem with a 53µL diazotization zone (26cm of 0.02"ID Teflon® tubing) and a 2.5mL substitution zone (310cm of 0.04" ID Teflon® tubing). Solutions of 0.1M 5-AT **5-1** in 1.5M sulfuric acid, aqueous 0.4M $NaNO_2$, 1M citric acid in 5M NaOH, and a 4M NaOH quench were flowed through the system at ratio of 1:1:0.9:0.9 to provide a substitution zone pH of 4.5 (measurements confirmed a pH between pH 4.5 and pH 5). Flow rates from 50µL/min to 100µL/min of 5-AT **5-1** corresponding to maximum NaNT **5-3** production rates of 0.05 to 0.1 g/hr-chain were tested.

The reaction zone volumes were sized to provide conversions of 5-AT **5-1** to NaNT **5-3** between 50% and 75% at 25°C for the flow rates tested. HPLC analysis of the reactor effluent, however, indicated conversions between 37% and 54%. This disparity was believed to be caused by the increased gas evolution observed during operation. For the reaction at a 5-AT **5-1** flow rate of 50µL/min a 10 cm length at the exit of the substitution reaction zone was marked and the speed of the gas and liquid slugs traversing this section were measured to be 0.52 cm/s, corresponding to a total volumetric flow rate of 253 µL/min. Recalculating for this 43% reduction in residence time gives expected conversions of 32% and 54% conversion showing good agreement with the experimental results.

5.6 Conclusions

With the enhanced safety of working with minimal volumes of material, new conditions that were previously considered hazardous could be explored thoroughly. By increasing the range of conditions available to test it was discovered that, as long as local drying of the diazonium salt **5-2** was avoided, the production of NaNT **5-3** could be safely carried out at temperatures well above the previous 18°C ceiling for safe operation. Additionally, it was determined that the speed of mixing greatly affected the nitrite substitution reaction as the reacting species are in competing equilibria with non-reactive forms. The rapid mixing within the modular micromixers enabled, a study of the effect of pH by manipulating the flow rate of a citrate buffer solution.

In utilizing a modular design for the exploration of multi-step syntheses, the mass transfer and safety advantages of microsystems were incorporated into a modular architecture. This flexible design provided greater freedom to manipulate the relative reaction times for each step of the synthesis. This enabled a kinetic study of both steps of the synthesis of sodium nitrotetrazolate **5-3** with a single set of microfluidic modules. Additionally, the modular design presented an improved ability to directly probe the conditions of the reaction. Through the use of reversible fittings, the pH of the reaction media was measured using standard, bench-top techniques and the system was immediately reconnected to allow continued production. With this system, both the kinetics of this multi-step synthesis and the equilibrium constant of the intermediate (Table 5.3) were determined for the synthesis of an energetic compound that, due to the hazards involved in batch processing could not safely be studied using traditional means.

A second generation mixing module was also fabricated in silicon to enable higher flow rates and superior chemical compatibility. These silicon modules were designed to provide a scaled-out system which could provide on-demand NaNT **5-3** synthesis for BNCP production. These silicon-based mixing modules were found to be capable of excellent mixing at flow rates up to 2mL/min and reaction tests produced consistent results with those observed in the kinetic study.

Table 5.3: Kinetic Parameters for the Direct Synthesis of NaNT (5-3)

	ln(A) ($M^{-1}s^{-1}$)	E_A (kJ/mol)	k_{298K} ($M^{-1}s^{-1}$)
Diazonium Formation $Rate = k'_{diazo}[5-AT][NaNO_2]$	16.2 ± 2.7	38.5 ± 6.5	2.0
NO_2 Substitution $Rate = k_{sub}[Diazonium^+][NO_2^-]$	24.2 ± 3.6	69.7 ± 8.8	$1.9 \cdot 10^{-2}$
pK_{diazo}= 7.9 ± 1.0			

References

1. Senturia, S.D., *Microsystem design*. 2001, Boston: Kluwer Academic Publishers.
2. Madou, M.J., *Fundamentals of microfabrication : the science of miniaturization*. 2nd ed. 2002, Boca Raton, Fla.: CRC Press.
3. Bassous, E., H.H. Taub, and L. Kuhn, *Ink jet printing nozzle arrays etched in silicon.* Applied Physics Letters, 1977. **31**(2): p. 135-137.
4. Terry, S.C., J.H. Jerman, and J.B. Angell, *Gas-Chromatographic Air Analyzer Fabricated on a Silicon-Wafer.* Ieee Transactions on Electron Devices, 1979. **26**(12): p. 1880-1886.
5. Manz, A., N. Graber, and H.M. Widmer, *Miniaturized Total Chemical-Analysis Systems - a Novel Concept for Chemical Sensing.* Sensors and Actuators B-Chemical, 1990. **1**(1-6): p. 244-248.
6. Golay, M.J.E., *Vapor Phase Chromatography and the Telegrapher's Equation.* Analytical Chemistry, 1957. **29**(6): p. 928-932.
7. Giddings, J.C., *Comparison of the Theoretical Limit of Separating Ability in Gas and Liquid Chromatography.* Analytical Chemistry, 1964. **36**(10): p. 1890-1892.
8. Van Sant, M.J., *Gas Chromatography*, in *Handbook of instrumental techniques for analytical chemistry*, F.A. Settle, Editor. 1997, Prentice Hall PTR: Upper Saddle River, NJ. p. 125-146.
9. Knox, J.H. and M.T. Gilbert, *Kinetic Optimization of Straight Open-Tubular Liquid-Chromatography.* Journal of Chromatography, 1979. **186**(DEC): p. 405-418.
10. Jorgenson, J.W. and E.J. Guthrie, *Liquid-Chromatography in Open-Tubular Columns - Theory of Column Optimization with Limited Pressure and Analysis Time, and Fabrication of Chemically Bonded Reversed-Phase Columns on Etched Borosilicate Glass-Capillaries.* Journal of Chromatography, 1983. **255**(JAN): p. 335-348.
11. Knox, J.H., *Theoretical Aspects of Lc with Packed and Open Small-Bore Columns.* Journal of Chromatographic Science, 1980. **18**(9): p. 453-461.
12. Manz, A., Y. Miyahara, J. Miura, Y. Watanabe, H. Miyagi, and K. Sato, *Design of an Open-Tubular Column Liquid Chromatograph Using Silicon Chip Technology.* Sensors and Actuators B-Chemical, 1990. **1**(1-6): p. 249-255.
13. Harrison, D.J., K. Fluri, K. Seiler, Z.H. Fan, C.S. Effenhauser, and A. Manz, *Micromachining a Miniaturized Capillary Electrophoresis-Based Chemical-Analysis System on a Chip.* Science, 1993. **261**(5123): p. 895-897.
14. Zhang, C.X. and A. Manz, *Narrow sample channel injectors for capillary electrophoresis on microchips.* Analytical Chemistry, 2001. **73**(11): p. 2656-2662.

15. Incropera, F.P. and D.P. DeWitt, *Fundamentals of heat and mass transfer*. 4th ed. 1996, New York: Wiley.
16. E.I. DuPont de Nemours and Company, 1996, Ashmead, J.W., C.T. Blaisdell, M.H. Johnson, J.K. Nyquist, J.A. Perrotto, and J.F. Ryley, Jr., *Integrated Chemical Processing Apparatus and Processes for the Preparation Thereof*, Patent **5,534,328**, United States of America
17. E.I. DuPont de Nemours and Company, 1997, Ashmead, J.W., C.T. Blaisdell, M.H. Johnson, J.K. Nyquist, J.A. Perrotto, and J.F. Ryley, Jr., *Integrated Chemical Processing Apparatus and Processes for the Preparation Thereof*, Patent **5,960,763**, United States of America
18. E.I. DuPont de Nemours and Company, 1998, Ryley, J.F., Jr., J.A. Perrotto, M. Oren, and R.J. Riegert, *Waveguide Sensing Element for Use in a Sample Medium and Method of Rear-Firing Electromagnetic Radiation*, Patent **5,724,151**, United States of America
19. Ehrfeld, W., V. Hessel, and H. Löwe, *Microreactors : new technology for modern chemistry*. 1st ed. 2000, Weinheim ; New York: Wiley-VCH. xi, 288 p.
20. Srinivasan, R., I.M. Hsing, P.E. Berger, K.F. Jensen, S.L. Firebaugh, M.A. Schmidt, M.P. Harold, J.J. Lerou, and J.F. Ryley, *Micromachined reactors for catalytic partial oxidation reactions.* AIChE Journal, 1997. **43**(11): p. 3059-3069.
21. Chambers, R.D., J. Hutchinson, and G. Sandford, *Recent studies at Durham on direct fluorination.* Journal of Fluorine Chemistry, 1999. **100**(1-2): p. 63-73.
22. Lal, G.S., G.P. Pez, and R.G. Syvret, *Electrophilic NF fluorinating agents.* Chemical Reviews, 1996. **96**(5): p. 1737-1755.
23. de Mas, N., A. Gunther, M.A. Schmidt, and K.F. Jensen, *Microfabricated multiphase reactors for the selective direct fluorination of aromatics.* Industrial & Engineering Chemistry Research, 2003. **42**(4): p. 698-710.
24. Quiram, D.J. and Massachusetts Institute of Technology. Dept. of Chemical Engineering., *Characterization and systems integration of microreactors*. 2001. p. 327 leaves.
25. Ajmera, S.K., M.W. Losey, K.F. Jensen, and M.A. Schmidt, *Microfabricated packed-bed reactor for phosgene synthesis.* AIChE Journal, 2001. **47**(7): p. 1639-1647.
26. Fogler, H.S., *Elements of chemical reaction engineering*. 3rd ed. Prentice-Hall international series in the physical and chemical engineering sciences. 1999, Upper Saddle River, N.J.: Prentice Hall PTR. xxx, 967 p.
27. Ajmera, S.K., *Microchemical Systems for Kinetic Studies of Catalytic Processes*, in *Chemical Engineering*. 2002, Massacusetts Institute of Technology: Cambridge, MA. p. 274.
28. Muller, A., K. Drese, H. Gnaser, M. Hampe, V. Hessel, H. Lowe, S. Schmitt, and R. Zapf, *Fast preparation and testing methods using a microstructured modular reactor for parallel gas phase catalyst screening.* Catalysis Today, 2003. **81**(3): p. 377-391.
29. Mills, P.L. and J.F. Nicole, *A novel reactor for high-throughput screening of gas-solid catalyzed reactions.* Chemical Engineering Science, 2004. **59**(22-23): p. 5345-5354.

30. Jensen, K.F., *Microreaction engineering - is small better?* Chemical Engineering Science, 2001. **56**(2): p. 293-303.
31. Williamson, K.L., *Macroscale and microscale organic experiments*. 2nd ed. 1994, Lexington, Mass.: D.C. Heath and Company.
32. Plante, O.J., E.R. Palmacci, and P.H. Seeberger, *Automated solid-phase synthesis of oligosaccharides.* Science, 2001. **291**(5508): p. 1523-1527.
33. Seeberger, P.H., *Automated carbohydrate synthesis to drive chemical glycomics.* Chemical Communications, 2003(10): p. 1115-1121.
34. Hong, J.W. and S.R. Quake, *Integrated nanoliter systems.* Nature Biotechnology, 2003. **21**(10): p. 1179-1183.
35. Haswell, S.J., R.J. Middleton, B. O'Sullivan, V. Skelton, P. Watts, and P. Styring, *The application of micro reactors to synthetic chemistry.* Chemical Communications, 2001(5): p. 391-398.
36. Jähnisch, K., V. Hessel, H. Löwe, and M. Baerns, *Chemistry in microstructured reactors.* Angewandte Chemie-International Edition, 2004. **43**(4): p. 406-446.
37. Inoue, T., E.R. Murphy, M.A. Schmidt, and K.F. Jensen. *Microreactor Direct Synthesis of hydrogen Peroxide from Hydrogen and Oxygen*. in *7th International Conference on Microreaction Technology (IMRET 7)*. 2003. Lausanne, Switzerland.
38. Perozziello, G., *Packaging of Microsystems*, in *Microsystem engineering of lab-on-a-chip devices*, O. Geschke, H. Klank, and P. Tellemann, Editors. 2004, Wiley-VCH: Weinheim. p. 183-212.
39. Lee, Y.C., B.A. Parviz, J.A. Chiou, and S.C. Chen, *Packaging for microelectromechanical and nanoelectromechanical systems.* Ieee Transactions on Advanced Packaging, 2003. **26**(3): p. 217-226.
40. Fredrickson, C.K. and Z.H. Fan, *Macro-to-micro interfaces for microfluidic devices.* Lab on a Chip, 2004. **4**(6): p. 526-533.
41. Jensen, K.F., *Silicon-based microchemical systems: Characteristics and applications.* Mrs Bulletin, 2006. **31**(2): p. 101-107.
42. Jhunjhunwala, M., *Control of Fluid Path on Microscale*, in *Chemical Engineering*. 2003, Massachusetts Institute of Technology: Cambridge, MA.
43. Khan, S.A., A. Günther, M.A. Schmidt, and K.F. Jensen, *Microfluidic synthesis of colloidal silica.* Langmuir, 2004. **20**(20): p. 8604-8611.
44. McDonald, J.C., D.C. Duffy, J.R. Anderson, D.T. Chiu, H.K. Wu, O.J.A. Schueller, and G.M. Whitesides, *Fabrication of microfluidic systems in poly(dimethylsiloxane).* Electrophoresis, 2000. **21**(1): p. 27-40.
45. Günther, A., S.A. Khan, M. Thalmann, F. Trachsel, and K.F. Jensen, *Transport and reaction in microscale segmented gas-liquid flow.* Lab on a Chip, 2004. **4**(4): p. 278-286.
46. Arana, L.R., S.B. Schaevitz, A.J. Franz, M.A. Schmidt, and K.F. Jensen, *A microfabricated suspended-tube chemical reactor for thermally efficient fuel processing.* Journal of Microelectromechanical Systems, 2003. **12**(5): p. 600-612.
47. Arana, L.R. and Massachusetts Institute of Technology. Dept. of Chemical Engineering., *High-temperature microfluidic systems for thermally-efficient fuel processing*. 2003. p. 238 p.

48. Nittis, V., R. Fortt, C.H. Legge, and A.J. de Mello, *A high-pressure interconnect for chemical microsystem applications.* Lab on a Chip, 2001. **1**(2): p. 148-152.
49. Meng, E., S.Y. Wu, and Y.C. Tai, *Silicon couplers for microfluidic applications.* Fresenius Journal of Analytical Chemistry, 2001. **371**(2): p. 270-275.
50. Gray, B.L., D. Jaeggi, N.J. Mourlas, B.P. van Drieenhuizen, K.R. Williams, N.I. Maluf, and G.T.A. Kovacs, *Novel interconnection technologies for integrated microfluidic systems.* Sensors and Actuators a-Physical, 1999. **77**(1): p. 57-65.
51. Pan, T., A. Baldi, and B. Ziaie, *A reworkable adhesive-free interconnection technology for microfluidic systems.* Journal of Microelectromechanical Systems, 2006. **15**(1): p. 267-272.
52. Han, K.H. and A.B. Frazier, *Reliability aspects of packaging and integration technology for microfluidic systems.* Ieee Transactions on Device and Materials Reliability, 2005. **5**(3): p. 452-457.
53. Gonzalez, C., S.D. Collins, and R.L. Smith, *Fluidic interconnects for modular assembly of chemical microsystems.* Sensors and Actuators B-Chemical, 1998. **49**(1-2): p. 40-45.
54. Igata, E., M. Arundell, H. Morgan, and J.M. Cooper, *Interconnected reversible lab-on-a-chip technology.* Lab on a Chip, 2002. **2**(2): p. 65-69.
55. Lee, W.W., L.T. Nguyen, and G.S. Selvaduray, *Solder joint fatigue models: review and applicability to chip scale packages.* Microelectronics Reliability, 2000. **40**(2): p. 231-244.
56. Nah, J.W. and K.W. Paik, *Investigation of flip chip under bump metallization systems of Cu pads.* Ieee Transactions on Components and Packaging Technologies, 2002. **25**(1): p. 32-37.
57. Tu, K.N. and K. Zeng, *Tin-lead (SnPb) solder reaction in flip chip technology.* Materials Science & Engineering R-Reports, 2001. **34**(1): p. 1-58.
58. Pang, J.H.L., D.Y.R. Chong, and T.H. Low, *Thermal cycling analysis of flip-chip solder joint reliability.* Ieee Transactions on Components and Packaging Technologies, 2001. **24**(4): p. 705-712.
59. Goldmann, L.S. and B. Krall, *Measurement of solder--flux--vapor surface tension by a modified maximum bubble pressure technique.* Review of Scientific Instruments, 1976. **47**(3): p. 324-325.
60. Gusak, A.M. and K.N. Tu, *Kinetic theory of flux-driven ripening.* Physical Review B, 2002. **66**(11): p. -.
61. Kim, P.G., J.W. Jang, T.Y. Lee, and K.N. Tu, *Interfacial reaction and wetting behavior in eutectic SnPb solder on Ni/Ti thin films and Ni foils.* Journal of Applied Physics, 1999. **86**(12): p. 6746-6751.
62. Katsura, K., T. Hayashi, F. Ohira, S. Hata, and K. Iwashita, *A Novel Flip-Chip Interconnection Technique Using Solder Bumps for High-Speed Photoreceivers.* Journal of Lightwave Technology, 1990. **8**(9): p. 1323-1327.
63. Hunziker, W., W. Vogt, H. Melchior, D. Leclerc, P. Brosson, F. Pommereau, R. Ngo, P. Doussiere, F. Mallecot, T. Fillion, I. Wamsler, and G. Laube, *Self-Aligned Flip-Chip Packaging of Tilted Semiconductor Optical Amplifier Arrays on Si Motherboard.* Electronics Letters, 1995. **31**(6): p. 488-490.

64. Wale, M.J. and C. Edge, *Self-Aligned Flip-Chip Assembly of Photonic Devices with Electrical and Optical Connections.* Ieee Transactions on Components Hybrids and Manufacturing Technology, 1990. **13**(4): p. 780-786.
65. Boyce, M.P., *Transport and Storage of Fluids*, in *Perry's Chemical Engineers' Handbook*, R.H. Perry, D.W. Green, and J.O. Maloney, Editors. 1997, McGraw-Hill: New York. p. 10-83.
66. Swanson, P., R. Gelbart, E. Atlas, L. Yang, T. Grogan, W.F. Butler, D.E. Ackley, and E. Sheldon, *A fully multiplexed CMOS biochip for DNA analysis.* Sensors and Actuators B-Chemical, 2000. **64**(1-3): p. 22-30.
67. Yang, J.M., J. Bell, Y. Huang, M. Tirado, D. Thomas, A.H. Forster, R.W. Haigis, P.D. Swanson, R.B. Wallace, B. Martinsons, and M. Krihak, *An integrated, stacked microlaboratory for biological agent detection with DNA and immunoassays.* Biosensors & Bioelectronics, 2002. **17**(6-7): p. 605-618.
68. Enikov, E.T. and J.G. Boyd, *Electroplated electro-fluidic interconnects for chemical sensors.* Sensors and Actuators a-Physical, 2000. **84**(1-2): p. 161-164.
69. Tsau, C.H., S.M. Spearing, and M.A. Schmidt, *Characterization of wafer-level thermocompression bonds.* Microelectromechanical Systems, Journal of, 2004. **13**(6): p. 963-971.
70. Peles, Y., V.T. Srikar, T.S. Harrison, C. Protz, A. Mracek, and S.M. Spearing, *Fluidic packaging of microengine and microrocket devices for high-pressure and high-temperature operation.* Journal of Microelectromechanical Systems, 2004. **13**(1): p. 31-40.
71. London, A.P., A.A. Ayon, A.H. Epstein, S.M. Spearing, T. Harrison, Y. Peles, and J.L. Kerrebrock, *Microfabrication of a high pressure bipropellant rocket engine.* Sensors and Actuators a-Physical, 2001. **92**(1-3): p. 351-357.
72. Timko, M.T. and Massachusetts Institute of Technology. Dept. of Chemical Engineering., *Acoustic emulsions of liquid, near-critical carbon dioxide and water : application to synthetic chemistry through reaction engineering*. 2004. p. 2 v. (372 leaves).
73. Timko, M.T., K.A. Smith, R.L. Danheiser, J.I. Steinfeld, and J.W. Tester, *Reaction rates in ultrasonic emulsions of dense carbon dioxide and water.* AIChE Journal, 2006. **52**(3): p. 1127-1141.
74. Watanabe, K. and E.R. Murphy, *Nickel Coated Microfluidic Devices for Cryogenic Hypofluorite Synthesis.* Unpublished Data, 2004.
75. Ratner, D.M., E.R. Murphy, M. Jhunjhunwala, D.A. Snyder, K.F. Jensen, and P.H. Seeberger, *Microreactor-based reaction optimization in organic chemistry glycosylation as a challenge.* Chemical Communications, 2005(5): p. 578-580.
76. Sears, P. and C.H. Wong, *Enzyme action in glycoprotein synthesis.* Cellular and Molecular Life Sciences, 1998. **54**(3): p. 223-252.
77. Varki, A., *Biological Roles of Oligosaccharides - All of the Theories Are Correct.* Glycobiology, 1993. **3**(2): p. 97-130.
78. Lehmann, J., *Carbohydrates : structure and biology*. Thieme organic chemistry monograph series. 1998, Stuttgart ; New York: G. Thieme Verlag. xiv, 274 p.
79. Sears, P. and C.H. Wong, *Toward automated synthesis of oligosaccharides and glycoproteins.* Science, 2001. **291**(5512): p. 2344-2350.

80. Toshima, K. and K. Tatsuta, *Recent Progress in O-Glycosylation Methods and Its Application to Natural-Products Synthesis.* Chemical Reviews, 1993. **93**(4): p. 1503-1531.
81. Carlson, R. and J.E. Carlson, *Design and optimization in organic synthesis*. 2nd rev. and enl. ed. Data handling in science and technology, v. 24. 2005, Amsterdam ; San Diego, CA: Elsevier. xx, 574 p.
82. Garegg, P.J. and T. Norberg, *Observations on Silver Trifluoromethane Sulfonate-Promoted Syntheses of 1,2-Trans-Glycosides from Acylated Glycosyl Bromides.* Acta Chemica Scandinavica Series B-Organic Chemistry and Biochemistry, 1979. **33**(2): p. 116-118.
83. Fügedi, P., A. Lipták, P. Nanasi, and A. Neszmélyi, *Retention of the Anomeric Configuration in the Imidate Procedure - Synthesis of Disaccharides Containing Alpha-L-Rhamnopyranosyl and Alpha-D-Mannopyranosyl Groups.* Carbohydrate Research, 1982. **107**(1): p. C5-C8.
84. Ratner, D.M., *Solution-phase and automated solid-phase synthesis of high-mannose oligosaccharides : application to carbohydrate microarrays and biological studies*, in *Chemistry*. 2004, Massachusetts Institute of Technology: Cambridge, MA. p. 355.
85. Geankoplis, C.J., *Transport processes and unit operations*. 3rd ed. 1993, Engelwood Cliffs, N.J.: PTR Prentice Hall. xiii, 921 p.
86. Guram, A.S. and S.L. Buchwald, *Palladium-Catalyzed Aromatic Aminations with in-Situ Generated Aminostannanes.* Journal of the American Chemical Society, 1994. **116**(17): p. 7901-7902.
87. Hartwig, J.F., M. Kawatsura, S.I. Hauck, K.H. Shaughnessy, and L.M. Alcazar-Roman, *Room-temperature palladium-catalyzed amination of aryl bromides and chlorides and extended scope of aromatic C-N bond formation with a commercial ligand.* Journal of Organic Chemistry, 1999. **64**(15): p. 5575-5580.
88. Old, D.W., J.P. Wolfe, and S.L. Buchwald, *A highly active catalyst for palladium-catalyzed cross-coupling reactions: Room-temperature Suzuki couplings and amination of unactivated aryl chlorides.* Journal of the American Chemical Society, 1998. **120**(37): p. 9722-9723.
89. Schoenbe.A, Bartolet.I, and R.F. Heck, *Palladium-Catalyzed Carboalkoxylation of Aryl, Benzyl, and Vinylic Halides.* Journal of Organic Chemistry, 1974. **39**(23): p. 3318-3326.
90. Schoenbe.A and R.F. Heck, *Palladium-Catalyzed Amidation of Aryl, Heterocyclic, and Vinylic Halides.* Journal of Organic Chemistry, 1974. **39**(23): p. 3327-3331.
91. Schlummer, B. and U. Scholz, *Palladium-catalyzed C-N and C-O coupling - A practical guide from an industrial vantage point.* Advanced Synthesis & Catalysis, 2004. **346**(13-15): p. 1599-1626.
92. Plante, O.J., S.L. Buchwald, and P.H. Seeberger, *Halobenzyl ethers as protecting groups for organic synthesis.* Journal of the American Chemical Society, 2000. **122**(29): p. 7148-7149.
93. Nishiyama, M., T. Yamamoto, and Y. Koie, *Synthesis of N-arylpiperazines from aryl halides and piperazine under a palladium tri-tert-butylphosphine catalyst.* Tetrahedron Letters, 1998. **39**(7): p. 617-620.

94. Singer, R.A. and S.L. Buchwald, *Preparation of 2-amino-2 '-hydroxy-1,1 '-binaphthyl and N-arylated 2-amino-1,1 '-binaphthyl derivatives via palladium-catalyzed amination.* Tetrahedron Letters, 1999. **40**(6): p. 1095-1098.
95. Guram, A.S., R.A. Rennels, and S.L. Buchwald, *A Simple Catalytic Method for the Conversion of Aryl Bromides to Arylamines.* Angewandte Chemie-International Edition in English, 1995. **34**(12): p. 1348-1350.
96. Beller, M., M. Eckert, F. Vollmuller, S. Bogdanovic, and H. Geissler, *Palladium-catalyzed amidocarbonylation - A new, efficient synthesis of N-acyl amino acids.* Angewandte Chemie-International Edition in English, 1997. **36**(13-14): p. 1494-1496.
97. Riermeier, T.H., A. Zapf, and M. Beller, *Palladium-catalyzed C-C- and C-N-coupling reactions of aryl chlorides.* Topics in Catalysis, 1997. **4**(3-4): p. 301-309.
98. Perry, R.H., D.W. Green, and J.O. Maloney, *Perry's Chemical Engineers' Handbook*. 7th ed. 1997, New York: McGraw-Hill.
99. Blaser, H.U., A. Indolese, F. Naud, U. Nettekoven, and A. Schnyder, *Industrial R&D on catalytic C-C and C-N coupling reactions: A personal account on goals, approaches and results.* Advanced Synthesis & Catalysis, 2004. **346**(13-15): p. 1583-1598.
100. Miller, P.W., N.J. Long, A.J. de Mello, R. Vilar, J. Passchier, and A. Gee, *Rapid formation of amides via carbonylative coupling reactions using a microfluidic device.* Chemical Communications, 2006(5): p. 546-548.
101. Felder, R.M. and R.W. Rousseau, *Elementary principles of chemical processes*. 2nd ed. Wiley series in chemical engineering. 1986, New York: Wiley. xix, 668 p.
102. Al-Qahtani, M.H. and V.W. Pike, *Palladium(II)-mediated C-11-carbonylative coupling of diaryliodonium salts with organostannanes - a new, mild and rapid synthesis of aryl [C-11]ketones.* Journal of the Chemical Society-Perkin Transactions 1, 2000(6): p. 1033-1036.
103. Kihlberg, T. and B. Långström, *Biologically active C-11-labeled amides using palladium-mediated reactions with aryl halides and C-11 carbon monoxide.* Journal of Organic Chemistry, 1999. **64**(25): p. 9201-9205.
104. Rahman, O., T. Kihlberg, and B. Långström, *Synthesis of ^{11}C-/^{13}C-ketones by Suzuki coupling.* European Journal of Organic Chemistry, 2004(3): p. 474-478.
105. Itsenko, O., T. Kihlberg, and B. Långström, *Synthesis of aliphatic [carbonyl-^{11}C]esters using [^{11}C]carbon monoxide.* European Journal of Organic Chemistry, 2005(17): p. 3830-3834.
106. Långström, B., T. Kihlberg, M. Bergström, G. Antoni, M. Björkman, B.H. Forngren, T. Forngren, P. Hartvig, K. Markides, U. Yngve, and M. Ögren, *Compounds labelled with short-lived β^+-emitting radionuclides and some applications in life sciences. The importance of time as a parameter.* Acta Chemica Scandinavica, 1999. **53**(9): p. 651-669.
107. Rahman, O., T. Kihlberg, and B. Långström, *Aryl triflates and [^{11}C]/(^{13}C)carbon monoxide in the synthesis of ^{11}C-/^{13}C-amides.* Journal of Organic Chemistry, 2003. **68**(9): p. 3558-3562.
108. Chen, J.T. and A. Sen, *Mechanism of Transition-Metal-Catalyzed Double Carbonylation Reactions - Synthesis and Reactivity of Benzoylformyl Complexes*

of Palladium(Ii) and Platinum(Ii). Journal of the American Chemical Society, 1984. **106**(5): p. 1506-1507.
109. Pangborn, A.B., M.A. Giardello, R.H. Grubbs, R.K. Rosen, and F.J. Timmers, *Safe and convenient procedure for solvent purification.* Organometallics, 1996. **15**(5): p. 1518-1520.
110. Prausnitz, J.M., R.N. Lichtenthaler, and E.G.d. Azevedo, *Molecular thermodynamics of fluid-phase equilibria*. 3rd ed. 1999, Upper Saddle River, N.J.: Prentice-Hall PTR. xvii, 860 p.
111. Fronabarger, J., A. Schuman, R.D. Chapman, W. Fleming, and W.B. Sanborn. *Chemistry and Development of BNCP, A Novel DDT Explosive*. in *31st AIAA-Joint Propulsion Conference*. 1995. San Diego, CA: American Institute of Aeronautics and Astronautics Inc.
112. 1978, Gilligan, W.H. and M.J. Kamlet, *Method of Preparing The Acid Copper Salt of 5-Nitrotetrazole*, Patent **4,093,623**, U.S.A.
113. Bates, L.R. *The Potential of Tetrazoles in Initiating Explosive Systems*. in *Thirteenth Symposium on Explosives and Pyrotechnics*. 1986. Hilton Head, SC.
114. Williams, M.D. to K.F. Jensen, E.R. Murphy, and J.K. Kralj, *Project Sponsor Conference Call*. 2005, Pacific Scientific: Chandler, AZ and Cambridge, MA.
115. Morosin, B., R.G. Dunn, R. Assink, T.M. Massis, J. Fronabarger, and E.N. Duesler, *The secondary explosive tetraammine-cis-bis(5-nitro-2H-tetrazolato-N^2)cobalt(III) perchlorate at 293 and 213 K.* Acta Crystallographica Section C-Crystal Structure Communications, 1997. **53**: p. 1609-1611.
116. Wootton, R.C.R., R. Fortt, and A.J. de Mello, *On-chip generation and reaction of unstable intermediates-monolithic nanoreactors for diazonium chemistry: Azo dyes.* Lab on a Chip, 2002. **2**(1): p. 5-7.
117. Fortt, R., R.C.R. Wootton, and A.J. de Mello, *Continuous-flow generation of anhydrous diazonium species: Monolithic microfluidic reactors for the chemistry of unstable intermediates.* Organic Process Research & Development, 2003. **7**(5): p. 762-768.
118. Günther, P.M., F. Möller, T. Henkel, J.M. Köhler, and G.A. Groß, *Formation of monomeric and novolak azo dyes in nanofluid segments by use of a double injector chip reactor.* Chemical Engineering & Technology, 2005. **28**(4): p. 520-527.
119. Hegarty, A.F., *Kinetics and mechanisms of reactions involving diazonium and diazo groups*, in *The chemistry of diazonium and diazo groups*, S. Patai, Editor. 1978, Wiley: Chichester ; New York. p. 511-591.
120. Ridd, J.H., *Nitrosation, Diazotisation, and Deamination.* Quarterly Reviews of the Chemical Society, 1961. **15**(4): p. 418-441.
121. Larkworthy, L.F., *Nitrosation, Diazotisation and Deamination. Part VIII. The Diazotisation of Weakly Basic Amines in Dilute Perchloric Acid.* Journal of the Chemical Society, 1959: p. 3304-3308.
122. de Fabrizio, E.C.R., E. Kalatzis, and J.H. Ridd, *Nitrosation, Diazotisation, and Deamination. Part XIII. Substituent Effects of the Nitrosation of Anilinium Ions.* Journal of the Chemical Society B: Physical Organic, 1966: p. 533-539.
123. Froment, G.F. and K.B. Bischoff, *Chemical reactor analysis and design*. 2nd ed. Wiley series in chemical engineering. 1990, New York: Wiley. xxxiv, 664 p.

124. *Dissociation Constants of Inorganic Acids and Bases*, in *CRC Handbook of Chemistry and Physics*, D.R. Lide, Editor. 2004, CRC Press.
125. Galli, C., *Substituent Effects on the Sandmeyer Reaction - Quantitative Evidence for Rate-Determining Electron-Transfer.* Journal of the Chemical Society-Perkin Transactions 2, 1984(5): p. 897-902.
126. McDonald, J.C. and G.M. Whitesides, *Poly(dimethylsiloxane) as a material for fabricating microfluidic devices.* Accounts of Chemical Research, 2002. **35**(7): p. 491-499.
127. Chapra, S.C. and R.P. Canale, *Numerical methods for engineers : with programming and software applications*. 3rd ed. 1998, Boston: WCB/McGraw-Hill. xix, 924 p.
128. Awtrey, A.D. and R.E. Connick, *Absorption spectra of I_2, I_3^-, I^-, IO^-,$S_4O_6^{--}$, and $S_2O_3^{--}$. Heat of the reaction $I_3^- = I_2 + I^-$.* Journal of the American Chemical Society, 1951. **73**: p. 1842-1843.
129. Panic, S., S. Loebbecke, T. Tuercke, J. Antes, and D. Boškovic, *Experimental approaches to a better understanding of mixing performance of microfluidic devices.* Chemical Engineering Journal, 2004. **101**(1-3): p. 409-419.

Appendix A: Fabrication Details

The fabrication processes for the devices described in this thesis are presented as run sheets. The run sheets provide the facility, cleanliness grade, and equipment used for each process step. Unless otherwise specified, devices were fabricated in one of the Microsystem Technology Laboratories (MTL) at MIT. MTL consists of 3 facilities: Integrated Circuits Laboratory (ICL), Technology Research Laboratory (TRL), and Exploratory Materials Laboratory (EML). Cleanliness is described by a color scale where brown is CMOS compatible, green indicates general silicon processing, yellow is KOH etch or Pyrex® compatible, red is for gold and III-V metals general processing, and purple indicates SU-8 processing. The equipment used is listed by its abbreviated name in the CORAL scheduling and management software for the Microsystems Technology Laboratory at MIT. A subset of the more common machines and their abbreviations are presented in Table A.1.

Table A.1: CORAL Abbreviations

Abbreviation	Equipment
A2-WetOxBond	MRL Industries Model 718 System Atmospheric Oxidation Furnace
diesaw	Disco Abrasive System Model DAD-2H/6T
EbeamAu	Temescal Semiconductor Products Electron Beam Evaporator
EV1	Electronic Visions EV620 Mask Aligner
EV501	Electronic Visions EV620-501 Wafer Aligner/Bonder
LAM490B	Lam Research Model 490B Reactive Ion Etch
Postbake	Blue M Model DDC-146C (120°C)
Prebake	Blue M Model DDC-146C (95°C)
sts-1	ICP Deep Trench Etching System (4” wafers)
sts-2	ICP Deep Trench Etching System (6” wafers)

Devices for Solder Packaging Testing

General process: First grow a protective oxide on the wafers for sts etching. Then pattern and etch the backside of the silicon wafer to create the through-holes for the inlet and outlet ports. Then, etch the backside of the silicon wafer to create flow channels. Next, anodically bond the pyrex wafer to seal the flow channels. Finally deposit copper around the flow ports and diesaw the devices.

Starting material: 4-inch Double Side Polished Silicon Wafer
4-inch Pyrex Wafer

STEP	FAC	MACHINE	ACTION	NOTES	CODE
1			**Pattern and etch flow ports**		
1.1			*Grow protective oxide for STS Etch*		
1.1.1	TRL	rcaTRL	RCA clean		
1.1.2	TRL	A2-WetOxBond	Grow 5000Å wet oxide		
1.2			*Photolithography for BOE Etch*		
1.2.1	TRL	HMDS	Coat wafer with HMDS	Program 3	
1.2.2	TRL	coater	Spin Coat photoresist AZP5460 to 10µm		
1.2.3	TRL	prebake	Bake at 90°C for 60 minutes		
1.2.4	TRL	EV1	Expose resist for 22.5 seconds to UV	Mask 1	
1.2.5	TRL	photowet-1	Development, 3min		
1.2.6	TRL	prebake	Postbake at 90°C for 30 minutes		
1.2.7	TRL	coater	Spin Coat photoresist OCG825 to 1µm on backside		
1.2.8	TRL	prebake	Bake at 90°C for 30 minutes		
1.3			*Pattern Oxide with BOE Etch*		
1.3.1	TRL	acidhood2	BOE Etch 7min		
1.4			*STS etch topside flow ports*		
1.4.1	TRL	STS1	STS etch, recipe MIT69, 200µm		
1.4.2	TRL	acidhood2	Remove resist using piranha		
2			**Pattern and etch flow channels**		
2.1			*Photolithography for BOE Etch*		
2.1.1	TRL	HMDS	Coat wafer with HMDS		
2.1.2	TRL	coater	Spin Coat photoresist AZP5460 to 10µm		
2.1.3	TRL	prebake	Bake at 90°C for 60 minutes		
2.1.4	TRL	EV1	Expose resist for 22.5 seconds to UV	Mask 2	
2.1.5	TRL	photowet-1	Development, 3min		
2.1.6	TRL	prebake	Postbake at 90°C for 30 minutes		
2.1.7	TRL	coater	Spin Coat photoresist OCG825 to 1µm on frontside		
2.1.8	TRL	prebake	Bake at 90°C for 30 minutes		
2.2			*Pattern Oxide with BOE Etch*		
2.2.1	TRL	acidhood2	BOE Etch 7min		
2.3			*STS etch backside flow ports*		
2.3.1	TRL	STS1	STS etch, recipe MIT69, 300µm		
2.3.2	TRL	acidhood2	Remove resist using piranha		

3			**Bond Pyrex wafer and deposit copper**		
3.1			*Wafer Bonding*		
3.1.1	TRL	EV501-620	Bond Pyrex and silicon wafers		
3.2			*Apply Photoresist for Liftoff Processing*		
3.2.1	TRL	HMDS	Coat wafer with HMDS		
3.2.2	TRL	coater	Spin Coat image reversible resist		
3.2.3	TRL	prebake	Bake at 90°C for 25 minutes		
3.2.4	TRL	EV1	Expose resist for 1.5 seconds to UV	Mask 3	
3.2.6	TRL	prebake	Postbake at 104°C for 28 minutes		
3.2.5	TRL	photowet-1	Development, 2min		
3.3			*Deposit and pattern copper*		
3.3.1	TRL	ebeamAu	Deposit 200nm of Copper		
3.3.2	TRL	Au solvent hood	Acetone liftoff		
3.4	ICL	diesaw	diesaw devices		

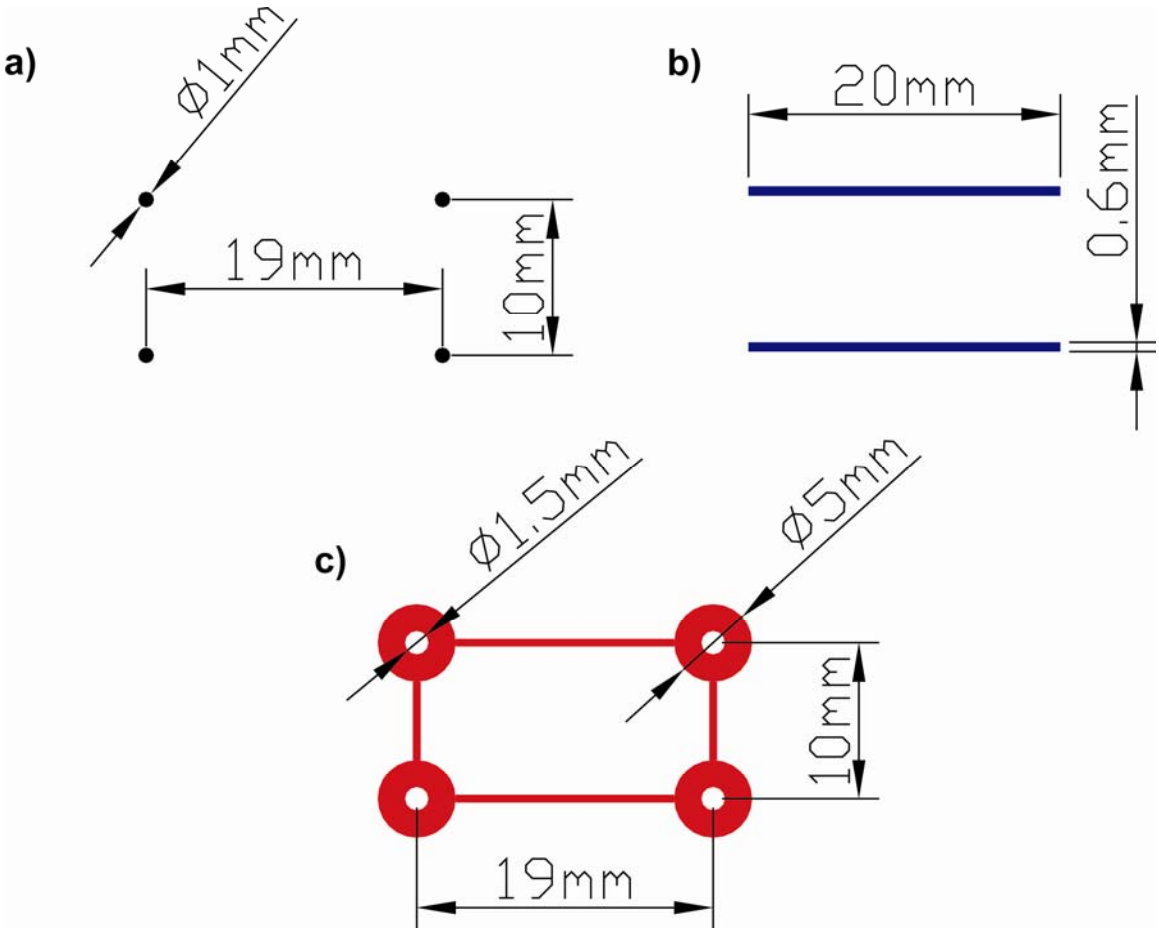

Figure A-1: Packaging Test Device Masks
a) Mask 1: Front-Side Through Holes
b) Mask 2: Back-Side Channels
c) Mask 3: Front-Side Connected Metal Bond Pads

Oligosaccharide and Carbonylation 5-Port Silicon Microreactor

General process: First grow a protective oxide on the wafers for sts etching. Then pattern and etch the backside of the silicon wafer to create the through-holes for the inlet and outlet ports. Then, etch the frontside of the silicon wafer to create flow channels. Next, oxidize and anodically bond the pyrex wafer to seal the flow channels. Finally deposit copper around the flow ports and diesaw the devices.

Starting material: 6-inch Double Side Polished Silicon Wafer
6-inch Pyrex Wafer

STEP	FAC	MACHINE	ACTION	NOTES	CODE
1			**Pattern and etch flow ports**		
1.1			*Grow protective oxide for STS Etch*		
1.1.1	TRL	rcaTRL	RCA clean		
1.1.2	TRL	A2-WetOxBond	Grow 5000Å wet oxide		
1.2			*Photolithography for BOE Etch*		
1.2.1	TRL	HMDS	Coat wafer with HMDS	Program 3	
1.2.2	TRL	coater	Spin Coat photoresist AZ9260 to 10µm		
1.2.3	TRL	prebake	Bake at 90°C for 60 minutes		
1.2.4	TRL	EV1	Expose resist for 45 seconds to UV in 3 intervals of 15sec	Mask 1	
1.2.5	TRL	photowet-1	Development, 3min AZ440		
1.2.6	TRL	coater	Coat photoresist OCG825 on frontside		
1.2.7	TRL	prebake	Bake at 90°C for 30 minutes		
1.3			*Pattern Oxide with BOE Etch*		
1.3.1	TRL	acidhood2	BOE Etch 7min		
1.4			*STS etch bottomside side flow ports*		
1.4.1	TRL	STS2	STS etch, 300µm	recipe MIT69A	
1.4.2	TRL	acidhood2	Remove resist using piranha		
2			**Pattern and etch flow channels**		
2.1			*Photolithography for BOE Etch*		
2.1.1	TRL	HMDS	Coat wafer with HMDS	Program 3	
2.1.2	TRL	coater	Spin Coat photoresist AZ9260 to 10µm		
2.1.3	TRL	prebake	Bake at 90°C for 60 minutes		
2.1.4	TRL	EV1	Expose resist for 45 seconds to UV in 3 intervals of 15sec	Mask 2	
2.1.5	TRL	photowet-1	Development, 3min AZ440		
2.1.6	TRL	coater	Coat photoresist OCG825 to 1µm on backside		
2.1.7	TRL	prebake	Bake at 90°C for 30 minutes		
2.2			*Pattern Oxide with BOE Etch*		
2.2.1	TRL	acidhood2	BOE Etch 7min		
2.3			*STS etch topside flow channels*		
2.3.1	TRL	coater	handlewafer mount		
2.3.2	TRL	STS2	STS etch, 400µm	recipe MIT69A	
2.3.3	TRL	acidhood2	Remove resist using piranha		

2.4			*Remove mask oxide and Coat channels with themal oxide*		
2.4.1	TRL	acidhood2	BOE Etch 7min		
2.4.2	TRL	acidhood2	Piranha clean wafers		
2.4.3	TRL	rcaTRL	RCA clean		
2.4.4	TRL	A2-WetOxBond	Grow 2000Å wet oxide		
3			**Bond Pyrex wafer and deposit copper**		
3.1			*Wafer Bonding*		
3.1.1	TRL	acidhood	Piranha clean wafers for bonding		
3.1.2	TRL	EV501-620	Bond Pyrex and silicon wafers		
3.3			*Deposit and pattern copper*		
3.3.1	TRL	coater	Apply shadowmask	Mask 3	
3.3.2	TRL	ebeamAu	Deposit 100nm Ti and 500nm of Copper		
3.4	ICL	diesaw	diesaw devices		

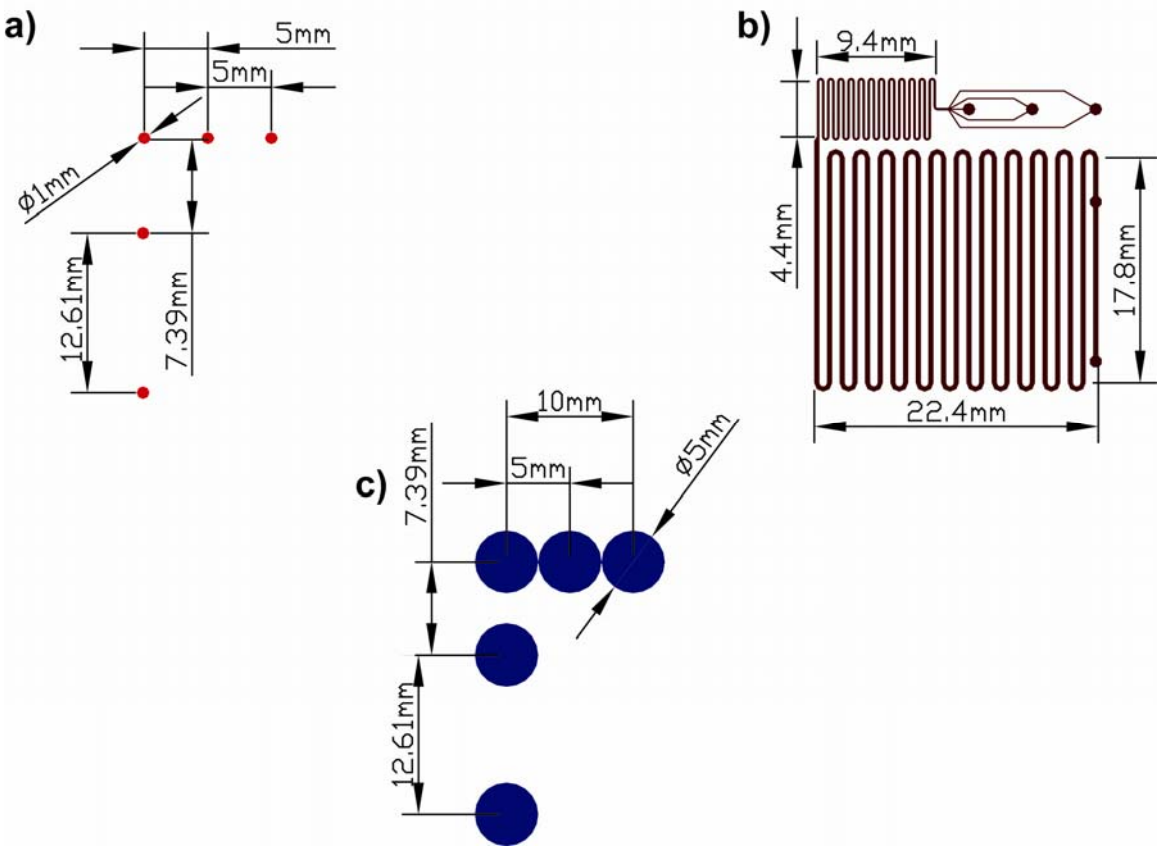

Figure A-2: 5-Port Silicon Microreactor Masks
a) Mask 1: Back-Side Through Holes
b) Mask 2: Front-Side Channel
c) Mask 3: Shadow Mask

PDMS micromixers for NaNT synthesis

General process: Construct an SU-8 mold on a silicon wafer for PDMS micromolding. Silanze the mold and cure PDMS over the mold to form devices.

Starting material: 4in Silicon wafers, Test grade, Single-side polished.

STEP	FAC	MACHINE	ACTION	NOTES	CODE
1			***Patterning of SU8 layer***		
1.1	TRL	hot plate	Dehydration bake @ 200 Celsius (60 min)		
1.2	TRL	pispinner	Spin coat 3mL of SU8-2050	750rpm for 15s then 1000rpm for 60s	
1.3	TRL	hot plate	Bake 65C 1min + ramp to 95C and hold for 30 min		
1.2	TRL	pispinner	Spin coat 3mL of SU8-2050	750rpm for 15s then 1000rpm for 60s	
1.3	TRL	hot plate	Bake 65C 1min + ramp to 95C and hold for 30 min		
1.4	TRL	EV1	UV Exposure (EV1, 9x5 seconds with 2s interval)		
1.3	TRL	hot plate	Bake 65C 1min + ramp to 95C and hold for 12 min		
2			***Development of the wafer***		
2.1	TRL	photowet	Development in PGMEA 30 min		
3			***Silanize and mold PDMS***		
3.1	66-125	bell jar	Expose to silanizing agent under vacuum	6 hours	
3.2	66-125	Oven	Pour degassed PDMS and bake at 70C	3 hours	

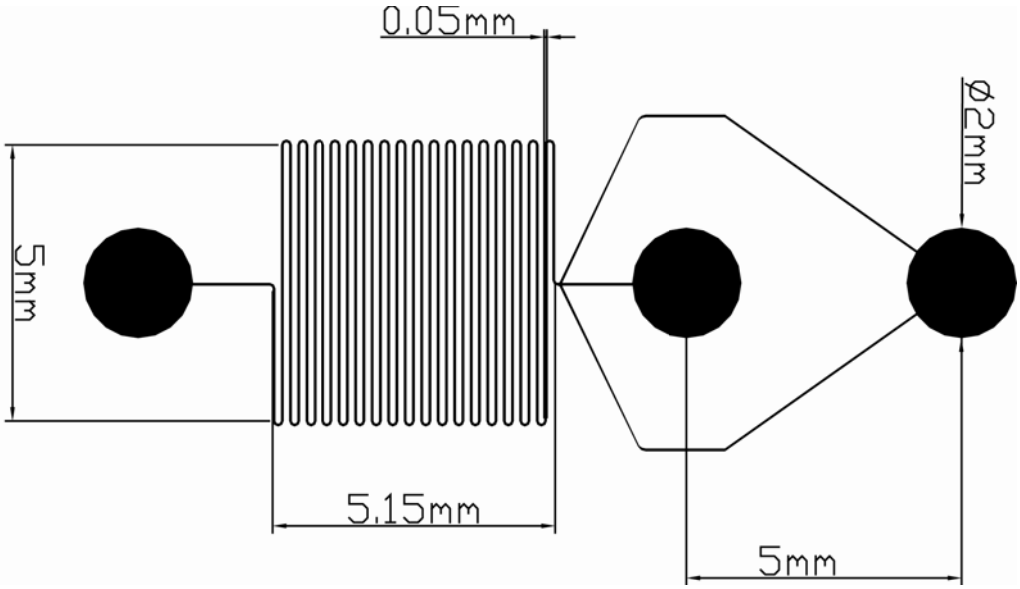

Figure A-3: SU-8 Master Mask

Silicon Micromixers for NaNT Packaging

General process: The wafers are oxidized to act as a mask for shallow KOH etching of the backside flow channels. The frontside is then patterned and etched to reveal the major flow channels through the oxide layer. Photoresist protects the exposed Si to pattern through holes for connecting to the backside flow channels. DRIE is used to partially etch these holes, the photoresist is then removed and the etching process finishes the through holes and defines the main flow channels. Lastly, two anodic bonds using pyrex wafers are used to seal the flow channels.

Materials: 6-in, double-side polished (100) Si wafer
6-in PYREX predrilled wafer
6-in PYREX

STEP	FAC	MACHINE	ACTION	NOTES	CODE
1			**OXIDIZE WAFER**		
1.1			*OXIDIZE WAFER*		
1.1.1	TRL	RCA	RCA clean wafer		
1.1.2	TRL	A2-WetOxBond	Grow 5000Å wet oxide		
2			**DEFINE BACKSIDE CHANNELS**		
2.1			*Photolithography*		
2.1.1	TRL	HMDS	Coat wafer with HMDS		
2.1.2	TRL	coater	Spincoat OCG 825 to define backside channels		
2.1.3	TRL	prebake	Bake at 95°C for 30 minutes		
2.1.4	TRL	EV1	Expose resist for 1.5 seconds (dP channel mask)	Mask 1	
2.1.5	TRL	photowet-1	Develop OCG 934:1:1, 1-3min		
2.1.6	TRL	postbake	Postbake at 95°C for 30 minutes		
2.1.7	TRL	acidhood2	BOE patterned SiO2	Need ~ 5 min in BOE	
2.1.8	TRL	acidhood2	piranha clean wafer		
2.2			*KOH Etch channels*		
2.2.1	ICL	TMAH-KOH hood	25%, 70°C KOH etch wafer to ~35 µm (~1 hr)		
2.2.2	TRL	acidhood	post KOH clean (2 piranhas; 50:1 HF dip)		
3			**OXIDIZE WAFER**		
3.1			*OXIDIZE WAFER*		
3.1.1	TRL	RCA	RCA clean wafer		
3.1.2	TRL	A2-WetOxBond	Grow 10000Å wet oxide		

4			**DEFINE FRONTSIDE CHANNELS & THRUHOLES**		
4.1			*Define frontside channels*		
4.1.1	TRL	HMDS	Coat wafer with HMDS		
4.1.2	TRL	coater	Spincoat OCG 825 to define frontside channels		
4.1.3	TRL	prebake	Bake at 95°C for 30 minutes		
4.1.4	TRL	EV1	Expose resist for 1.5 seconds (main channel mask)	Mask 2	
4.1.5	TRL	photowet-1	Develop OCG 934:1:1, 1-3min		
4.1.6	TRL	postbake	Postbake at 120°C for 30 minutes		
4.1.7	TRL	acidhood2	BOE patterned SiO_2		
4.1.8	TRL	acidhood2	piranha clean wafer		
4.2			*Define through holes*		
4.2.1	TRL	HMDS	Coat wafer with HMDS		
4.2.2	TRL	coater	Double spincoat thick photoresist AZP4620 on frontside to ~20mm		
4.2.3	TRL	prebake	Bake at 95°C for 30+ minutes		
4.2.4	TRL	EV1	Expose resist for 40 seconds to UV (Flowthrough Mask)	Mask 3	
4.2.5	TRL	photowet-1	Development, 5min		
4.2.6	TRL	prebake	Postbake at 95°C for 30 minutes		
4.3			*Attach handle wafer*		
4.3.1	TRL	coater	spincoat thick resist on handle wafer, attach wafer 1	use "target" pattern to attach wafers	
4.3.2	TRL	prebake	Postbake at 95°C 30 min		
4.4			*STS ETCH THRU HOLES*		
4.4.1	TRL	STS2	STS etch, recipe ole3, 650 um		
4.4.2	TRL	acidhood	piranha clean wafer		
4.5			*Attach handle wafer*		
4.5.1	TRL	coater	spincoat thick resist on handle wafer, attach wafer 1	"target" pattern	
4.5.2	TRL	prebake	Postbake at 95°C 30 min		

4.6			*STS ETCH THRU HOLES and MAIN CHANNELS*		
4.6.1	TRL	STS2	STS etch, recipe ole3, 200 µm		
4.6.2	TRL	acidhood	piranha clean wafer		
4.6.3	TRL	acidhood2	BOE etch to remove oxide		
4.7			*OXIDIZE WAFER*		
4.7.1	TRL	RCA	RCA clean wafer		
4.7.2	TRL	tube-a2	Grow 2000Å wet oxide		
5			**DEVICE PACKAGING**		
5.1			*CAP DEVICE*		
5.1.1	TRL	acidhood	Piranha clean wafers		
5.1.2	TRL	EV620	Align and bond predrilled-pyrex and Si wafers		
5.1.3	TRL	EV620	Align and bond wafer stack and pyrex bottom wafer	drilled pyrex from 5.1.2 will allow electric access to Si for 2nd anodic bonding step	
5.2			*DICE DEVICE*		
5.2.1	ICL	diesaw	score devices along break-away section	cut 700um deep	
5.2.2	ICL	diesaw	dice devices	cut 700um deep	

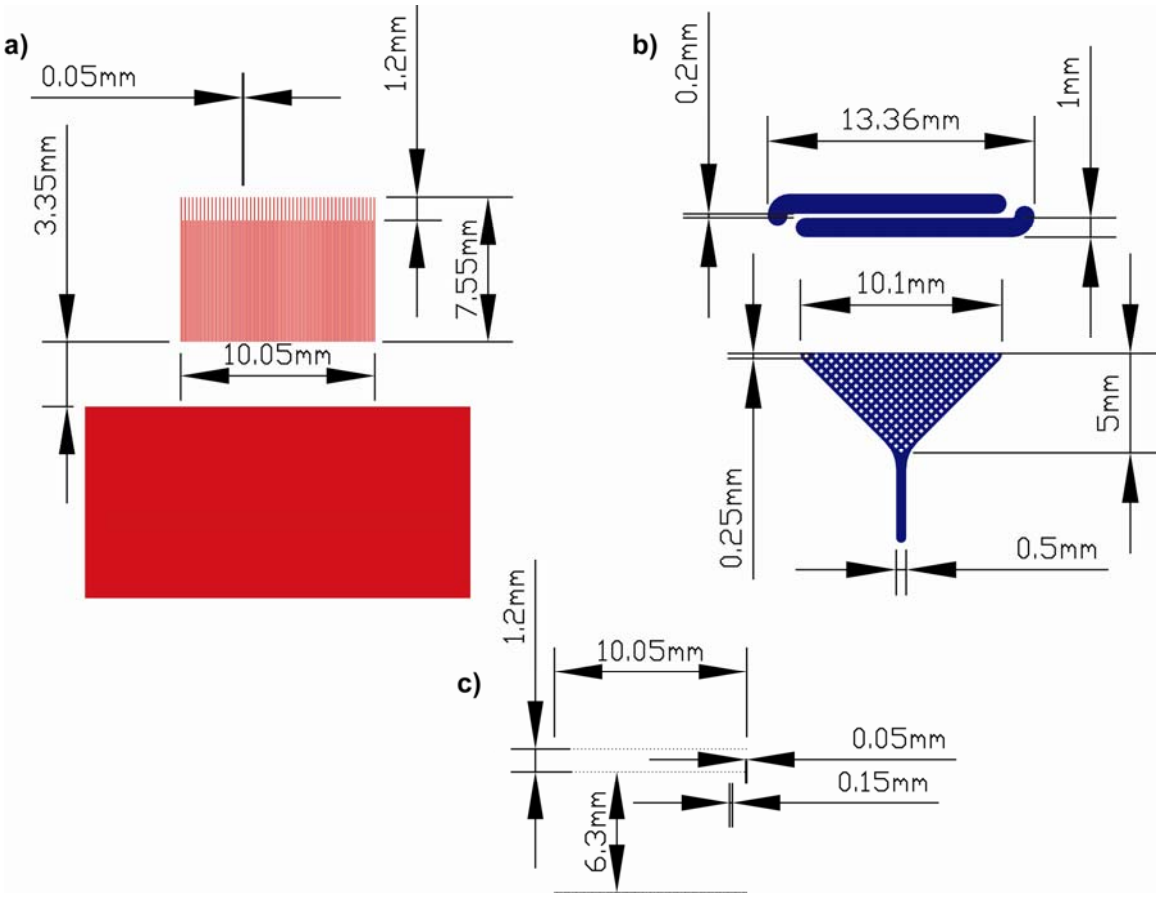

Figure A-4: Silicon Mixer Masks
a) Mask 1: Back-Side Pressure Drop Channels
b) Mask 2: Front-Side Mixing Channel
c) Mask 3: Front-Side Through Holes